

Extended Defects in Germanium

Fundamental and Technological Aspects

Bearbeitet von
Cor Claeys, Eddy Simoen

1. Auflage 2009. Buch. xx, 300 S. Hardcover
ISBN 978 3 540 85611 5
Format (B x L): 15,5 x 23,5 cm
Gewicht: 701 g

[Weitere Fachgebiete > Technik > Werkstoffkunde, Mechanische Technologie > Werkstoffkunde, Materialwissenschaft: Forschungsmethoden](#)

Zu [Inhaltsverzeichnis](#)

schnell und portofrei erhältlich bei


DIE FACHBUCHHANDLUNG

Die Online-Fachbuchhandlung beck-shop.de ist spezialisiert auf Fachbücher, insbesondere Recht, Steuern und Wirtschaft. Im Sortiment finden Sie alle Medien (Bücher, Zeitschriften, CDs, eBooks, etc.) aller Verlage. Ergänzt wird das Programm durch Services wie Neuerscheinungsdienst oder Zusammenstellungen von Büchern zu Sonderpreisen. Der Shop führt mehr als 8 Millionen Produkte.

Electrical and Optical Properties

2.1 Introduction

The first observations of plastically deformed germanium made immediately clear that dislocations introduced during a high-temperature deformation create acceptor states [1–5]. N-type Ge became p-type after deformation, while the resistivity of p-Ge did not exhibit important changes. Soon after, several hypotheses on the nature of the dislocation-related acceptor states were launched. It was Shockley who put forward the idea of the acceptor operation of the dangling bonds (DBs) in the core of a dislocation [6]; the dangling bonds originate from the threefold coordination of the germanium atoms. This has been illustrated in Fig. 1.9 of Chap. 1. In principle, both donor (giving up the unbound electron) and acceptor action can be expected, although originally only acceptor operation was found [1–4]. Based on that, Read formulated a theory for the occupation statistics of the acceptor states in covalent semiconductors [7, 8]. The difference with a point-defect related deep level is that the energy position of the dislocation acceptor level shifts with its occupation due to the Coulomb repulsion between the electrons on the DB sites. At the same time the line charge induces a surrounding space charge cylinder by interaction with the mobile charges in the semiconductor material.

This theory has long been the basis for the interpretation of the experimental results, mainly relying on Hall effect measurements as a function of temperature. It was only with the work of Schröter and co-workers [9, 10] that it became clear that the intrinsic electrical properties of dislocations are better described in terms of a one-dimensional band of states, showing both acceptor and donor activity, depending on the position of the Fermi level, that is, on the doping density and temperature.

Early theoretical calculations indicated that there is another potential source of electron states in the band gap of Ge, namely, the elastic strain field surrounding the dislocation core [11, 12]. Indeed, because of the strain field, the interatomic distance in the neighborhood of a dislocation is modified, which results in a local change of the band gap energy. Initial calculations showed a

splitting of the electron states of the conduction band in the range of 3 meV below E_C [11], which is negligibly small. However, later calculations, including the impact of the shear strain, suggested that for a screw dislocation in Ge a bound state at $E_C - 0.05$ eV could be split off from the conduction band, giving rise to electrical activity.

One overall problem in the quantification of the density of dangling bonds is the fairly large error bar in the determination of the dislocation density N_d in deformed material (see Chap. 1). Using simple preferential etching, N_d can be determined within a factor of 3. A more accurate quantification can be achieved by TEM, although this is more time consuming and provides less insight in the uniformity of the dislocation distribution and only works for high densities $N_d (>10^8 \text{ cm}^{-2})$.

However, besides the intrinsic activity of dislocation dangling bonds or strain-related states, it became soon clear that plastic deformation, even if the necessary precautions to avoid metal contamination are taken, can introduce point defects [4]. These deformation-induced point defects (PDs) can be annealed out by a subsequent heat treatment, thereby reducing the acceptor concentration. It was originally speculated that the PDs were vacancies or vacancy-related complexes, resembling the thermal defects introduced by quenching from high temperatures or created by particle irradiation [13].

Another source of electrical activity of dislocations is the elastic interaction of PDs with dislocations, described in Chap. 1 and leading to the formation of a Cottrell atmosphere [14]. These impurities have their own levels in the band gap, which may be shifted by the fact that they are now residing in the strain field of a dislocation. This is also the reason why it has shown advantageous to study deformation-induced dislocations rather than grown-in ones, as one can better control the dislocation-dopant (or PD) interaction by choosing appropriate deformation conditions (temperature, duration, cooling rate, atmosphere, etc.).

A further element to account for is the fact that there exist different dislocation types in the diamond lattice (see Chap. 1). This means that each type may have its own energy level(s) and electrical behavior.

Based on this, it is clear that the study of the electrical activity of dislocations is a complex matter, whereby one has to ascertain that “clean” dislocations of preferably one dominant type are studied. At the same time, the concept of dangling bonds has been questioned, particularly in the case of silicon. This is related to the fact that dislocations were shown to be split for most of their length by weak-beam TEM [15] and theoretical calculations indicate that the resulting 30° or 90° partials could well have a reconstructed (i.e., paired) core structure, whereby no electron states in the band gap occur.

A first section describes the electronic states of dislocations, based on experimental data from electrical techniques (Hall measurements, capacitance–voltage, DLTS; microwave, and DC conductance). The basic features of the main theories will be highlighted and the experimental conditions to obtain “pure” dislocations will be described. The next sections deal with the impact

of dislocations on the carrier mobility (scattering at charged dislocations), lifetime and trapping, low-frequency noise, and device operation (p-n junctions). The study of the optical properties of germanium has provided firm evidence of the distributed nature of the electronic states. From the obtained absorption, photoconductivity (PC) or photoluminescence (PL) spectra, a more or less complete and complex picture of the distribution of the 1D electron bands across the band gap has been established. The Chapter will be wrapped up in a conclusions section.

2.2 Electronic States of Dislocations

Shockley proposed that the acceptor nature of dislocations stems from the dangling bonds in the core of the line defect, introducing a 1D band of acceptor states in the band gap [6]. The spacing of the DBs is given by [5–7]

$$c = 0.866b \operatorname{cosec}\alpha, \quad (2.1)$$

with b the magnitude of the Burgers or lattice translation vector (0.4 nm in Ge) and α the angle between the dislocation line and the Burgers vector. The DB spacing is minimum for a pure edge ($\alpha = 90^\circ$) dislocation and maximum for a screw dislocation ($\alpha = 0$ and $c \rightarrow \infty$). In other words, (2.1) predicts no DBs for a screw dislocation and based on that, no electrical activity. As will be seen later, this is not confirmed by experiments, indicating one of the shortcomings of the Shockley–Read theory. In what follows, the evolution of the insight in the electrical activity of dislocations is sketched, starting from the Read model. The experiments leading to these theories are summarized. In recent years, interest has turned to the conduction along a dislocation, as it may represent a one-dimensional conductor.

2.2.1 Read’s Acceptor Level Model

Starting from the DB concept, a theory should enable explaining why only a fraction f_{ed} of the DBs with line density $1/c$ (cm^{-1}) contributes to the electrical activity. In other words, $f_{\text{ed}} = a_{\text{ed}}/c$, with a_{ed} the average spacing between acceptor states along the dislocation.¹ This leads to a negative line charge density q/a_{ed} , which repels the free electrons from the neighborhood of the dislocations (collective action of the line of charges²). As a consequence, a cylindrical space charge is formed around the dislocation – and assuming

¹ In fact, Read assumed a constant spacing between the occupied DB states in the most simple approximation [7,8].

² The charged DB sites can be regarded as a (continuous) line charge when $c/f_{\text{ed}} <$ mean spacing between donors or acceptors ($1/N_{\text{D,A}}^{1/3}$). In the other case (high(er) T or f_{ed} or high(er) doping), it can be regarded as a row of point charges.

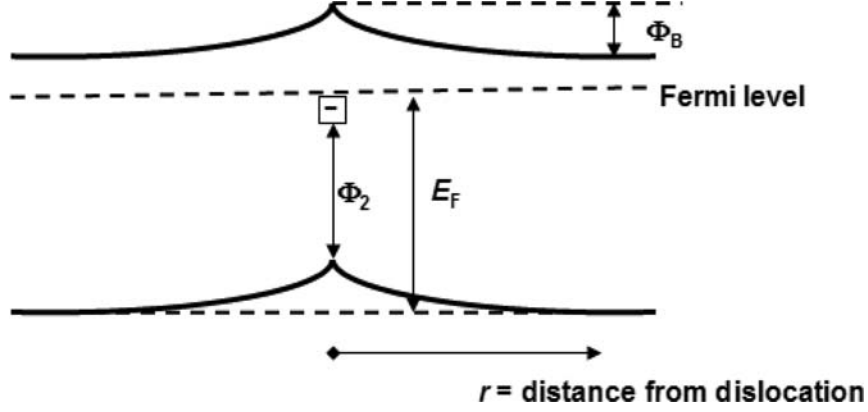


Fig. 2.1. Variation of energy bands with distance r from a dislocation. (after [7])

that the screening by the free electrons is negligible, which is valid at low temperatures – with radius R given by [7, 8]

$$\pi R^2 (N_D - N_A) = 1/a_{ed} = f_{ed} \cdot c \quad (2.2)$$

and schematically represented in Fig. 2.1. N_D and N_A are the donor and acceptor concentration, respectively, so that $N_D - N_A$ is the net doping density in the undeformed material, outside the dislocation region. As a consequence, a potential barrier Φ_B develops around a charged dislocation, which depends on its occupation (charge density Q), while the bands are bent, like in Fig. 2.1. At the same time, the energy position of the dislocation acceptor level (E_d) will increase with increasing charge, according to the relation

$$E_d(Q) = E_0 + E_e(Q), \quad (2.3)$$

with E_0 the level for $f_{ed} = 0$ ($Q = 0$), the neutral dislocation limit and $E_e(Q)$ the electrostatic energy associated with the Coulombic interaction between the occupied DBs. E_0 has to be derived experimentally, while E_e can be theoretically calculated under certain assumptions.

For the calculation of the electrostatic energy, one can in principle not rely on Fermi–Dirac statistics [7, 8], as the neighboring occupied sites repel each other. Assuming equally spaced occupied acceptors, Read obtained in the 0 K approximation

$$E_e = \{q^2 f_{ed} / (2p\varepsilon_0\varepsilon_{Ge}c)\} \{3/2 \ln(f_{ed}/f_c) - 0.866\}, \quad (2.4)$$

with q the elementary charge; ε_0 the permittivity of vacuum, and ε_{Ge} the dielectric constant of germanium, while f_c is defined by [7, 8]

$$f_c = c[\pi(N_D - N_A)]^{1/3} \quad (2.5)$$

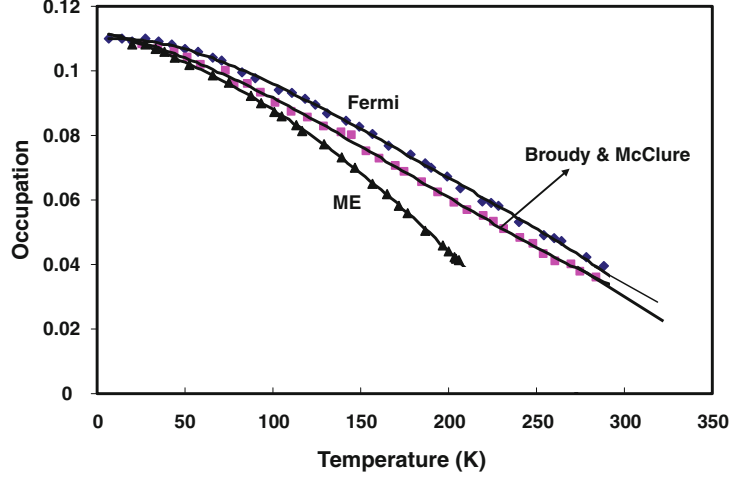


Fig. 2.2. Comparison of various statistical treatments for the occupation of dislocation acceptors by Read [7, 8] and Broudy and McClure [16] ($N_D - N_A = 10^{15} \text{ cm}^{-3}$, $E_C - E_0 = 0.225 \text{ eV}$, $f_c = 0.00586$). *ME* minimum energy approximation with constant spacing between occupied sites, *Fermi* Fermi-Dirac statistics (after [15])

and following from (2.2) for $R = a_{\text{ed}}$. It is also assumed that the bands shift rigidly with the charging of the dislocation, thereby, neglecting elastic field changes. Equations (2.4)–(2.5) are strictly speaking only valid for $T = 0 \text{ K}$ (no entropy contribution and fixed distance a_{ed} between acceptor states). Read has also worked out the statistics for a number of limiting cases [7,8], considering line charge fluctuations and nonuniformities, and hence, a nonzero entropy term. A further refinement was performed by Broudy and McClure [16,17]. Based on (2.4)–(2.5), the occupation fraction f_{ed} of the acceptor states can be calculated, yielding the result of Fig. 2.2. From this figure, one can derive that the fractional occupancy of the dangling bond acceptors states is maximum $\sim 12\%$ and reduces with increasing temperature to reach only a few % at room temperature. It is also clear from Fig. 2.2 that the Fermi-Dirac statistics overestimates the dislocation occupancy, although the Broudy–McClure approach leads to a formally equivalent expression [16].

Early assessment of the electrical activity of dislocations was performed by Hall measurements vs. temperature. It should be remarked that in such a case, only states at the Fermi level E_F (in thermodynamical equilibrium) are probed. A method that has been largely followed is to measure the free carrier (hole) concentration p as a function of T in the deformed (p-type) material, which yields E_F through [9]

$$E_F = kT \ln \left(\frac{CT^{3/2}}{p} \right) (E_F > kT), \quad (2.6)$$

with $C = 1.17 \times 10^{15} \text{ cm}^{-3} \text{ K}^{-3/2}$ in p-type Ge. At the same time, one can derive f_{ed} from [9]

$$f_{\text{ed}} = (p - N_{\text{A}}) / N_{\text{s}}, \quad (2.7)$$

N_{s} is the DB volume density in cm^{-3} equal to N_{d}/b , with N_{d} the dislocation density (assumed of one type for simplicity). The increase in free hole density in the deformed p-type material $p-N_{\text{A}}$ is then supposed to originate solely from the occupied dislocation DB states, neglecting all other mechanisms (deformation-induced point defects; split off strain states; impurity decoration; etc.). The neutral level according to (2.7) then corresponds to the temperature (or Fermi level) at which $p = N_{\text{A}}$, in the frame of the Read model.

Applying this theory, a wide range of values for the neutral dislocation level has been obtained, from $E_{\text{C}} - 0.225 \text{ eV}$ [7] to $E_{\text{C}} - 0.5 \text{ eV}$ [17]. Other groups found intermediate values [18]. Krylow and Auleytner concluded that the dislocation acceptor level in n-type Ge was at $E_{\text{C}} - 0.13$ to 0.18 eV , independent of the dislocation type [19]. Finally, in twisted n-type Ge with predominantly screw dislocations, no acceptor levels were observed within the resolution of the conductivity measurements employed [20]. In principle, E_0 should only depend on the dislocation core and not on the doping type or dislocation density, which was obviously not observed here.

2.2.2 Schröter's 1D Band Model

The wide scatter in E_0 level derived from the application of Read's model was puzzling and different explanations have been advanced, either pointing to a nonuniformity of the dislocation density or type or to an interaction with impurities or point defects. However, there was also evidence of the formation of donor states in deformed highly p-doped Ge [14,21], which cannot be explained in the frame of Read's model. This suggests rather a half-filled 1D band of states associated with dislocations than a single acceptor level, as originally suggested by Shockley [6] and also considered by Mueller in the interpretation of his data [22].

A breakthrough came with the study of plastically deformed p-type Ge by Schröter et al. [9,10,23]. The main experimental result is shown in Fig. 2.3 [24], comparing the free hole density for the undeformed and plastically deformed p-type Ge. At high temperatures, the deformed sample shows a higher p concentration, indicating the introduction of dislocation-related acceptors. It should also be noted that there is no leveling off at higher temperature [9], suggesting that the dislocation states are not fully occupied yet. However, there is a continuous reduction in p with lower T , which crosses the chemical acceptor density ($p = N_{\text{A}}$) of the starting material at $T \sim 80 \text{ K}$ and drops below N_{A} . This strongly suggests a donor operation of the dislocation states, when the Fermi level is sufficiently close to the valence band.

The cross-over in Fig. 2.3 marks a continuous transition from donor-type to acceptor-type behavior, which has been interpreted in terms of partially filled

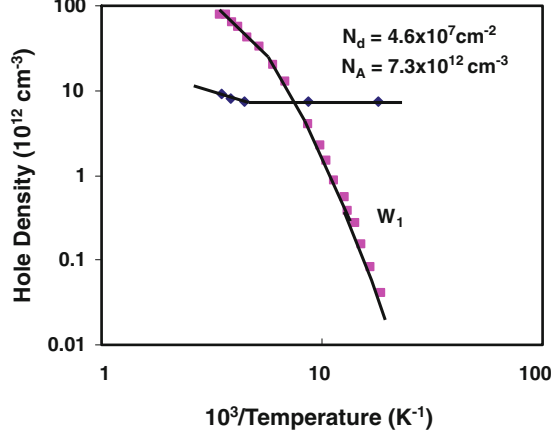


Fig. 2.3. Hall effect of deformed (W1: after static compression at 580 °C) and reference Ge. Hole density as a function of the inverse temperature before and after introduction of edge-type dislocations. At the intersection of the two curves the dislocations are neutral ($f_{ed} = 0$), while for lower temperatures they are positive, and for higher temperatures they are negatively charged (after [24])

dislocation states and, in combination with Shockley's dangling-bond concept, has led to the model of a half-filled dangling-bond band [9]. The occupation limit of this band coincides with the Fermi level given by (2.6), as long as the band does not become totally emptied or filled with electrons. From the cross-over temperature T_0 , the occupation limit of the neutral dislocation is obtained $E_0 = E_F(T_0, N_A)$. If the dislocation density is measured in addition, the line charge of the dislocation is $Q = q(p - N_A)/N_d$ so that the function $E_F(Q)$ is proportional to the electrostatic shift $E_e(Q)$ of the dislocation band on the energy scale.

To interpret these results, it was assumed that dislocations give rise to a 1D band of states, whereby E_F is the occupation limit and E_0 is now interpreted as the neutral occupation limit within the band, corresponding with zero line charge. Assuming that the doping density of chemical acceptors N_A in the p-Ge is not changed in the space charge region surrounding the dislocations in the deformed material (no deformation-induced PDs, which requires a $T_{def} > 773$ K or $0.6T_m$ typically), one can derive the fractional occupation of the dislocation states from

$$E_F - [E_0 - E_e(f_{ed})] \approx 2f_{ed}kT \quad \text{for } |f_{ed}| \ll 1. \quad (2.8)$$

In writing (2.8), it is assumed that the band is half-filled at $E_F = E_0$ and that each state is twofold degenerate, accepting electrons with spin up and spin down. This can be further developed into a linear function of f_{ed} [9]:

$$E_F - E_0 = E_e(f_{ed}) + (\Delta E_s/2\delta)f_{ed}, \quad (2.9)$$

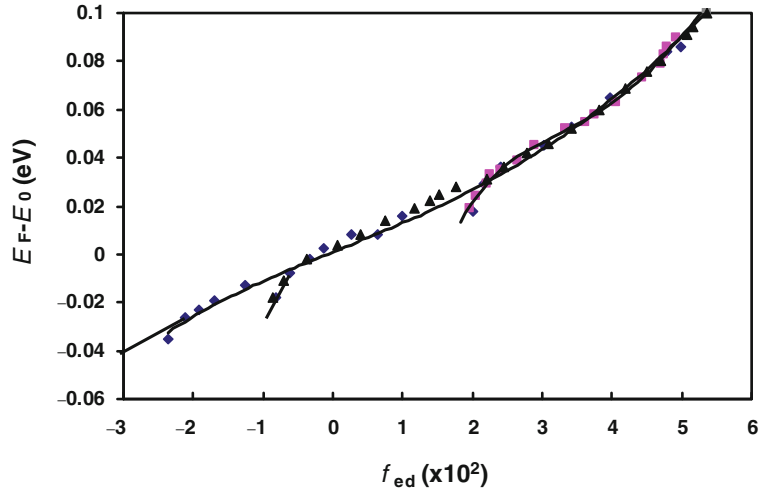


Fig. 2.4. $E_F(f_{ed}) - E_0$ as a function of f_{ed} for different highly deformed and doped samples (after [9])

with ΔE_s and δ constants for a given dislocation type. Note that according to (2.4) E_e is in the first instance a linear function of f_{ed} . The expression obtained by Read for E_e neglects screening of the charge on a dislocation line by free carriers, which is a good approximation in the low-temperature limit. The linear dependence predicted by (2.9) was fully supported by the experiments of Schröter [9], as shown in Fig. 2.4.

According to Fig. 2.5, one has to consider different interactions in a row of dangling bonds in order to calculate the occupation statistics [25]. In a simple one-electron-approximation, only the interaction of an additional electron with the line charge and the free carriers is taken into account. It was shown, moreover, that the effect of hybridization and intrabond Coulomb interaction on the DB states associated with 60° dislocations is rather small, so that the simple DB concept gives a fair description of the localized states associated with dislocations [26]. In the original band model, it is assumed that the screening of the DB charges occurs by the free carriers and not in a sharp space charge cylinder, with typical radius $\lambda = \sqrt{kT\varepsilon_0\varepsilon_{Ge}/q^2|p-n|}$ (the Debye screening length) [10,26]. This is valid for the dislocation barrier height in the range kT (small f_{ed} and thus higher T). For lower T , there is a transition to the space charge cylinder model of Read. Implementing the corresponding occupation statistics, expressions for E_F and E_e have been derived [9,10,15,27].

A further improvement was implemented by Veth and Lannoo [28], who took into account a better approximation for the short-range interaction of electrons on DB sites, resulting in an E_e , given by

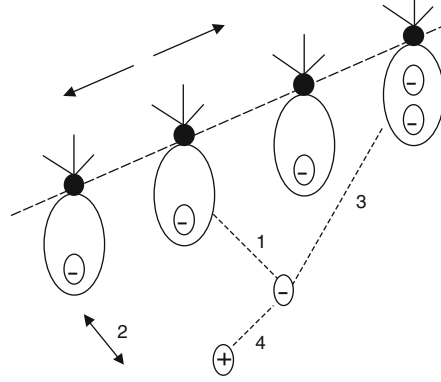


Fig. 2.5. Different interactions of an electron in the dislocation core are discussed for a row of dangling bonds: (a) the electron, added to a DB is repelled by the electron already present in it: intrabond Coulomb energy (1); (b) electrons may hop between dangling bonds and bulk states: hybridization, transition rate Δ/\hbar , with \hbar the reduced constant of Planck (2); (c) in a simple one-electron-approximation only the interaction of an additional electron with the line charge (3) and free charge carriers (4) is taken into account (after [25])

$$E_e = \frac{U f_{ed}}{\varepsilon_{Ge}} + \frac{q^2 f_{ed}}{2\pi\varepsilon_{Ge}\varepsilon_0 c} \ln\left(\frac{\lambda}{c}\right) \quad (2.10a)$$

$$\text{or } E_e = \frac{U f_{ed}}{\varepsilon_{Ge}} + \frac{q^2 f_{ed}}{2\pi\varepsilon_{Ge}\varepsilon_0 c} \left[\ln\left(\frac{R}{c}\right) - 0.616 \right] \quad (2.10b)$$

for the Schröter–Labusch (SL) or the Read case, respectively [15, 28]. In this theory, account is made for the discrete nature of the charge distribution along a dislocation, instead of considering it as a line of charge as in the SL case [28]. The screening length (or limiting radius between short and long-range Coulomb potential) is in this approach independent on the screening model applied [28] in contrast to the Read model [7, 8], while the energy shift ΔE (first term in the rhs of (2.10)) is assumed proportional with the excess electron charge and also independent on the screening model. The energy U is the intra-atomic Coulomb interaction between an excess charge and the electrons already present in the neutral state, represented by (1) in Fig. 2.5 [28].

Application of the band model led to the diagram of Fig. 2.6 for edge type (60°) dislocations: a neutral level E_0 at 0.09 eV from the valence band. The width of the 1D band has been extracted from capacitance–voltage (C – V) measurements on Schottky barriers, made on deformed Ge [29, 30]. It was hereby assumed that the DB acceptors can be treated as point defects with respect to their impact on the doping density in the depletion region of the diode [29]. A band width of 0.18 eV was derived from the C – V analysis [30].

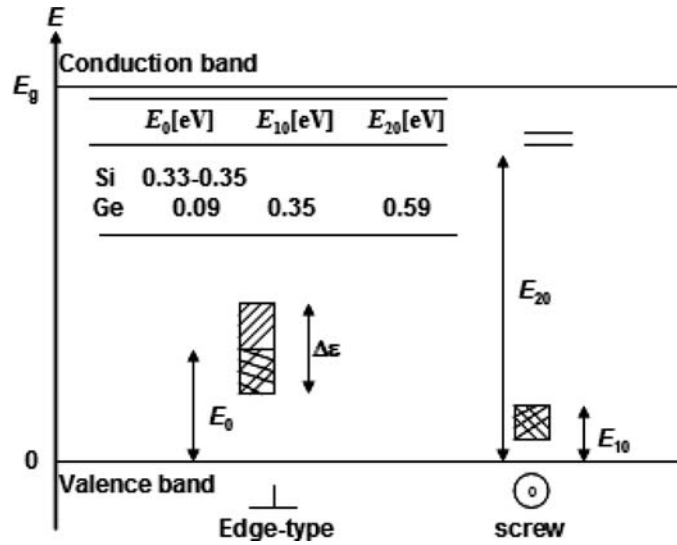


Fig. 2.6. Parameters of dislocation states for Si and Ge, as derived from measurements of the Hall effect: upper edge E_{10} of the full band and lower edge E_{20} of the empty band at a neutral screw dislocation, and the occupation limit E_0 of the half-filled band at a neutral edge-type dislocation (after [24])

A similar analysis has also been performed for samples with a large fraction of screw dislocations. It was concluded that the latter give rise to a fully occupied band at $E_V + 0.035$ eV (upper limit) and an empty band with lower limit at $E_V + 0.589$ eV [31, 32]. The question rises of course what the origin of these states is, since according to (2.1) there are no DB associated with screws. The answer is that most likely, the elastic strain field is creating these states [31, 32]. In first order, a screw dislocation has a pure shear strain. However, calculations have shown that this results only in split off states from the conduction band [12]. In second instance, there is a dilatation field associated with a screw and resulting in states split off from both valence and conduction band. The experimental results suggest that the binding energy of the shear field is larger than that for the dilatation one, in qualitative agreement with theory [11, 12]. The corresponding density of states is equal to the number of atoms along the dislocation line, that is, $1/b$ states per unit length of dislocation [32].

While the half-filled band model provides a fair interpretation of the Hall measurements on deformed germanium, some experimental evidence does not fit into the picture. As will be detailed later, the absence of microwave conductivity along dislocations in n-type material compared with p-type and the complex structure of the photoconductivity (PC) and absorption spectra point against the simple 1D band picture [33]. Also some Hall results did not completely agree with the interpretation by the Göttingen Group [33, 34].

Kolyubakin and Shevchenko arrive at a lower neutral edge dislocation level at $E_V + 0.07$ to 0.075 eV, independent of the starting conductivity [33], for small values of f_{ed} (< 0.005). This position was independent of dislocation density and cooling rate, suggesting that it was an intrinsic property rather than related with deformation-induced point defects. It was concluded that the band structure in the lower half of E_G was more complex and probably contains two acceptor bands with different widths and one donor band, separated by a gap [33]. The gap between the donor and acceptor states is rather narrow and in the range 30 [33] to 50 meV [34]. The lowest donor band (at $E_1 = 0.055$ – 0.075 eV) is fully occupied for the neutral dislocation, while the bottom of the second highest acceptor band is at $E_V + 0.25$ eV [33]. The first acceptor band is expected at $E_V + 0.07$ to 0.09 eV. It was also suggested that the complexity of the dislocation bands was due to their splitting [33]. This band complexity will be further detailed in the section on the optical properties.

2.2.3 First Principles Calculations and EPR Results: Do DBs Exist in Split Dislocations?

The original theoretical work focused on the electronic states associated with the strain field of dislocations [11, 12, 35–37]. Later calculations also considered the electronic states of dangling bonds in the dislocation core [38–45] and usually predicted a 1D half-filled band of states in the band gap, associated with 60° dislocations [40, 43]. More recent calculations also accounted for the fact that the dislocations are split over most part of their length [46–48]. This implies that the electrical activity in the first place stems from the partial dislocations (and/or the stacking fault bound by them) and not from the unsplit segments of the dislocation. Figure 2.7 compares the structure of a 30° -partial of the glide set unreconstructed (with DBs) and reconstructed (no DBs) [15]. According to calculations, the reconstructed 30° and 90° partials are more stable, leaving the question whether DBs are really responsible for

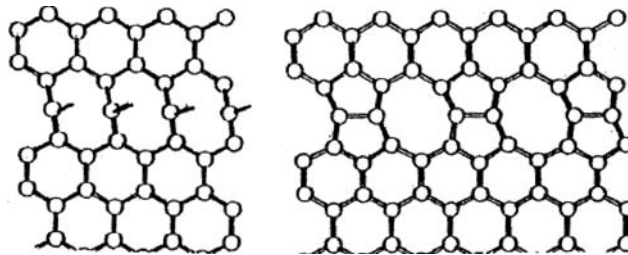


Fig. 2.7. 30° -partial dislocation of the glide set, unreconstructed (*left*) and reconstructed (*right*). Screw dislocations of the glide set dissociate into two 30° -partials, 60° -dislocations of the glide set into one 90° -partial and one 30° -partial (after [15])

the electrical activity of dislocations in Si and Ge. This also strongly questions existing Read and Schröter theories based on the DB concept.

Summarizing the current view of the theory of dislocation states in Si (and Ge) [15]: deep states originate in the indirect band gap in core configurations of three- and fivefold coordination, and are missing for cores with fourfold coordination. This means that dangling bonds, that is, threefold coordination, are a sufficient condition for deep levels associated with it. The dangling-bond carrying core of the 30° -partial gives rise to a broad one-dimensional band of states extending over the whole indirect band gap [15]. On core reconstruction, this wide band splits into two narrow bands, one occupied, the second empty, which move out of the band gap. In summary, the 30° -partial in silicon has a reconstructed core with no deep electronic states. This implies no electrical activity of screw dislocations, associated with DB states. Of course, there can still be electronic states associated with the strain field surrounding the dislocations, as mentioned earlier. These stress states probably correspond with the two 1D bands in Fig. 2.6 [24, 31, 32].

The question which of the four possible core states of the 90° -partial is the more stable one has not been clearly answered yet. It has been shown that the unreconstructed 90° -partial gives rise to two bands: the upper one is a resonant state near the center of the Brillouin zone and becomes a bound state near the zone boundary, while the lower band is bound over the entire zone [48]. However, it was concluded that the unreconstructed core configuration was rather unlikely, so that there exists serious doubt whether the electrical activity of 60° -dislocations can be ascribed to dangling bond states in the core of the 90° -partial. The available calculations show that the fourfold coordinated cores are more stable than the three- and fivefold ones, so that no states are expected in the band gap [15]. It is thus well possible that the 1D bands derived for dislocations in Ge (see Fig. 2.6, e.g.) are not related to DB centers but result from split-off strain states. Another source of electron states may be the stacking fault (SF) in between the two partials [15]. Calculations suggest that mainly due to the strain field of the partials, SF states may be shifted into the band gap [15]. Another question that has hardly been tackled is what the impact is of faults in the core structure, like jogs and kinks or points of intersection [48]. The fact is that most of the measured data can be satisfactorily explained within the DB band formalism.

In principle, the presence of dangling bonds in Ge can be demonstrated by the electron paramagnetic resonance (EPR) technique, which is structure sensitive and yields an unmistakable fingerprint of the unpaired electron on a Ge atom back-bonded by three Ge neighbors. There have been some reports of the EPR observation of DBs in Ge, associated with dislocations [49–51]. The most convincing result was obtained on as-grown dislocations [50, 51], where a highly sensitive photoconductivity (PC) technique was employed. Without optical excitation, no DB-like signals were observed. On the other hand, the PC persisted for hours after switching off the light, indicating that the free carriers reside in a long lifetime dislocation band, retaining a nonzero

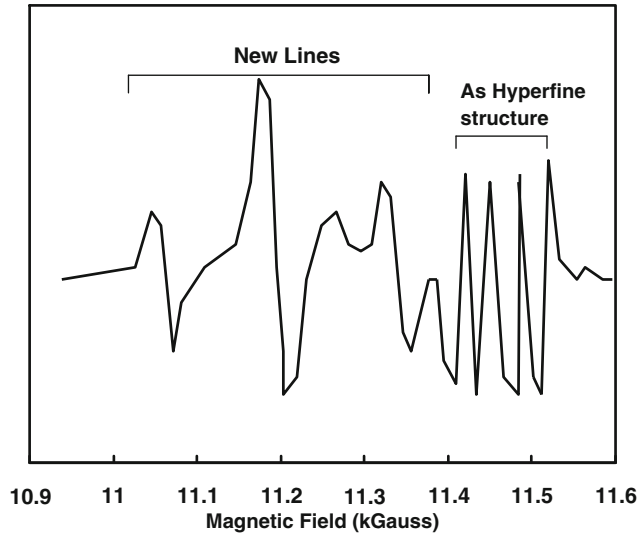


Fig. 2.8. Derivative curves of EPR in As-doped Ge ($N_D - N_A = 8 \times 10^{13} \text{ cm}^{-3}$). Magnetic field is oriented along a $\langle 100 \rangle$ direction. $T = 2 \text{ K}$, $f = 25.16 \text{ GHz}$. Note the sign reversal of the new lines as compared to the As hyperfine structure. Dislocation density $\sim 2 \times 10^4 \text{ cm}^{-2}$ (after [50])

spin-dependent mobility. In other words, the mobility of the photo-excited electrons was determined by spin-dependent scattering through DBs located in the core of dislocations within the crystal.³ The resulting spectrum is represented in Fig. 2.8 [50]. The derived symmetry of the lines yields evidence of a small well-defined distortion within dislocations [50].

2.2.4 One Dimensional Conduction Along Dislocations

Although the origin is far from resolved, it has been well established that 60° dislocations (or their partials) give rise to 1D bands in the band gap of germanium, which are intrinsic to the dislocation core. From a theoretical viewpoint, one would expect also a one-dimensional conduction along the dislocation line [52], even if account is made for the defects that could be present (splitting, kinks and jogs, internal mechanical stress, impurity atoms, etc.). In case the band is half-filled, as would be expected for a DB-related band, a metallic type of conductivity will result. Reconstruction between pairs of DBs (atoms) will split the 1D band into a full donor and an empty acceptor band, separated by a gap [52]. This could lead to a thermally activated conduction mechanism. One-dimensional conductors are also very sensitive to perturbations (defects) and easily break into segments, which are separated

³ No such signals were detected in essentially dislocation-free crystals [50,51].

by activation barriers. However, 1D conduction is not totally destroyed by these barriers but persists via thermally activated hopping.

Another possibility for thermally activated conduction is the opening of a gap at the Fermi level upon cooling to low temperatures, causing a Peierls or Hubbard transition from a 1D metal to a 1D semiconductor. In deformed Ge, there are generally only short, disconnected straight-line dislocation segments so that when the DC conductance is measured at low temperature, not enough current flow in a single direction is available [52], resulting in no observable dislocation conduction, if no special precautions (sample preparation) are taken. This calls for a high-frequency conductance measurement. This field has been explored by the Chernogolovka Group [53–57], resulting in firm evidence of dislocation conductance at liquid helium temperatures. Typical values were in the range $\sigma = 2.5 \times 10^{-9}$ to $1.4 \times 10^{-10} \Omega^{-1} \text{cm}^{-1}$, which is rather high for a 1D conductor, so that some caution in the interpretation of the results is required [52]. A possible alternative explanation for the observed effects is the decoration of the core by doping elements [52], although in some experiments this option has been clearly denied.

A typical result of the dislocation conductance at $f = 9.5$ GHz in deformed p-type germanium vs. $1/T$ is displayed in Fig. 2.9a [53]. There are two parts in the curves of Fig. 2.9: a σ_{micro} that is practically temperature independent from 4.2 to 10 K and a temperature activated part at higher T . It should be remarked that the DC conductance of the material is many decades lower at 4.2 K due to the freeze-out of the free carriers and the difference increases for lower T . Note also that the microwave conductance is absent in undeformed, low dislocation density material [53]. In other words, $\sigma_{\text{DC}} = \sigma_{\text{micro}}$ in reference samples. Moreover, the asymmetry of σ_{micro} follows the asymmetry of the dislocations.

A second relevant factor in the microwave conductance is the doping dependence, illustrated in Fig. 2.9b [53]. For a low doping density, the microwave conductance at 4.2 K and 9.5 GHz saturates at the point (N_{d}) where it is believed that the space charge cylinders (SCCs) start to overlap. Below this threshold, the SCC are separated by “normal” (but frozen-out) p-type germanium, above that, there is no more “neutral” material in-between. For higher doping densities (smaller R according to (2.2)) this transition takes place at a higher density N_{d} . This behavior cannot be explained by a conductivity mechanism based on hopping between empty acceptor states [53]. Furthermore, no anisotropy is expected for a dopant-related hopping mechanism. It was furthermore observed that the anisotropy of σ_{micro} was independent on N_{d} or the doping density, only on the dislocation structure [53].

Based on these observations, it was concluded that the dislocation states form two bands (an empty and a full one) separated by a small gap of 0.01 eV. This explains the thermally activated increase with T in Fig. 2.9a. A hole mobility at 9.5 GHz of $10^4 \text{cm}^2 \text{V}^{-1} \text{s}^{-1}$ was derived, which is about one decade smaller than that for the valence band at 4.2 K [53]. The fact that σ_{micro}

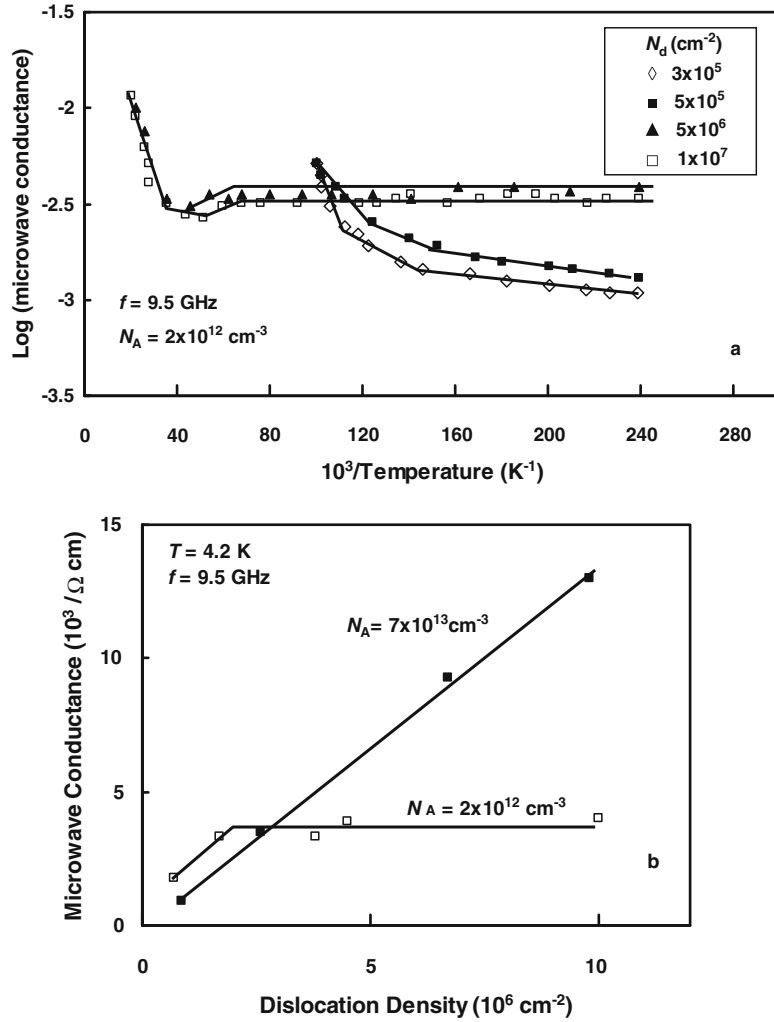


Fig. 2.9. (a) Temperature dependence of the microwave conductance for deformed samples with different dislocation density. (b) Dependence of the microwave conductance on the dislocation density at $T = 4.2 \text{ K}$ for deformed samples with initial acceptor concentration $2 \times 10^{12} \text{ cm}^{-3}$ (*open squares*) and $7 \times 10^{13} \text{ cm}^{-3}$ (*filled squares*) (after [53])

increases for lower T in Fig. 2.9a and high N_d is indicative of a metallic type of conductivity along the dislocations. In the case no overlap of the SCCs occurs, the microwave conductivity drops with temperature in Fig. 2.9a [53].

The microwave conductivity of deformed n-type Ge behaves qualitatively different than for p-type material [54]. It was found to be weakly temperature-dependent, increasing with T , while σ_{micro} decreases with N_d and disappears

for a sufficiently high dislocation density [54]. Such a contrasting behavior could be explained by considering at least three bands of dislocation states: a lower band that is completely filled in n-type and partially filled in p-Ge, a second band with a low mobility (discrete level?), and a third empty band. Finally, it was found that the microwave conductivity showed the same anisotropy as the dislocation structure [55], similar as in p-type material [53].

Another remarkable effect associated with the low-temperature conductance in deformed material is that no measurable Hall effect could be associated with both the observed DC and microwave conductance [56,57]. This made it impossible to determine the sign (type) of the carriers responsible for the one-dimensional σ_{DC} and σ_{micro} . However, using severely strained (50–70%) samples enabled the measurement of the Hall emf and demonstrated firmly hole-type conductivity [57]. The temperature dependence of the DC conductivity could be described by $\sigma_{\text{DC}} \sim T^y$, with $y = 0.15\text{--}1.5$. Putting together all experimental evidence from DC, Hall effect and microwave measurements resulted in a proposed energy band scheme represented in Fig. 2.10 [57], whereby the levels E_1 belong to the dislocation dangling bonds and E_2 is the band of energies of the extra electrons trapped in these bonds and separated by a gap Δ_{12} .⁴

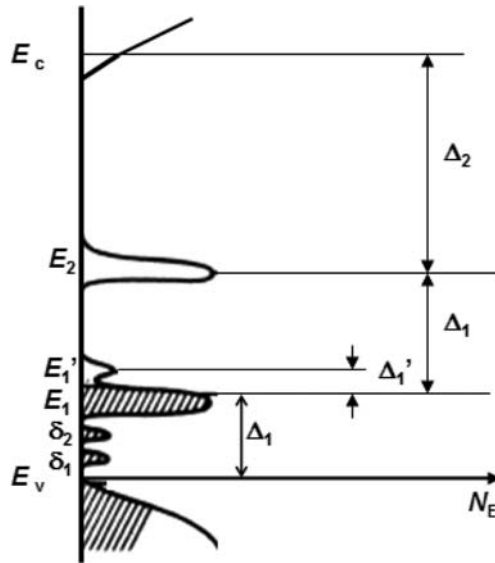


Fig. 2.10. Energy diagram of dislocation states in germanium. Here N_E is the density of states. $\Delta_1 = 0.07$ eV, $\Delta_1' < 0.03$ eV, $\Delta_{12} = 0.18$ eV, and $\Delta_2 = 0.49$ eV (after [57])

⁴ It should be noted that E_1 and E_1' are equivalent to the edge dislocation band in Fig. 2.6. The difference is a different interpretation of the Hall effect data, as described in Refs [33] and [34].

A model has been proposed for the dislocation microwave conductance, describing it in terms of the characteristic length l_d of the conducting segment and its resistance R_d [52, 58]. A suitable parameter of the core states is the specific conductance $\Sigma = 1/R_d$. An appropriate model for this object is a slender ellipsoid of length l_d and radius $r \ll l_d$. This finally resulted in [52, 58]

$$\sigma_{\text{micro}} = \sigma_B + (2\pi/3)\nu l_d \Sigma. \quad (2.11)$$

In (2.11), ν is the volume density of dislocation segments and σ_B is the conductivity of the matrix. It has been generally found that Σ decreases with dislocation density. This was thought to be a fingerprint of the fact that the core states are only conductive if they are “doped” by shallow impurities in the matrix. An alternative picture is that the density of core defects increases with N_d , resulting in a drop in σ_{micro} [52]. It was also found that l_d is on the order of 9–12 μm in Ge with a dislocation density of about 10^7 cm^{-2} [58] and that the dislocation conductance in Ge ($\sim 10^{-10} \Omega^{-1} \text{ cm}^{-1}$) was much higher than in Si [58].

More recently, renewed attempts have been made to measure the DC conductance along one or a small group of similar straight dislocations running from top to bottom through a Ge sample [59]. Assuming that a charged dislocation in n-type Ge is surrounded by a space charge cylinder, it will behave like a rectifying or Schottky contact, as already demonstrated by Hogarth and Baynham in the fifties [60]. The conduction of a dislocation to the bulk n-Ge looks like a soft diode, as in Fig. 2.11 [59]. This is consistent with the idea of a dislocation as a thin Schottky tube and supports the SCC idea. The softness of the characteristics may be described by tunneling of electrons through

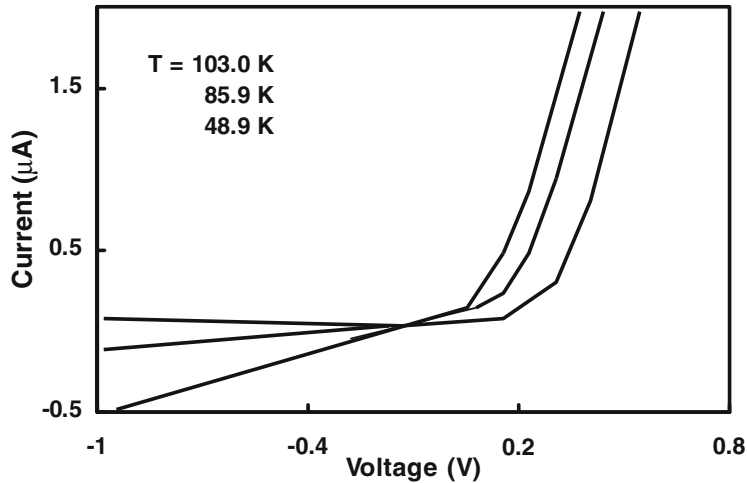


Fig. 2.11. Current–voltage plots for conduction from dislocations to n-type bulk Ge (after [59])

the barrier. If 60° dislocations are the dominant recombination centers in deformed Ge, one can derive a carrier lifetime equal to [59]

$$\tau = \frac{r_d l_d}{\partial U / \partial Q}, \quad (2.12)$$

with Q the trapped charge per unit length on the dislocation and r_d the differential resistance of the diode of Fig. 2.11 at zero voltage. Based on the data of Fig. 2.11 ($r_d = 10^8 \Omega$, $l_d = 115 \mu\text{m}$, and $\partial U / \partial Q \sim 3\text{--}5 \text{ V}$ times c/q , with c the distance between the dangling bonds in the dislocation core), one obtains a lifetime $\tau \sim 1 \mu\text{s}$, which is much smaller than the observed recombination lifetimes [59], so that it is concluded that single 60° dislocations are possibly not the rate limiting recombination centers in deformed Ge [59]. For groups of dislocations, this may be related to the overlap of the potential barriers, so that the tunneling probability would be strongly reduced and the recombination time increased.

The conductance through a small group of dislocations has also been measured by making ohmic contacts on the top and bottom of the thinned sample ($100 \mu\text{m}$) with reach-through dislocations [59]. The resulting I - V characteristics are shown in Fig. 2.12 at different temperatures for a small group of 60° dislocations. It was found that there was no specific dependence on the doping density so that it is an intrinsic property of the dislocation. The zero volt conductance has a 25 meV activation energy as shown in Fig. 2.13 [59] and was attributed to a $\sim 50 \text{ meV}$ gap in the band structure of dislocations caused by a Peierls transition and, therefore, always centered around the Fermi level.

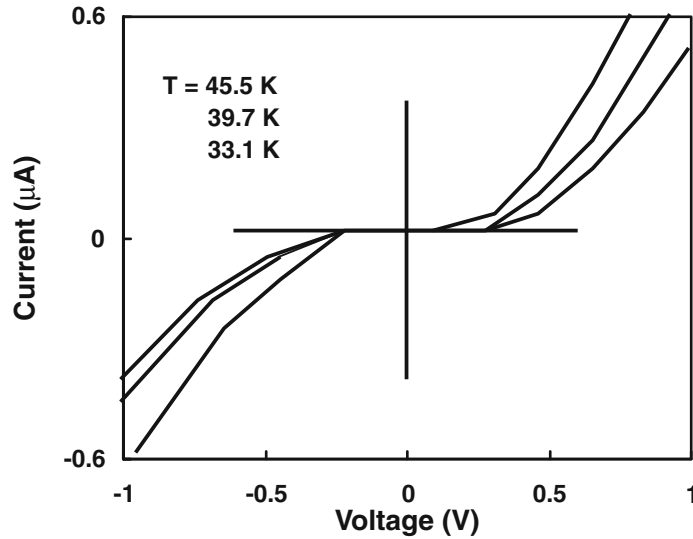


Fig. 2.12. Current–voltage characteristics of various samples at different temperatures (after [59])

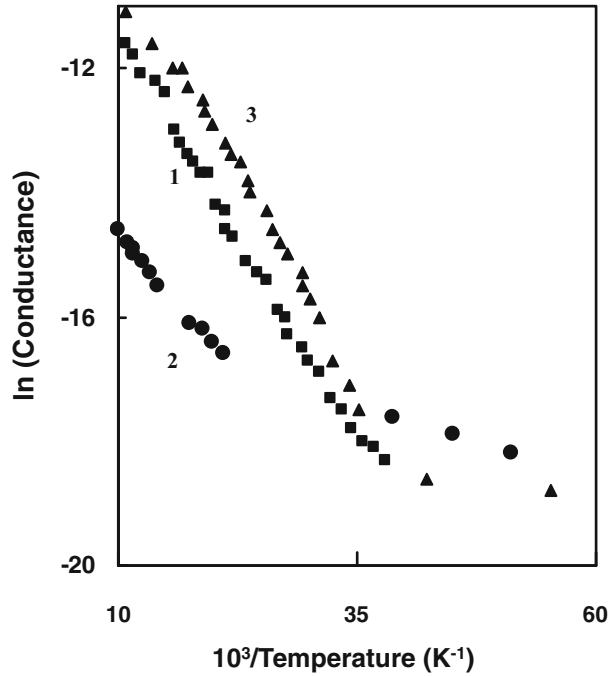


Fig. 2.13. Logarithm of the conductance σ at 0 V against reciprocal temperature for samples with different doping (N_D) and dislocation density (N_d) and characteristic length l_d . 1: $N_D = 10^{13} \text{ cm}^{-3}$, 40 dislocations, $l_d \sim 100 \mu\text{m}$; 2: $N_D = 10^{15} \text{ cm}^{-3}$, 15 dislocations, $l_d = 200 \mu\text{m}$; 3: $N_D = 3 \times 10^{13} \text{ cm}^{-3}$, the number of dislocations could not be determined, $l_d = 115 \mu\text{m}$ (after [59])

In n-type Ge, sufficient electrons are trapped so that the Fermi level is in the upper of the two resulting bands. This confirms the band diagram of Fig. 2.10.

2.2.5 Deformation-Induced Point Defects

Already in the early days of semiconductor research, it was recognized that deformation at high temperatures could also induce point defects, like vacancies and vacancy aggregates [4, 13]. It was a possible explanation for the n- to p-type conversion of plastically deformed Ge. Later, Krylow suggested that the results by Schröter could be well explained by PDs, with a donor level at $E_V + 0.22 \text{ eV}$ [61]. A more rigorous study was undertaken by the Chernogolovka Group [62] and they came to the conclusion that deformation at $420 \text{ }^\circ\text{C}$ creates PDs with levels at $E_V + 0.01 \text{ eV}$, $E_V + 0.022 \text{ eV}$, and $E_V + 0.036 \text{ eV}$, based on Hall effect measurements. Annealing at $550\text{--}600 \text{ }^\circ\text{C}$ increased the activation energy of the shallow levels to 60 meV . They may be annealed out in the range $680\text{--}700 \text{ }^\circ\text{C}$, similar as quenched-in point defects.

There was a strong suspicion that the $E_V + 0.036$ eV level was due to substitutional copper [63], affecting the dissociation width of screw-like dislocations.

Perhaps the most systematic studies of plastic-deformation-induced PDs in Ge have been performed by Cavallini et al. [64–68]. They demonstrated by Hall effect measurements that low-temperature deformations ($T < 430$ °C) introduce shallow acceptor states at $E_V + 0.02$ eV, probably connected with the strain field around the dislocations [68]. Higher temperature deformations (at 580 °C) introduce the typical $E_V + 0.09$ eV dislocation-related states. It was also noted that low temperature deformations favor widely dissociated screw dislocations [66]. Annealing of these 0.02 eV shallow dislocation states at temperatures from 480 to 580 °C leads to a progressive inactivation. At the same time, levels at $E_V + 0.05$ to 0.06 eV are introduced, probably due to impurity introduction along the dislocation themselves [68].

The spectra of the PDs have also been studied with deep level transient spectroscopy (DLTS) [69–71]. A spectrum for LT ($< 0.6T_m$) deformed n-type Ge is shown in Fig. 2.14 [71]. After annealing at 580 °C, the number of etch pits has not changed, while the DLTS peak has dropped by a factor of 10 in amplitude. This points to a reduction of the related deep levels, which, furthermore, behave as ordinary noninteracting point defects after anneal, that is, they follow exponential trap filling kinetics. The corresponding activation

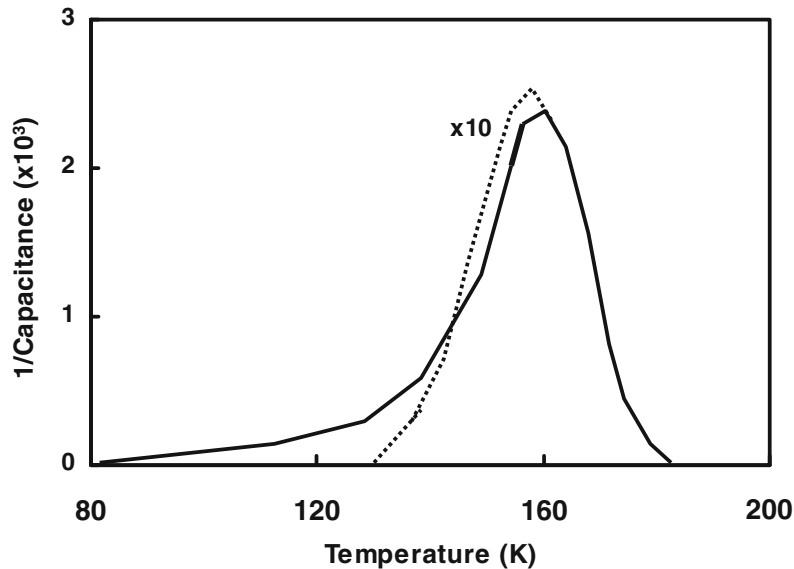


Fig. 2.14. DLT-spectrum as measured for n-type germanium, deformed at 420 °C (*solid line*). Annealing the deformed specimen at 580 °C ($=0.7 T_m$) for 70 min does not, within the limit of error, reduce the dislocation density, as measured by etch pit counting, while the amplitude of the DLTS line decreases about an order of magnitude (*dotted line*). Dislocation density $N_d = 1.5 \times 10^7$ cm⁻² (after [71])

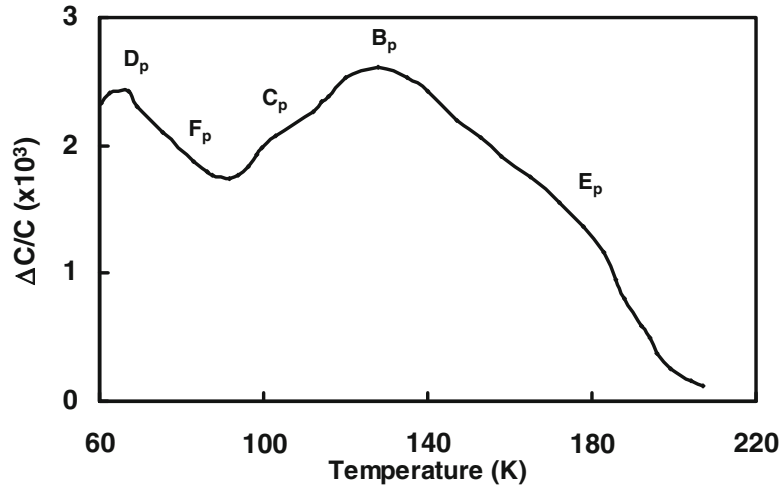


Fig. 2.15. Capacitance transient spectrum of the p-type Ge sample deformed at 580 °C. The lines B_p, C_p, and D_p had been observed at the spectrum of the sample deformed at lower temperature, while the defect responsible for line A_p is not observed in the material deformed at 580 °C. $N_d = 7.5 \times 10^7 \text{ cm}^{-2}$ (after [70])

enthalpy is 0.29 eV from the conduction band [71]. It was concluded that point defect clouds surround the dislocations formed during plastic deformation and that these anneal out at high temperatures.

In $T_{\text{def}} > 0.6T_m$ deformed p-type Ge, a dominant dislocation peak at an activation enthalpy of 0.08 eV, close to the Hall effect data of 0.09 eV, has been found by DLTS [70]. A typical spectrum is represented in Fig. 2.15 [70]. The extended-defect nature of the peak is identified by the logarithmic trap filling of the centers, in other words, the peak amplitude grows according to $\ln(1 + t_{\text{fill}}/\tau_C)$, with τ_C the capture time constant and t_{fill} the filling pulse duration. For $T_{\text{def}} < 0.6T_m$ additional point-defect like features become obvious in the spectra, at $E_V + 0.19 \text{ eV}$, $E_V + 0.27 \text{ eV}$, and $E_V + 0.39 \text{ eV}$ [70].

2.2.6 Electrical Activity of Grown-In Dislocations

Usually, rather large dislocation densities are required to study their electrical and optical properties. This explains why most investigations have been carried out on plastically deformed material. Besides a reasonable control of the dominant dislocation structure and type, it also allows to minimize point-defect – dislocation interactions during the heat treatment, when performed above $T_{\text{def}} = 0.6T_m$. There exists nevertheless some scientific and practical interest in the study of grown-in dislocations, in particular for high-purity (HP) germanium, utilized for the fabrication of nuclear-radiation detectors. It is known that a small density of dislocations ($100 < N_d < 10^4 \text{ cm}^{-2}$) is

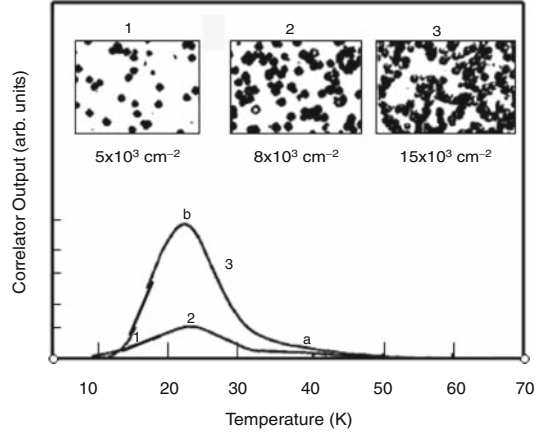


Fig. 2.16. Capacitive transient spectra of defect states associated with increasing dislocation density in a germanium crystal (grown in the [100] direction under 1 atm of H_2). Nearest neighbor distance between etch pits in picture 2 is $25\ \mu\text{m}$, in picture 3, $15\ \mu\text{m}$ (micrographs taken at $\times 50$). Below $\text{EPD} = 5 \times 10^3\ \text{cm}^{-2}$ no spectroscopic features could be seen. Activation energy of peak -b- is $E_V + 0.02\ \text{eV}$, half width ($k\Delta T$) is $0.95\ \text{meV}$. Half width of -a- is $\approx 2\ \text{meV}$. $N_A - N_D \sim 1 \times 10^{10}\ \text{cm}^{-3}$ (after [72])

required for obtaining a good detector resolution. Too high a density will cause carrier trapping and loss of resolution [72–74]. The fact is that the doping density in HP-Ge is low ($\sim 10^{10}\ \text{cm}^{-3}$) and using DLTS enabled the study of the deep levels associated with grown-in dislocations.

Typical results for p-type HP-Ge are illustrated in Fig. 2.16 [72], showing the presence of two broad bands of deep levels, increasing in peak amplitude with increasing etch pit density (EPD). A density of $\sim 10^4\ \text{cm}^{-2}$ is required to detect the deep levels in DLTS. The peak maximum position corresponds with an energy level at $E_V + 0.02\ \text{eV}$ and $E_V + 0.08\ \text{eV}$. The first band agrees quite well with the shallow dislocation states detected at $E_V + 0.02\ \text{eV}$ by Hall effect and ascribed to strain-states [68]. The second, smaller band corresponds with the well-known half-filled acceptor band at $E_V + 0.09\ \text{eV}$ [9, 10]. It was observed that the deeper band was higher for material, showing more lineage⁵ or clustering of dislocations.

Similar bands were obtained in [73], resulting in a peak position at $E_V + 0.035\ \text{eV}$ and $E_V + 0.08\ \text{eV}$. It was suggested that the band of shallow states was possibly related to screw dislocations. This is not in conflict with the association of the $E_V + 0.02\ \text{eV}$ states to the strain field surrounding dislocations. These levels are predominantly formed at low deformation temperatures, where mainly screws are introduced, characterized by a wide splitting [66, 68].

⁵ Lineage: any low angle grain boundary where the angle of misfit $< 1^\circ$.

The presence of these bands is sensitive to the crystal-growth atmosphere: N_2 -grown crystals exhibit much higher dislocation-related DLTS bands (deep level concentrations) than H_2 -grown material [72]. This suggests a passivation of the underlying defects (dangling bonds?) by hydrogen, as is also observed for other deep-level point defects in Ge, like metal-related deep acceptor states. The crystal growth orientation also plays a role, whereby $\{113\}$ p-type HP-Ge shows less hole trapping than $\{100\}$ [72].

DLT-spectra have also been obtained on n-type HP-Ge; a typical result is shown in Fig. 2.17 [73]. The peak maximum corresponds to an activation energy of $E_C - 0.1$ eV. It was also remarked that the peak width was 3–4 times higher than for a point-defect peak, suggesting a band of states close to the conduction band. They were associated with the strain field surrounding the dislocations [73]. An additional feature noted in Fig. 2.17 is the anomalous reduction of the steady-state capacitance with increasing temperature. This was thought to originate from the space charge cylinders surrounding the dislocations, leading to a junction capacitance of the form [73]

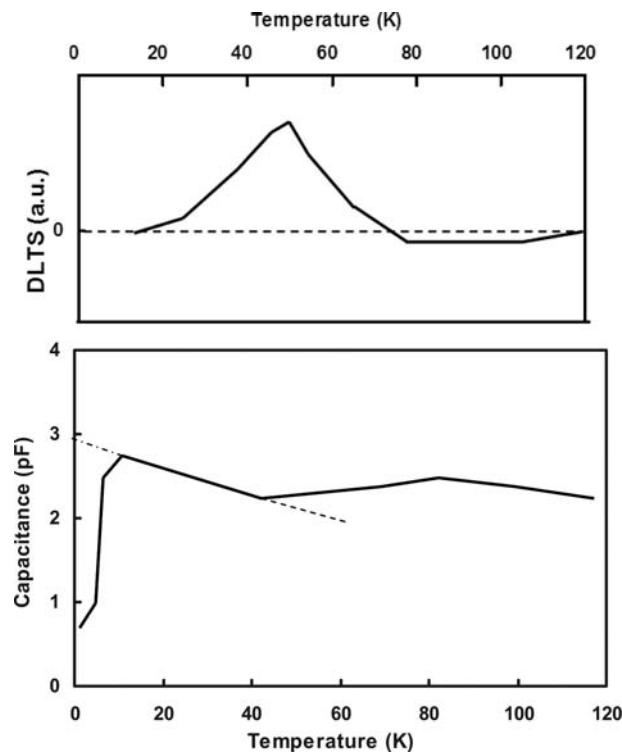


Fig. 2.17. (a) DLT-spectrum (rate window 6.16 ms) of an n-type Ge (Au)-barrier. Pulse from -4 to -2 V. (b) Corresponding C - T plot at a quiescent bias of -4 V. The *dashed line* indicates the linear drop of the capacitance with temperature (after [73])

$$C = C_0 \left[1 - \frac{N_d}{n} \frac{kT \epsilon_0 \epsilon_{\text{Ge}} \pi}{q^2} \right], \quad (2.13)$$

with C_0 the steady-state capacitance corresponding with a free carrier (doping) density n and $N_d = 0$ and normally constant (or slightly increasing) with T , for a dislocation-free substrate.

A more systematic study between grown-in dislocation type, identified by TEM, and DLTS levels was undertaken in [74]. The n-type 40 K level was shown correlated with the presence of [112] dislocations (pure edge and 30° type) – the correlation is shown in Fig. 2.18 [74]. From this, it is derived that an EPD of $5,000 \text{ cm}^{-2}$ corresponds with a DLTS peak concentration of 10^{10} cm^{-3} . N-type HP-Ge samples with predominant [100] edge (90°) dislocations exhibit a somewhat deeper DLTS band, peaking at 60 K and with an activation energy of 120 meV. These [100] dislocations occur mainly in the lineage or mosaic structure of [100]-grown n-type HP-Ge [74]. In p-type HP-Ge, the different types of dislocations could not be discriminated by DLTS: they all gave rise to the 20 K band at $E_V + 0.02 \text{ eV}$. There is, however, a correlation with the [112] type of edge and 30° dislocations [74]. The presence of mosaic or lineage (2D or 1D dislocation clustering) shifts the peak position towards slightly higher energies, in line with the observations of Hubbard and Haller [72]. Another interesting observation is that for the same EPD, the

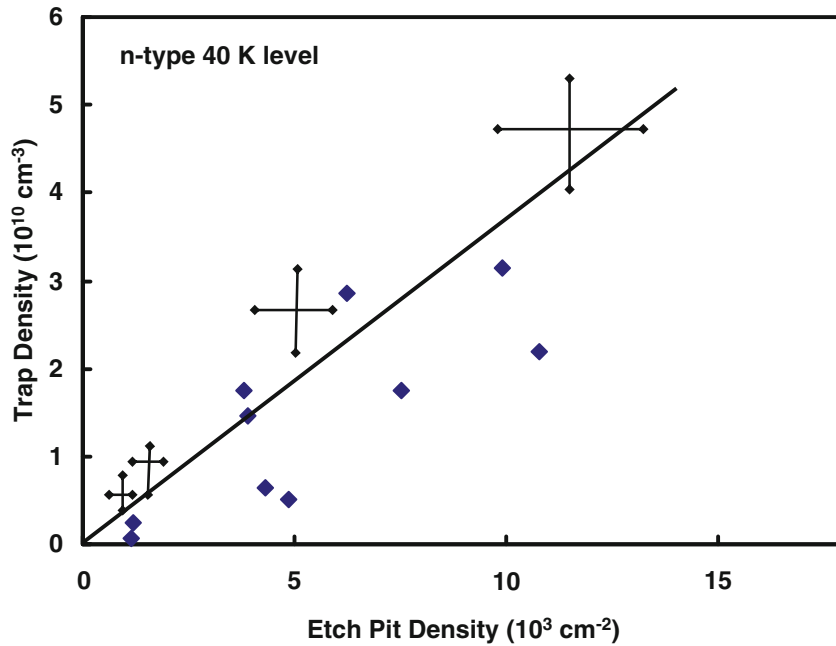


Fig. 2.18. Correlation between the etch pit density and the trap concentration of the 40 K level deduced from DLTS (after [74])

trap concentration derived from DLTS is five times lower in p- than in n-type HP-Ge. This indicates that the specifications for N_d are more stringent for n- compared with p-type material [74].

2.3 Impact of Dislocations on Carrier Mobility

Already in the earliest observations, it was realized that dislocations affect the mobility of carriers at low temperatures, where Coulombic scattering becomes important [3, 75, 76]. It was also demonstrated that the effect is anisotropic with respect to the dislocation orientation [75, 76]. Figure 2.19 shows the electron mobility vs. temperature for the direction parallel and perpendicular to the dislocations. A clear reduction is observed for current flow perpendicular to the dislocations [76]. A similar effect is observed for the hole drift velocity in deformed Ge as a function of the electric field in Fig. 2.20 [75]. This was confirmed by later experimental investigations [77–81].

Several calculations have been performed regarding scattering by charged dislocations and its impact on mobility [82–87]. In most cases, the results were interpreted in terms of Read's Space Charge Cylinder (SCC) model [83].

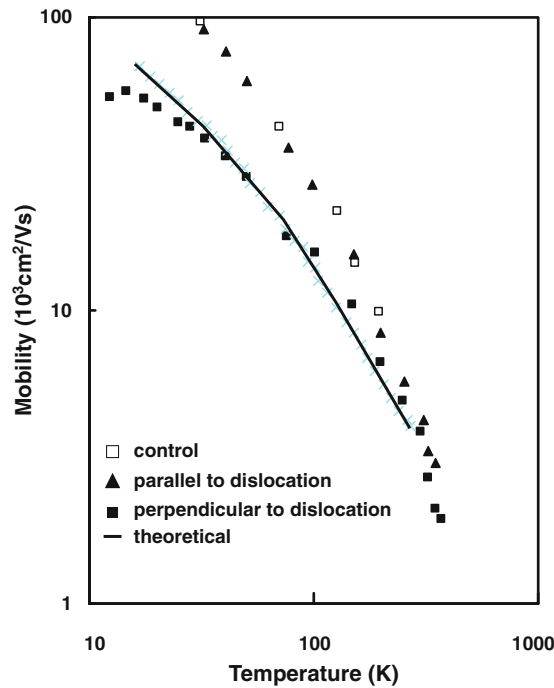


Fig. 2.19. Mobility as a function of temperature. *Solid line* is a theoretical curve (after [76])

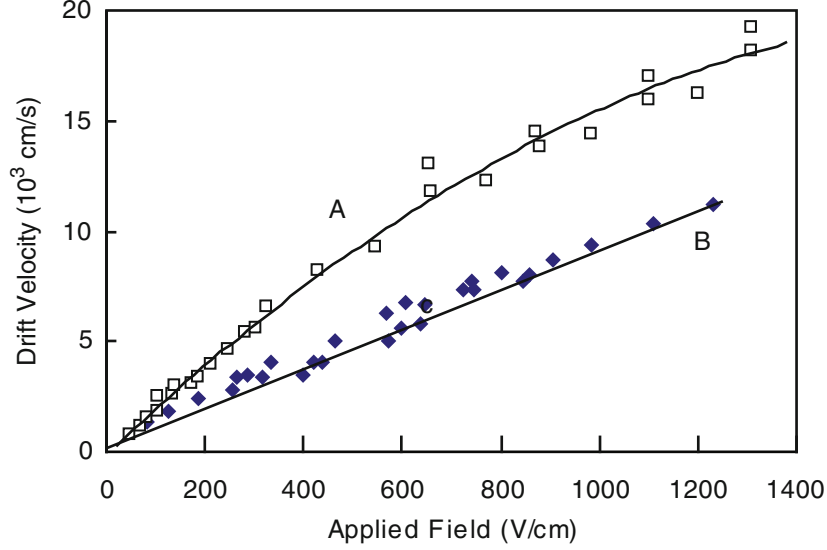


Fig. 2.20. Drift velocity of holes in dislocated n-type germanium as a function of applied electric field. *Curve A*: parallel to the dislocation array. *Curve B*: across the dislocation array (after [75])

The impact on the perpendicular mobility can be explained by considering two effects, namely, the increase in the average electric field E_{\perp} and the scattering at the charged dislocations [76]. Some corrections to the original concept have been introduced by Broudy [17], who took into account that the SCC has not a sharp boundary, so that scattering in the parallel direction occurs as well. A further refinement considers the high-density saturation effect, when the SCCs start to overlap [80, 81].

The next step was to reinterpret the mobility data in terms of the half-filled band model [88]. As shown in Fig. 2.21, the mobility in deformed Ge exhibits a maximum at low temperatures, which is not observed for reference undeformed material [88]. It has been demonstrated that the mobility maximum corresponds with neutral dislocations, where $f_{ed} = 0$ and $E_F = E_0$. A neutral dislocation only scatters through its elastic strain field [88]. Furthermore, μ follows the charging of the dislocations (or f_{ed}). Assuming spherical energy surfaces, one can calculate that the mobility due to scattering at dislocations is given by [88]

$$\mu_{de} = \frac{A}{A_0} \frac{T^{3/2}}{N_d f_{ed}^2 \lambda}, \quad (2.14)$$

with λ the appropriate screening length, that is, the SCC radius of (2.2) when $kT \ll q\Phi$ or the Debye screening length. A is a constant, which is 1,430 according to Kuznetsova [85] or 590 following Pödör [77] and $A_0 = 1 \text{ cm V}^{-1} \text{ s}^{-1} \text{ K}^{-3/2}$. A similar result was obtained for material containing

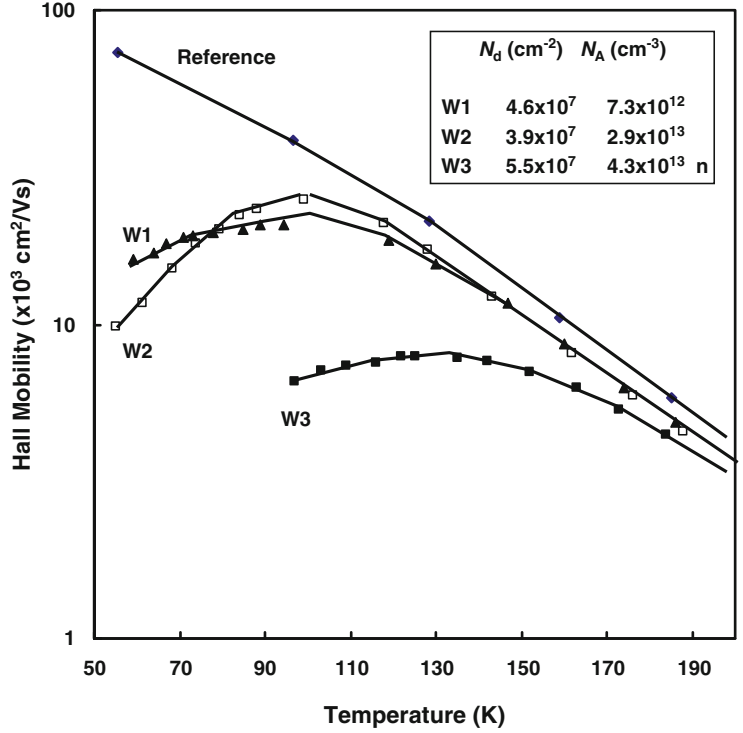


Fig. 2.21. Temperature dependence of the Hall mobility for samples with the same dislocation density but with different doping. For low temperature, one can notice the impact of the dislocation charge qf_{ed}/b (after [88])

mainly screw dislocations [31]. It was noticed there that the anisotropy of the mobility was larger in n- than in p-type samples, suggesting a larger electron than hole occupation.

Later results on deformed p-type Ge indicated an exponential temperature dependence $\mu \sim \exp(-B/kT)$ [89] for $T < 80$ K, due to hole scattering by dislocations in the region of the donor action ($f_{ed} < 0$). This could be explained by the exponential temperature dependence of the number of scattering centers on the dislocations.

Overall, in bulk Ge it is accepted that both the carrier mobility and diffusivity are relatively insensitive to dislocation scattering up to a density of 10^8 cm⁻² [90]. However, more recent concerns focus on the impact of threading dislocations (TDs) in thin heteroepitaxial layers⁶ on the carrier transport properties [90,91]. In that case, the mobility due to dislocations can be modeled as [91]

⁶ Usually deposited on Si(100) substrates, see Chapter 4 for more details.

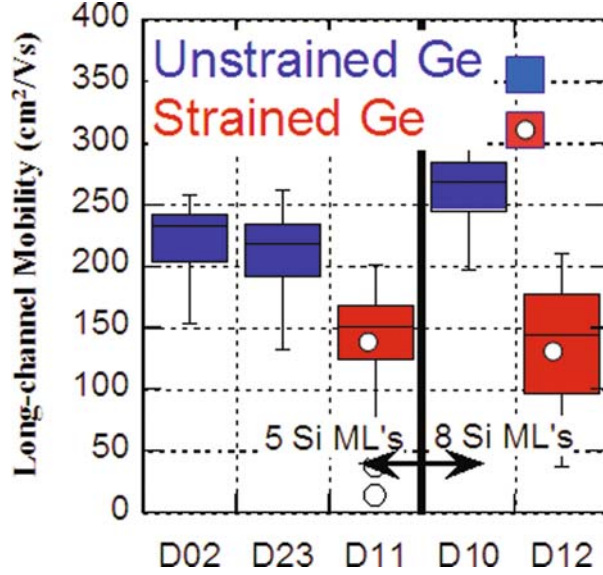


Fig. 2.22. Hole mobility extracted from long-channel pMOSFETs fabricated in unstrained 2 μm Ge-on-Si epitaxial layers (device D02, D23, and D10), with a TD density of $\sim 10^8 \text{ cm}^{-2}$, compared with μ_h for transistors fabricated in 20 nm strained-Ge-on-Si substrates (device D11 and D12), employing a thin $\text{Si}_{0.2}\text{Ge}_{0.8}$ relaxed buffer layer, with a TDD of $2.5 \times 10^{10} \text{ cm}^{-2}$. The TDD has been determined by defect etching and SEM inspection. The interface of the transistors was passivated by a few mono-layers (MLs) of epitaxial silicon (see Chap. 4) (after [92])

$$\mu_{\text{TD}} = \frac{q}{4\hbar L_{2\text{D}}} \sqrt{\frac{g_v g_s}{\pi n}} \frac{1}{N_{\text{TD}}}, \quad (2.15)$$

with \hbar the reduced Planck constant, N_{TD} the TD density, g_v the valley degeneracy, and g_s the spin degeneracy. Finally, $L_{2\text{D}}$ is the two-dimensional Debye screening length, given by

$$L_{2\text{D}} = \frac{q^2 n}{2\varepsilon_0 \varepsilon_{\text{Ge}}} \Delta E, \quad (2.16)$$

which is on the order of 0.3 μm [91], with ΔE the TD energy level. In practice, it has been observed that the inversion layer hole mobility in pMOSFETs fabricated in a thin Ge epitaxial layer on a (100) Si substrate is deteriorated for TD densities in the range $\sim 10^{10} \text{ cm}^{-2}$, while little effect is found for densities below 10^8 cm^{-2} , as illustrated by Fig. 2.22 [92].

2.4 Impact of Dislocations on Lifetime, Trapping, and Noise

This section is discussing the impact of dislocations on electrical device performance parameters such as minority carrier lifetime, charge trapping, and low frequency noise.

2.4.1 Impact on Carrier Recombination

Dislocations were shown to reduce the carrier lifetime in plastically deformed [1,93], heat treated and quenched [94] and as-grown germanium crystals with a high dislocation density [5,95–104]. Assuming simple Shockley–Read–Hall (SRH) statistics to be applicable, one arrives at the following formula for the bulk lifetime due to dislocations [95]:

$$\tau_d = 1/v_{th}\sigma_d\rho N_d, \quad (2.17)$$

with v_{th} the thermal velocity, ρ the density of active recombination centers (dangling bonds) on a dislocation line (cm^{-1}), and σ_d the capture cross section. Along the same lines, one obtains for the surface recombination velocity along a lineage grain boundary [95]

$$S_d = v_{th}\sigma_d\rho N_s. \quad (2.18)$$

In (2.18), N_s is the density of lineage boundary dislocations per centimeter. Assuming a $\rho = 6 \times 10^5 \text{ cm}^{-1}$, one arrives at a $\sigma_d = 4 \times 10^{-14} \text{ cm}^2$ at 300 K [95].

The factor $1/v_{th}\sigma_d\rho$ has also been termed the recombination activity of a dislocation and follows immediately from the measured τ_d vs. N_d characteristic. In agreement with (2.17), a hyperbolic relationship is typically found, as shown in Fig. 2.23 [96]. From this, an activity of $5.5 \times 10^{-4} \text{ cm}^{-1} \text{ s}^{-1}$ in high-resistivity and $3.5 \times 10^{-3} \text{ cm}^{-1} \text{ s}^{-1}$ in low-resistivity Ge has been derived [96]. It was also demonstrated that the recombination activity per dislocation depends on the crystal growth rate (Fig. 2.24) [97]. The density of grown-in dislocations increases with growth rate, yielding a more or less linear reduction of the lifetime of the material [97]. At the same time, the grown-in N_d depends on the crystal growth orientation, with the highest density for $\langle 111 \rangle$, followed by $\langle 100 \rangle$, and finally $\langle 211 \rangle$ [97]. With increasing growth rate, each dislocation becomes a less efficient recombination center. This was ascribed to the fact that during fast growth, less impurity atoms could reach the dislocation core to form a Cottrell atmosphere and associated SRH recombination centers [96,97].

The impact of the growth rate on lifetime in Ge crystals is once more illustrated in Fig. 2.25 [100]. A maximum lifetime is found for an $N_d \sim 10^3 \text{ cm}^{-2}$. Below that value, τ_d is determined by fast diffusing point defects (copper, nickel, etc.). For sufficiently high dislocation densities, these impurities condensate on the dislocations. For a higher growth rate, fast diffusing impurities

have less time to enter the crystal and to reduce the lifetime. This leads to a higher maximum τ_d for a smaller N_d [100]. It was proposed that the condensation of vacancies on the dislocation lines could explain the reduction of τ_d from 2 to 0.9 ms in Fig. 2.25 [100]. This is in line with the fact that for good HP-Ge detector material, a density of $\sim 10^3 \text{ cm}^{-2}$ dislocations is required to avoid the presence of vacancy-cluster-related trapping centers in the bulk of the crystal [72, 74]. On the other hand, dislocation-free HP-Ge suffers from trapping by vacancy-related point defect complexes.

Based on the data of Fig. 2.25, a hole cross section of $1.1 \times 10^{-14} \text{ cm}^2$ (300 K) was derived, slightly lower than Okada's value [95]. For deformed material (bent samples), a hole $\sigma_d \sim 3.6 \times 10^{-14} \text{ cm}^2$ was obtained, illustrating the importance of considering the impurity-dislocation interaction with respect to carrier lifetime [100]. This rather large capture cross section value(s) for holes – even larger than that for Cu_s at 300 K – was ascribed to the impact of the space charge region around the dislocations [100]. Finally, it was observed that the dislocation density impacts on the surface recombination velocity of germanium [100].

A summary of the early results on lifetime vs. dislocation density in n- and p-type Ge is given in Fig. 2.26 [93]. The following empirical relationship was derived for the lifetime in plastically deformed Ge [93]:

$$\tau_n = 0.7/N_d \text{ (p - Ge) ,} \quad (2.19a)$$

$$\tau_p = 2.5/N_d \text{ (n - Ge) .} \quad (2.19b)$$

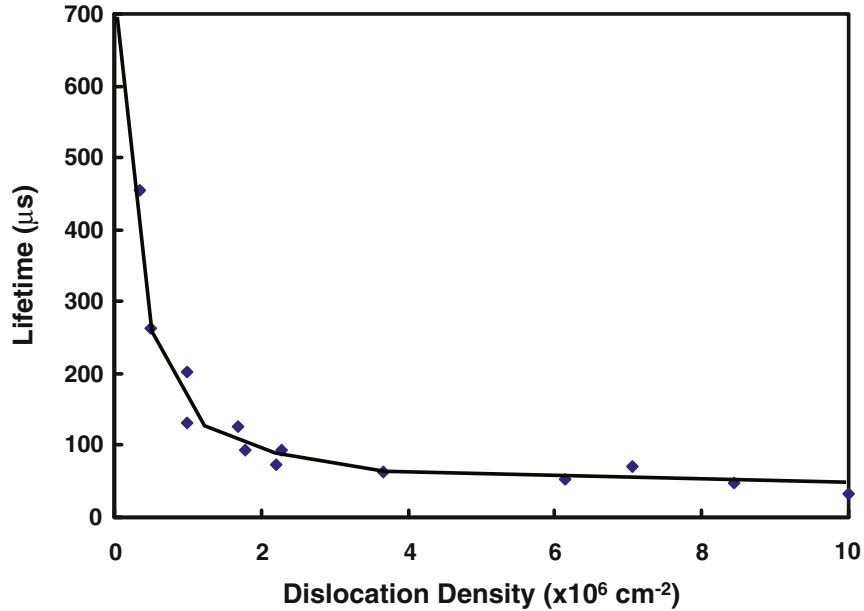


Fig. 2.23. Lifetime vs. dislocation density for high-resistivity germanium (after [96])

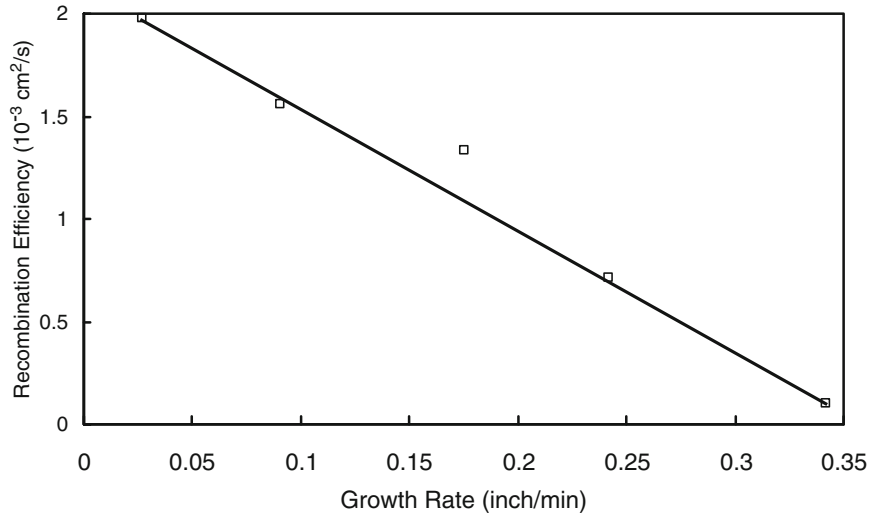


Fig. 2.24. Recombination efficiency per unit length of dislocation vs. growth rate (after [97])

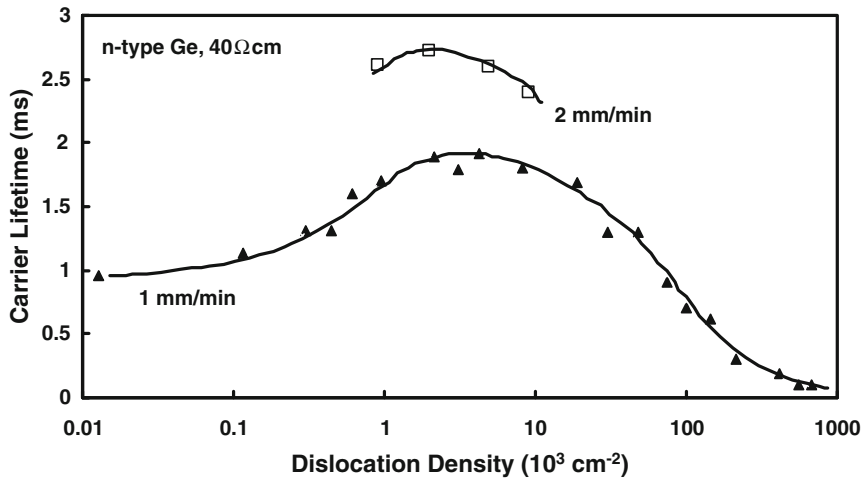


Fig. 2.25. Effect of edge dislocation density on carrier lifetime in n-type, 40 $\Omega \text{ cm}$ Ge crystals produced at different growth rates: 1 mm min^{-1} (filled triangles) and 2 mm min^{-1} (open squares) (after [100])

It is clear that recombination through dislocations happens faster in p-type germanium than in n-type, whereby hole capture is the faster of the two processes, due to the electron charge on the dislocations. Note that the dislocation activity in deformed material appears to be significantly larger than that for the as-grown case (see Fig. 2.24). One factor to take into account is

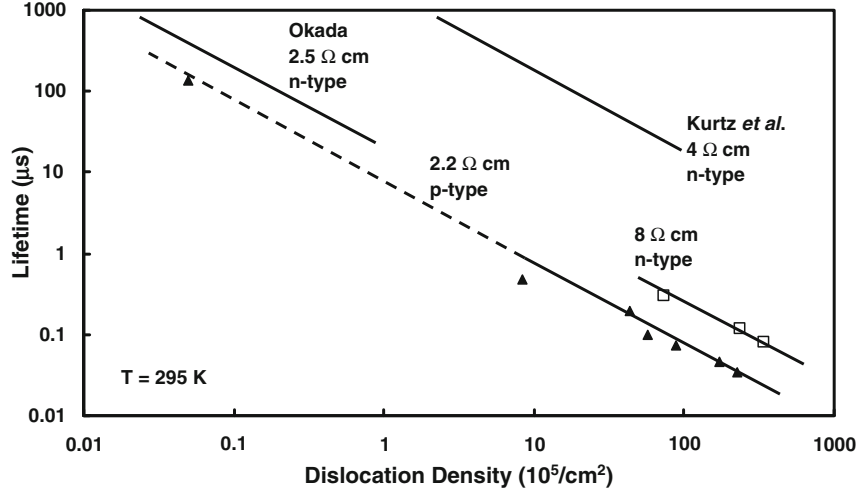


Fig. 2.26. Room-temperature lifetime in germanium with different dislocation densities (after [93])

the accuracy of the value of N_d , which largely depends on the used measurement technique. However, also for as-grown dislocations in p-Ge, an increase of the activity from $0.17 \text{ cm}^2 \text{ s}^{-1}$ at 300 K to $5 \text{ cm}^2 \text{ s}^{-1}$ at 125 K was observed for $7.7 \Omega \text{ cm}$ material [104]. This value increases to $0.33 \text{ cm}^2 \text{ s}^{-1}$ for $1.8 \Omega \text{ cm}$ p-Ge (300 K). In lineage (small angle grain) boundaries, a dislocation activity of $4.14 \text{ cm}^2 \text{ s}^{-1}$ (n-) and $1.22 \text{ cm}^2 \text{ s}^{-1}$ was obtained, corresponding with a capture radius of 0.115 nm (holes in n-type) and 0.28 nm (electrons in p-type) [101].

It was also observed that the lifetime in bent p-type samples increased with temperature, as shown in Fig. 2.27 [93], following a $T^{2.5}$ power law below room temperature. A similar dependency was found by Iglitsyn and Kolesnik [101]. Above room temperature, τ_d in Fig. 2.27 is thermally activated, with activation energy about half the band gap of Ge [93]. The capture radius of a dislocation, equal to $3.54 \times 10^{-8} \text{ cm}$ at room temperature for p-Ge, could be described by [93]

$$R_c = 3.4 \times 10^{-8} (300/T)^3 (\text{p-Ge}). \quad (2.20)$$

For n-type Ge, interpretation of the data was complicated by the presence of the SCC and could not be explained in terms of a simple SRH-like model [93].

It has also been observed that the carrier diffusion length in crystals with parallel arrays of edge dislocations is anisotropic [105]. This is illustrated in Fig. 2.28 [105], showing that the diffusion length is much smaller across the dislocations than parallel with it. Moreover, a stronger electron trapping effect was found during the photoconductivity measurements [105]. Assuming uniform carrier diffusivity, the anisotropy in diffusion length has been ascribed to anisotropy in the carrier recombination lifetime, which is, therefore, no longer a scalar but a tensor in dislocated Ge [105]. It was later demonstrated

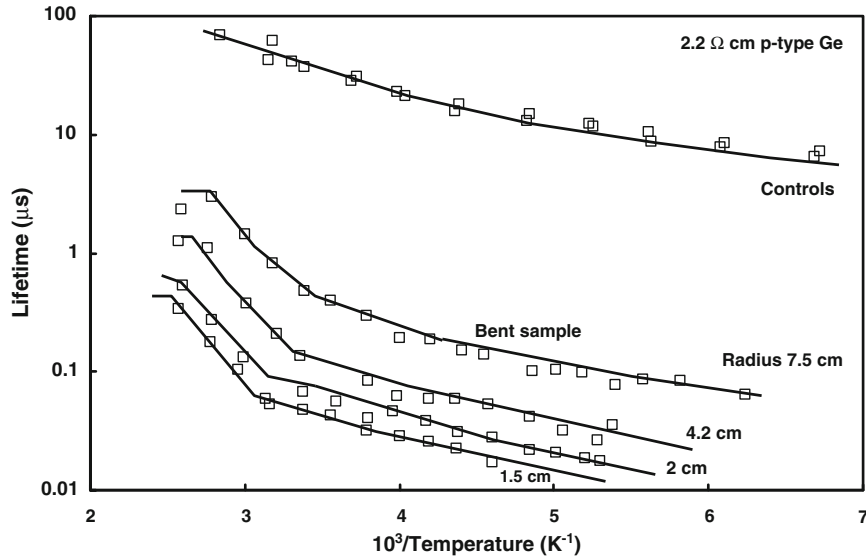


Fig. 2.27. Temperature dependence of lifetime in plastically deformed p-type germanium (after [93])

that D is isotropic in dislocated p-Ge, so that all diffusion length anisotropy is indeed in the lifetime [75]. In n-type Ge, on the other hand, both D and τ_d are anisotropic [75].

The fact that the parallel lifetime is higher is explained by the presence of the SCC, which forms a barrier for the penetration of the carriers. It was also found that dislocations ending at the surface enhance the surface recombination velocity by introducing surface states [105].

Regarding the origin of the recombination lifetime activity of dislocations in Ge, this was originally interpreted in terms of the electrical activity of impurity atoms condensed in a Cottrell atmosphere around the dislocations [96, 97, 106]. Three effects were considered in the early work. First, because of the strain field surrounding the dislocations, one can expect a narrowing of the band gap, which should facilitate carrier recombination. The presence of an impurity atmosphere will further facilitate recombination events. Finally, the possible role of dangling bond acceptor states was also acknowledged.

Subsequently, the interest of theorists focused on the effect of dangling bonds on carrier recombination [107, 108]. Attempts have also been made to model the capture cross section of a dislocation, accounting among other for the contribution of electron tunneling through the potential barrier of the space charge cylinder [109, 110]. A stronger temperature dependence for hole capture by a negatively charged dislocation in n-type Ge was calculated than for the case of a point defect [110].

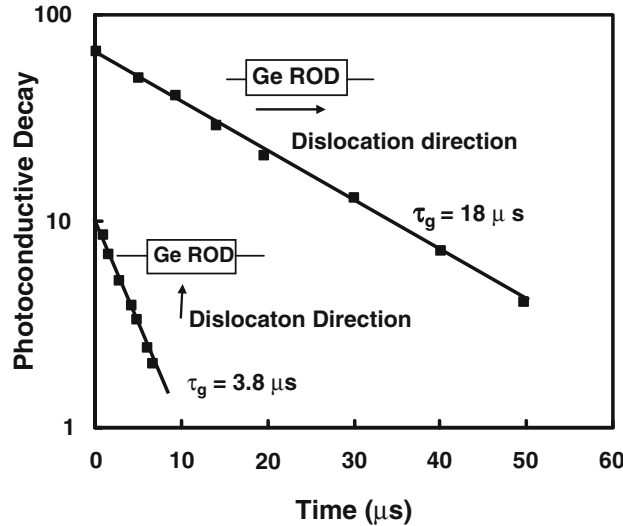


Fig. 2.28. The decay of photoconducance for two grown dislocated germanium specimens (after [105])

A better understanding of carrier recombination through dislocation states should consider the whole band scheme and not only the primary half-filled band, accessible by Hall effect measurements in equilibrium [111]. This has become obvious from the results of optical recombination studies, where the action of at least two bands, 0.5 eV apart, was demonstrated (see Sect. 2.6). Schröter has derived a recombination model, assuming that the transitions within one band were much faster (equilibrium fast established) compared with the interband transitions. He came to the picture represented schematically in Fig. 2.29 [111]. Basic features of the model are the following:

- The electron capture occurs via tunnel states at the dislocation (c-d) [109]
- The hole capture takes place in two steps: a first transition leads to bound hole states at the negatively charged dislocation (h-v) and is followed by a second transition from the hole band to one of the other dislocation bands (d-h)

This model enables to explain the observed temperature dependence of the lifetime and at the same time incorporates all features that have been deduced from electrical (and optical) measurements.

It was finally pointed out by Shikin et al. [112] that the capture/emission of a trapped electron through the Coulomb barrier is also strongly affected by the strain field. This is related to the fact that the deformation potential (which is not cylindrically symmetric) will determine the saddle point of the total electron potential.

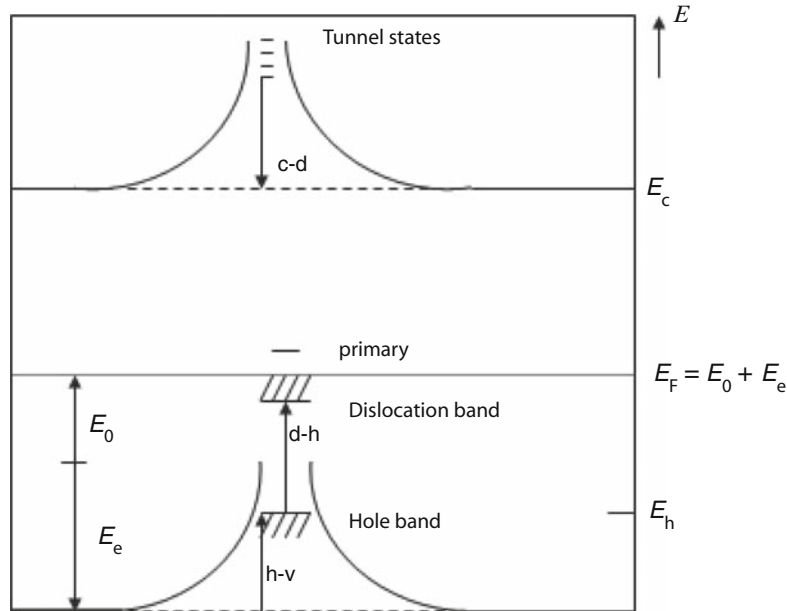


Fig. 2.29. Band scheme at a dislocation (after [111])

The recombination activity of dislocations has also been investigated by the electron beam induced current (EBIC) technique [113]. For EBIC, the electrons generated by a beam with a few kiloelectron volt energy are collected by a reverse-biased junction (or Schottky barrier). Regions with a high recombination activity usually show up as dark spots (contrast regions) in the SEM image and vice versa. From the analysis of the contrast, an estimate of the local diffusion length can be made with a resolution of $\sim 1 \mu\text{m}$ typically. Dislocations in Ge have been imaged in the normal EBIC mode but when a special sample configuration is used, with an array of dislocations connecting top and bottom of the sample, a different type of mechanism comes into play [113]. It has been shown that besides acting as a recombination site, dislocations can also collect electrons in their core and conduct them to the back-side of the sample. Using the back-side current, an image with opposite contrast is obtained where the dislocation cores show up as bright regions. This has been interpreted as additional proof for the one-dimensional conductivity of dislocations in germanium. In fact, the normal recombination mechanism is in competition with the collection/conduction mechanism and the ratio of the two will determine the nature of the contrast [113].

2.4.2 Impact on Low Frequency Noise

Dislocations enhance the $1/f$ noise in semiconductors [114–116]: as an illustration, the excess noise in a plastically deformed Ge sample is given in

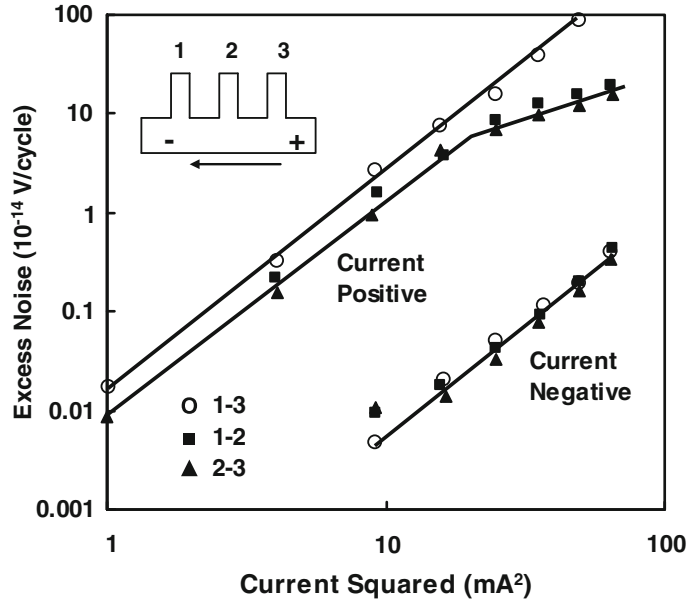


Fig. 2.30. Excess noise levels observed in plastically deformed Ge single crystal at 20 Hz (after [115])

Fig. 2.30 [115]. An unusual aspect is that the dislocation-related $1/f$ noise follows an I^4 power law instead of the expected I^2 dependence. Models have been proposed, which consider trapping in the space charge barrier [114] or diffusion of impurity atoms along the dislocation line [116]. The origin of the carrier transport fluctuations should probably be reinterpreted in terms of a 1D band model.

Generation-recombination noise spectra have also been studied in undeformed Ge and ascribed to grown-in dislocations [117]. The generation-recombination time constants and photoconductive decay lifetimes were interpreted in terms of a SRH model, yielding a dislocation level at $E_C - 0.15$ eV.

2.5 Impact of Dislocations on Ge Junction Devices

A few studies have been devoted to the impact of dislocations on the leakage (or generation) current of a Schottky barrier [30] or p-n junction [118–120]. It has been shown that the reverse current of a Schottky barrier on plastically deformed Ge contains different components, which relate to the depletion (generation) width, to surface generation along the perimeter of the barrier, and an ohmic component that could be associated with conduction along the dislocation core and becomes important below 180 K [30]. The generation current has been interpreted in terms of Schröter's carrier recombination

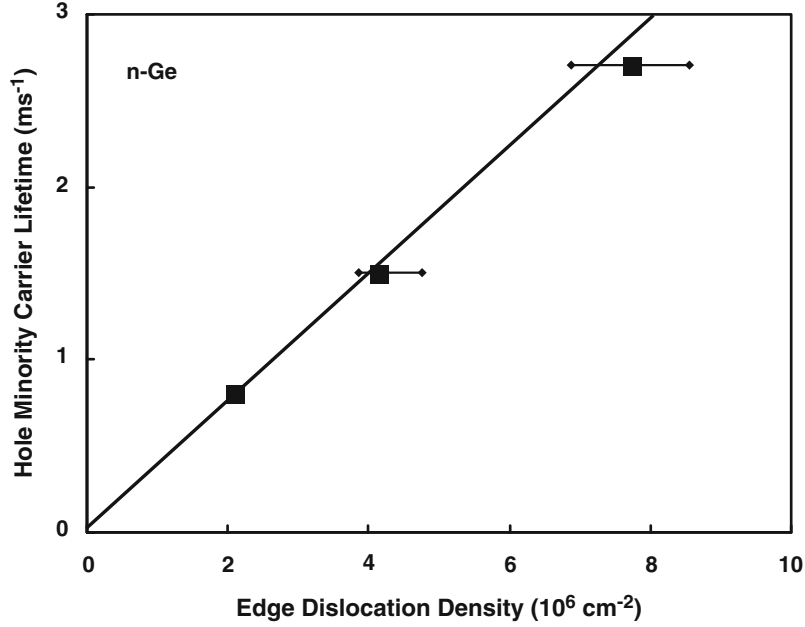


Fig. 2.31. Inverse of the hole minority carrier lifetime (τ_{p0}) vs. dislocation density of a set of deformed n-type Ge samples, derived from the reverse current of an Au Schottky barrier (after [30])

model [111]. Based on this analysis, the hole minority carrier lifetime of Fig. 2.31 was obtained in function of the edge dislocation density [30]. The corresponding capture rate and capture rate per dangling bond are

$$c_{p0} = 1.4 \times 10^{-11} \text{ cm}^{-3} \text{ s}^{-1} \quad \text{and} \quad \chi_{p0} = 3.7 \times 10^{-4} \text{ cm}^2 \text{ s}^{-1}. \quad (2.21)$$

These values are much smaller than the ones derived from lifetime measurements and Read's model for the dislocation states (see Sect. 2.3).

Earlier, some work has been performed on Ge p-n junctions containing dislocations created by plastic deformation [118]. Similar as in silicon, it was found that dislocations cause microplasma breakdown at sufficiently large reverse bias, giving rise to a soft reverse characteristic [118, 119]. It can be derived from Fig. 2.32 that the leakage current increases for increasing deformation or strain ε . To obtain good I - V characteristics it was concluded that the dislocation density crossing the junction should be well below $5 \times 10^6 \text{ cm}^{-2}$ [118]. The results were at that time interpreted in terms of the effect on the ideal diffusion current (lifetime). Using a lifetime value of $\tau_n = 2.07/N_d$ and $\tau_p = 0.61/N_d$, one can calculate the effect of dislocations on the diffusion current as shown in Fig. 2.33. From this, it was concluded that the effect is not high [118].

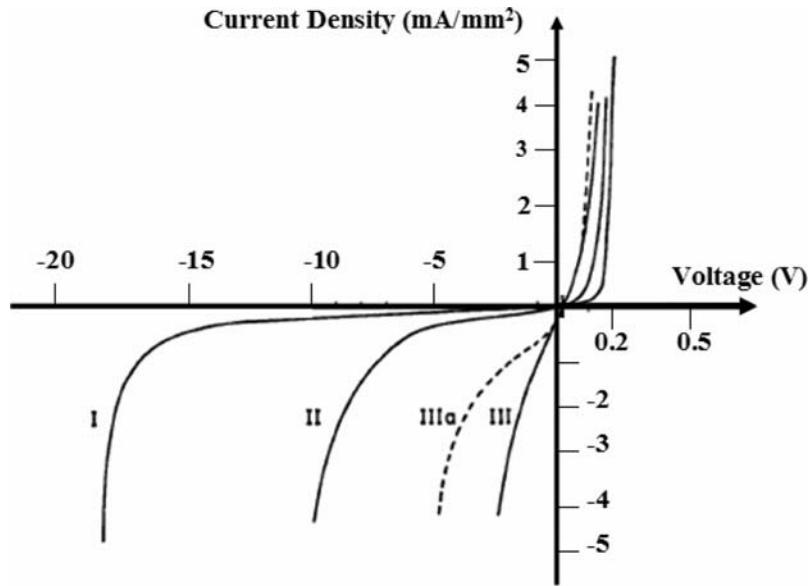


Fig. 2.32. Dependence of the I - V characteristic of a Ge p-n junction on the deformation. $\varepsilon_I = 2.9\%$, $\varepsilon_{II} = 10\%$, and $\varepsilon_{III} = 21\%$. Annealing for 105 min at 900°C transforms curve III into IIIa. Doping density: $N_A = 5 \times 10^{17}\text{ cm}^{-3}$, $N_D = 10^{17}\text{ cm}^{-3}$ (after [118])

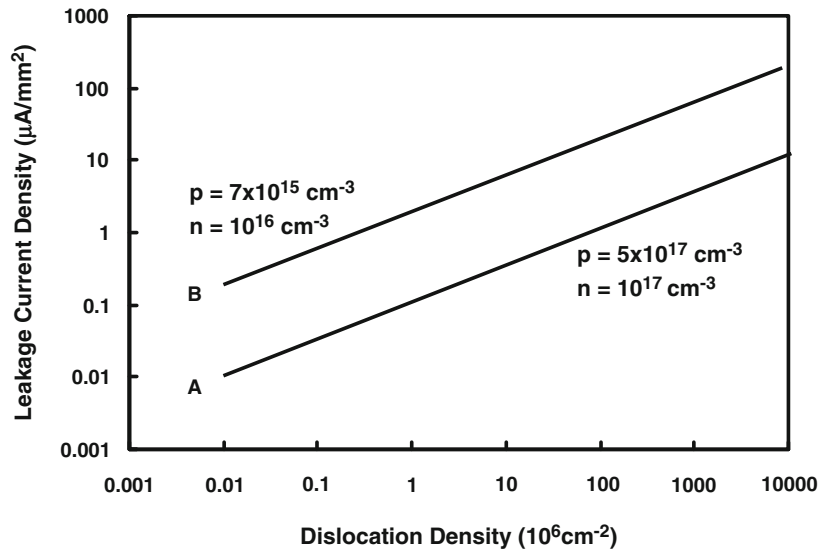


Fig. 2.33. Calculated leakage current density as a function of the dislocation density for $N_A = 5 \times 10^{17}\text{ cm}^{-3}$, $n = 10^{17}\text{ cm}^{-3}$ (curve A), and $N_A = 7 \times 10^{15}\text{ cm}^{-3}$, $n = 10^{16}\text{ cm}^{-3}$ (curve B) (after [118])

A more detailed study of the leakage current in deformed (twisted) Ge p-n junctions was carried out by Ryuzan [120]. There, a clear increase of both the forward recombination and the reverse generation current was observed, pointing to the existence of dislocation-related GR centers in the depletion region of the diode. The reverse current was found to increase with the amount of plastic deformation and with the twist angle θ_t [120]. Moreover, the generation current appears to be thermally activated with activation energy in the range of 0.35–0.43 eV, as indicated in Fig. 2.34 [120]. The increase of the recombination current with twist angle is represented in Fig. 2.35, showing a higher slope for the $\langle 100 \rangle$ twist axis compared with $\langle 111 \rangle$ [120]. It was found to obey the relationship

$$J_{\text{rg}} = \frac{\pi}{2} \frac{qn_i W_d}{V_{\text{bi}} \sqrt{\tau_{\text{p0}} \tau_{\text{n0}}}} V \quad (2.22)$$

for very small bias ($|V| < kT/q$). In (2.22), W_d is the depletion region width, V_{bi} is the built-in potential of the p-n junction and τ_{p0} , τ_{n0} is the minority carrier lifetime in the n-, respectively, p-side of the junction. The increase of the depletion region GR current upon plastic deformation will thus mainly come from a reduction of τ_{p0} and τ_{n0} . As will be seen later (see Sect. 2.6), the activation energy of 0.43 eV agrees quite well with data coming from photoconductivity experiments on deformed material [59]. The dependence of the reverse current at 1 V on twist angle is given in Fig. 2.36, showing an exponential variation, in agreement with the SRH theory for p-n junctions [120]. In other words, plastic deformation induces a number of point-defect-like GR centers in the depletion region. A similar conclusion was later reached for Schottky barriers on deformed material [29].

In lowly doped p-n junctions with a large transition region, negative differential resistance (NDR) behavior was observed in forward direction, as shown in Fig. 2.37a [120]. This points to the presence of a p-n-p-n structure induced by the space charge cylinders around the charged dislocations and schematically represented in Fig. 2.37b.

As mentioned earlier, high-purity Ge radiation detectors, which are basically large p-n junction structures that operate under full depletion voltage require a minimum dislocation density for good performance [72–74]. However, as shown in Fig. 2.38, above a dislocation density $\sim 10^4 \text{ cm}^{-2}$, the detector resolution expressed as full width at half maximum (FWHM) is deteriorated [121, 122]. This results from (electron) trapping, leading to incomplete charge collection and asymmetric detector peaks, with a tail towards low energies. Using exposure to collimated high-energy electrons demonstrates that the poor resolution regions correspond with the high dislocation density parts of the detector (e.g., lineage, cross-hatch, mosaic, etc) [121].

It was observed that p-type $\langle 113 \rangle$ HP-Ge material shows good performance for $N_d > 10^4 \text{ cm}^{-2}$. It could point to a different type of dominant dislocations (screws?) than in $\langle 100 \rangle$ Ge crystals with a lower activity. It was also noticed that the detector peak tailing only occurred when the p^+ -contact

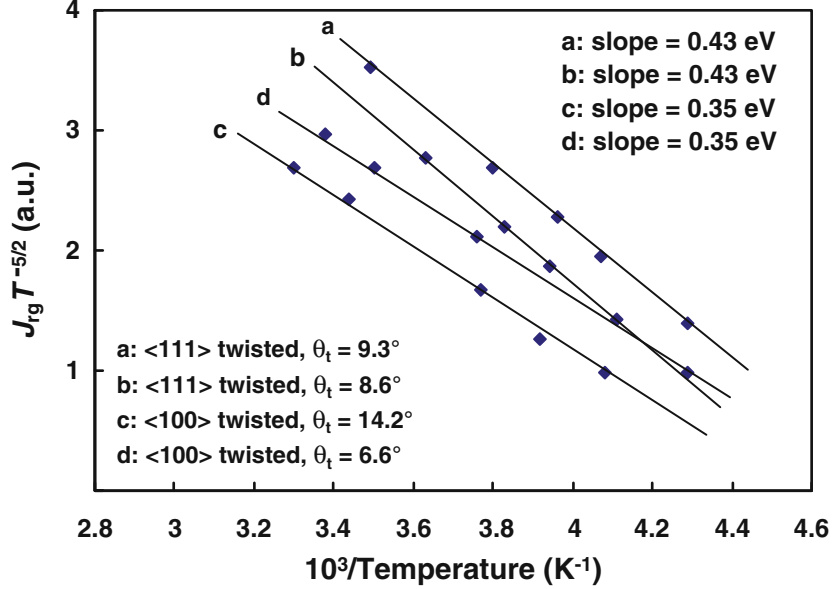


Fig. 2.34. Variation of reverse current at 2 V bias with temperature. $J_{rg}T^{-5/2}$ is plotted against T^{-1} for the $\langle 111 \rangle$ and the $\langle 100 \rangle$ twisted samples (after [120])

is scanned with the e-beam, pointing to electron trapping as the major cause, since the anode collects the electrons in the reverse-biased diode. Similar as in deformed material, Hall measurements showed the presence of a distribution of dislocation-related acceptor states with mean energy at 0.08 eV above the valence band [122].

In so-called Esaki-diodes, with a high doping density on either side of the junction, no effect has been observed by bending-induced dislocations with a density of 10^7 cm^{-2} [123].

Finally, anomalous I - V characteristics have been obtained for point-contact diodes on germanium [124]. This has been ascribed to the intersection of a dislocation with the surface.

2.6 Impact of Dislocations on Optical Properties

Because of the existence of dislocation states in the band gap of Ge, it is expected that these will affect the optical properties (absorption, photoconductivity, optical recombination, (photo-)luminescence, etc.) of the material. Moreover, using optical spectroscopy, one can obtain complementary information on the dislocation band structure. The advantage compared with Hall effect measurements is that all states are accessible at the same time, while

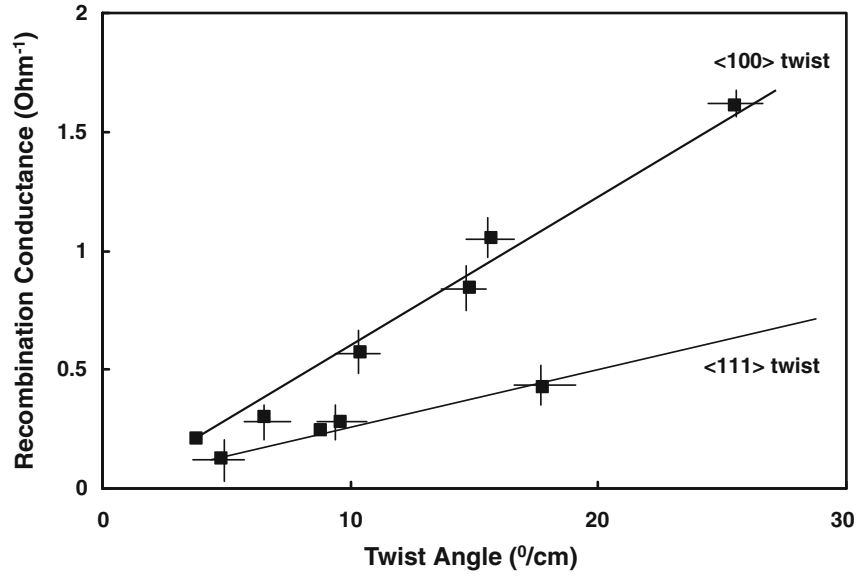


Fig. 2.35. Recombination conductance vs. twist angle (after [120])

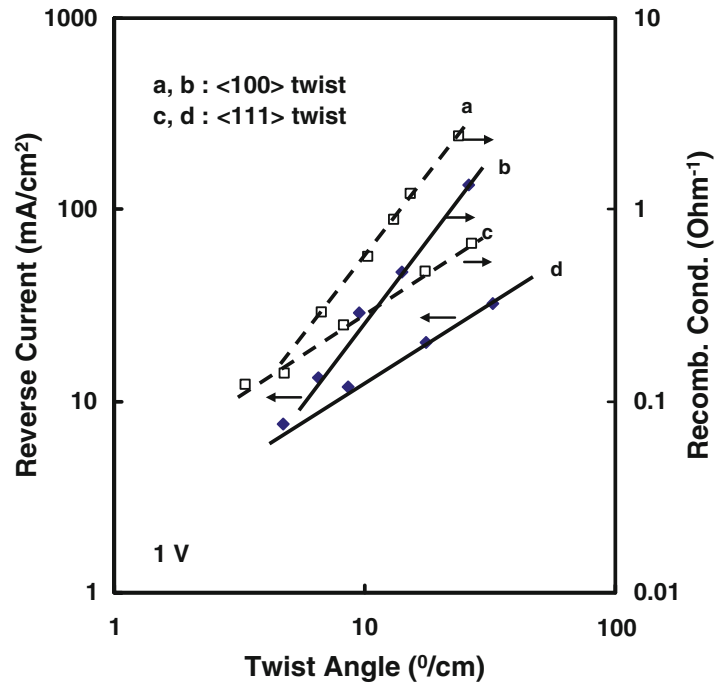


Fig. 2.36. Reverse current (*left*) at 1 V bias and recombination conductance (*right*) vs. twist angle (after [120])

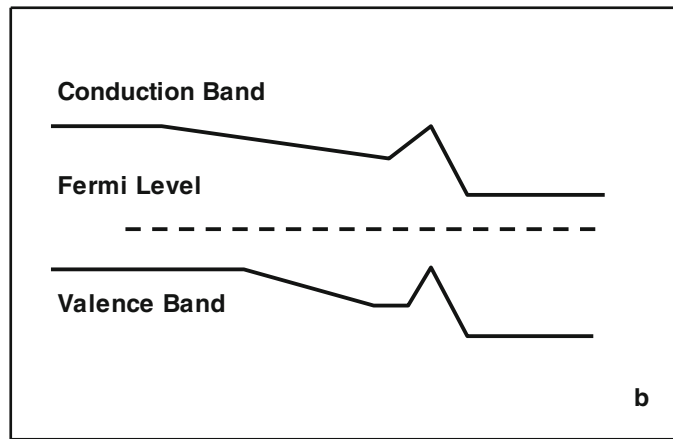
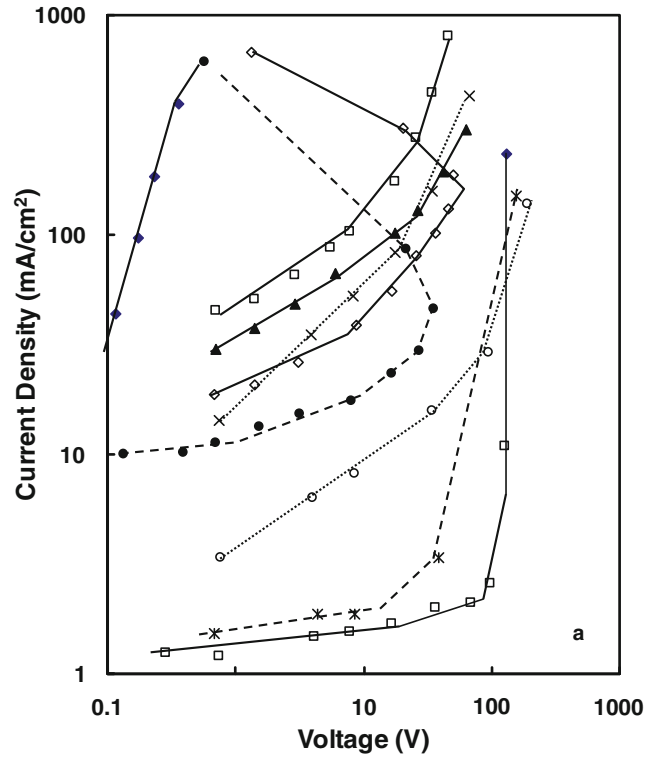


Fig. 2.37. (a) Current–voltage characteristics of the $\langle 111 \rangle$ twisted sample with twist angle as a parameter. (b) A probable energy band structure of the twisted samples, which have the anomalous characteristics in forward direction. The variations in local energy band are smoothed out (after [120])

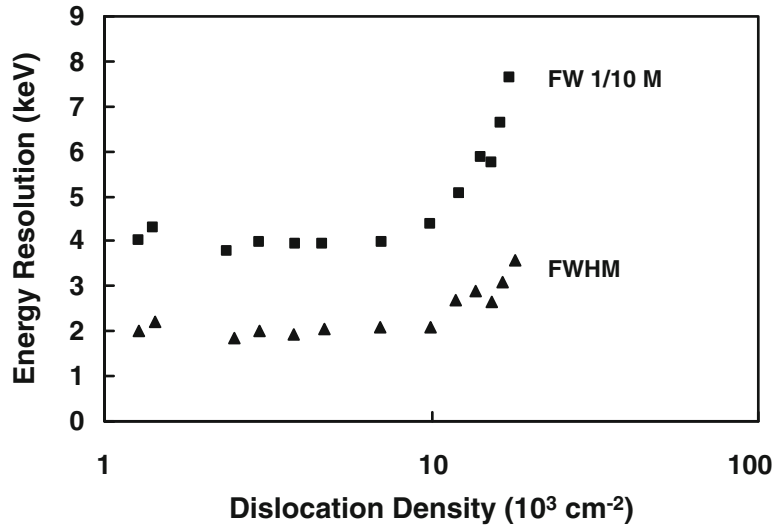


Fig. 2.38. Correlation between dislocation density and energy resolution shown by 1.34 MeV γ -irradiation of ^{60}Co of 13 planar high-purity germanium detectors. Detector area: approx. 10 cm^2 ; depletion width: 1 cm (after [121])

in the latter technique, only levels at the Fermi level contribute to the measurement. This means that from optical measurements one directly derives the distribution (density) of states, without uncertainties related to electrostatic charging of the dislocations. Of course, this assumes a rigid band model where all levels shift approximately the same amount due to the charge on the dangling bonds. Based on the results of the optical characterization, a more detailed band structure has been established, whereby, for example, the 1D nature could be clearly demonstrated.

2.6.1 Absorption and Recombination

Initial absorption experiments of plastically deformed germanium showed a shift of the intrinsic absorption edge to longer wavelengths (lower energies) plus an absorption tail at longer λ and increasing with increasing deformation [125]. The first effect was ascribed to a reduction of the band gap by the strain field. The extended tail was associated with the energy levels (acceptor states) induced by the dislocations [125].

Later experiments showed that the infrared (IR) absorption tail is dependent on the direction of the light propagation relative to the slip plane [126]. This was confirmed in [127], where a pronounced dichroism was observed. It was also established that the dipole moment of the absorbing centers was parallel to the glide direction, firmly linking it with the dislocation states. However, the absorption is fairly weak and only observable for large dislocation

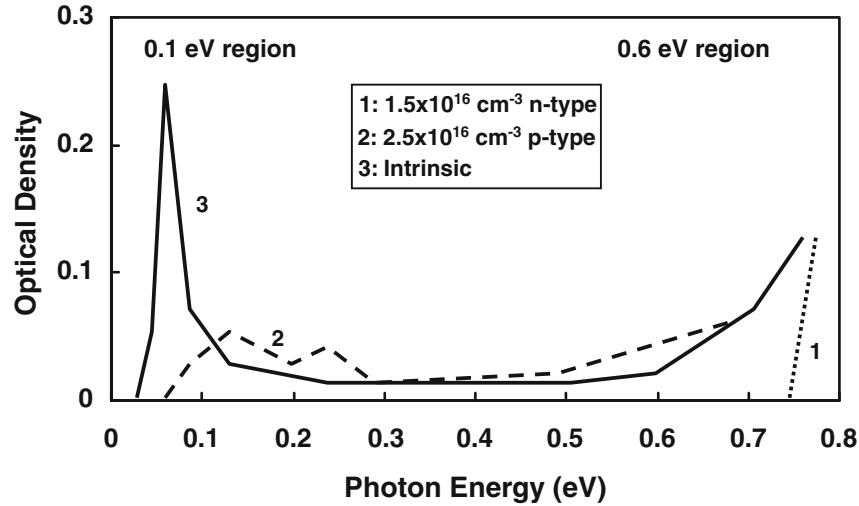


Fig. 2.39. Absorption spectra at 77 K of differently doped samples having the same etch pit density of $2 \times 10^7 \text{ cm}^{-2}$ and thickness ($d = 4.1 \text{ mm}$) (after [129])

densities ($>10^7 \text{ cm}^{-2}$) in n-type Ge [127]. In p-type material, it was hard to find dislocation-related absorption.

In the photon energy range $h\nu = 0.03\text{--}0.5 \text{ eV}$ an enhanced absorption for $h\nu < 0.22 \text{ eV}$ was observed in heavily deformed Ge [128]. This feature disappeared after annealing at 600°C , which could point to a correlation with deformation-induced PDs. However, it was not ruled out that the transitions involved electrons going from the valence band to the primary dislocation band at $E_V + 0.09 \text{ eV}$ or intraband transitions [128].

A more detailed and systematic study has been performed by Barth et al. [129], who showed that the infrared absorption in heavily dislocated Ge is characterized by two spectral peaks around 0.1 and 0.6 eV, as can be noted in Fig. 2.39. It was also shown that in n- and p-type Ge different transitions are responsible for the “0.6 eV” band [129]. The “0.1 eV” region, on the other hand, is strongly dependent on the doping concentration, as observed in Fig. 2.40. In other words, the intensity of the absorption is not governed by the dangling bond density but by the number of electrons trapped on it. In n-Ge, the 0.1 eV peak increases strongly for lower T and saturates below 80 K. This band also exhibits pronounced dichroism with dipole moment along the displacement (Burgers) vector. This means that the dipole of the underlying optical transition is parallel to the Burgers vector. In p-type samples, no dichroism was reported in [129].

The absorption data has been interpreted in terms of the band model of Fig. 2.41 [129]. In n- and p-type Ge two different dislocation states (bands) are involved in the optical transitions, giving rise to IR photon absorption. In p-type Ge, it is the $E_V + 0.13 \text{ eV}$ level and in n-Ge it is a state at 0.1 eV

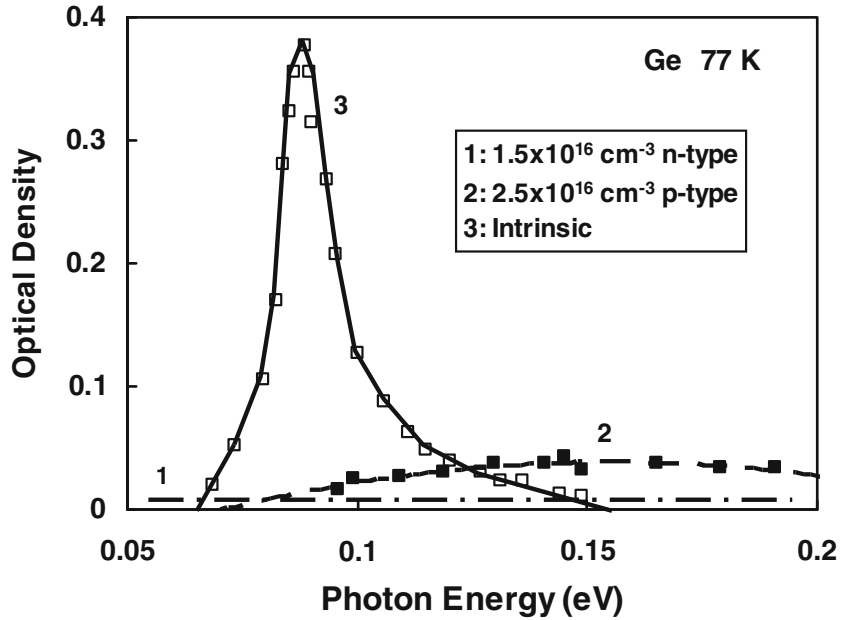


Fig. 2.40. Influence of doping type on the absorption in the 0.1 eV region of Ge at $T = 77$ K having an etch pit density of $3 \times 10^7 \text{ cm}^{-2}$ and $d = 4.1$ mm (after [129])

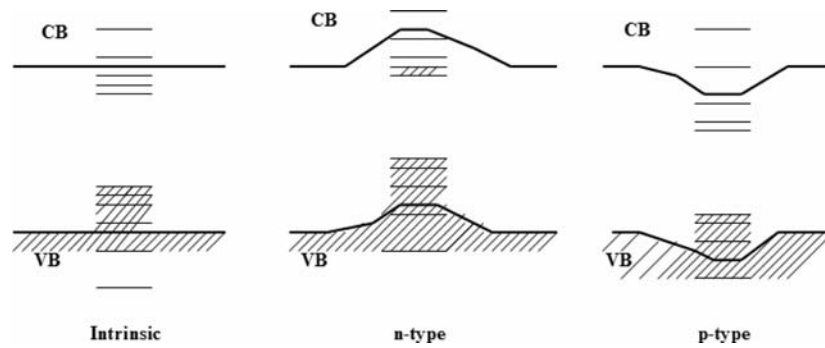


Fig. 2.41. Energy levels of edge dislocations. Filled states are indicated by *hatched lines* (after [129])

below the conduction band, related to the split off states in the dilation region. The “0.6 eV” peak is believed to correspond to complementary transitions: in p-Ge, absorption occurs from the valence band into the empty $E_C - 0.1$ eV states and in n-type Ge, electrons are excited from the occupied $E_V + 0.13$ eV level to the conduction band. It was also noted that the energy difference between the two dislocation states in Fig. 2.41 corresponded well with the

energy of the optical recombination energy [129] to be described later. The Authors also came to the conclusion that no absorption within a half-filled dislocation band occurred, in conflict with the general picture accepted by that time [129]. They assumed that both the 0.1 and 0.6 eV peaks involved split off strain states. Their argument is that the IR absorption coefficient (α_{IR}) is rather weak, which is unexpected if there would exist a half-filled band of states. In that case, one would always expect inter-band transitions with a higher α_{IR} [129]. It should finally be remarked that some theoretical discussion of the latter results was given by Winter [130].

2.6.2 Optical Recombination

A number of studies were devoted to the optical recombination radiation by 60° -dislocations [131–135]. Systematically, a peak at 0.5 eV was observed in plastically deformed Ge, as given in Fig. 2.42, showing the electroluminescence curves for different Ge p-n junctions operated in forward direction [131]. Besides the intrinsic recombination peak at 0.7 eV (band gap energy), there is an emission at 0.5 eV, which varies with a high power of the forward current (~ 5) in deformed material. It is not observed at 300 K or in heat-treated material only, reduces above 200 K, and is constant from 40–120 K [131].

The feature is most pronounced for electrons injected in p-type germanium. In later studies, it was derived that the recombination spectrum is related with hole transitions from the valence band to dislocations levels at $E_C - 0.22$ and $E_C - 0.14$ eV from the conduction band [133]. Another set of levels was found at $E_C - 0.18$ eV, while the half-width of the radiation line connected with the transition of a hole to one of these levels is 0.016 eV [133].

Employing higher-resolution optical measurements reveals some fine-structure in the band (Fig. 2.43) [135], whereby the line intensity increases for lower temperatures; the FWHM remains constant, however. For dislocation densities above $5 \times 10^6 \text{ cm}^{-2}$, the intensity drops [135]. The total intensity of the spectrum remains constant up to $N_d = 5 \times 10^6 \text{ cm}^{-2}$, whereby the spectral features between 0.5 and 0.6 eV grow at the expense of the intrinsic emission at 0.72 eV (82 K) [135]. The peak maximum shifts the same way as the intrinsic (or band-to-band) emission [135] and is illustrated in Fig. 2.44 [133]. The temperature shift has a linear slope of $2.6 \times 10^{-4} \text{ eV/K}$, similar as the temperature shift of the germanium band gap [133]. The kind of doping has no impact, suggesting that the presence of a Cottrell atmosphere around the dislocations does not play a role in the recombination events [134, 135]. Barth et al. interpreted their results in terms of a dislocation level at $E_C - 0.12$ eV, where recombination of electrons may proceed with holes from the valence band or with holes at the $E_V + 0.1$ eV acceptor level [135].

It was also observed that dislocations are rather inefficient recombination centers: only 10^{-4} recombination events are radiative at $T = 80 \text{ K}$ [135]. This led to the suggestion that the radiative centers could be different than the dangling bonds and are, in particular, defect sites in the core structure [133].

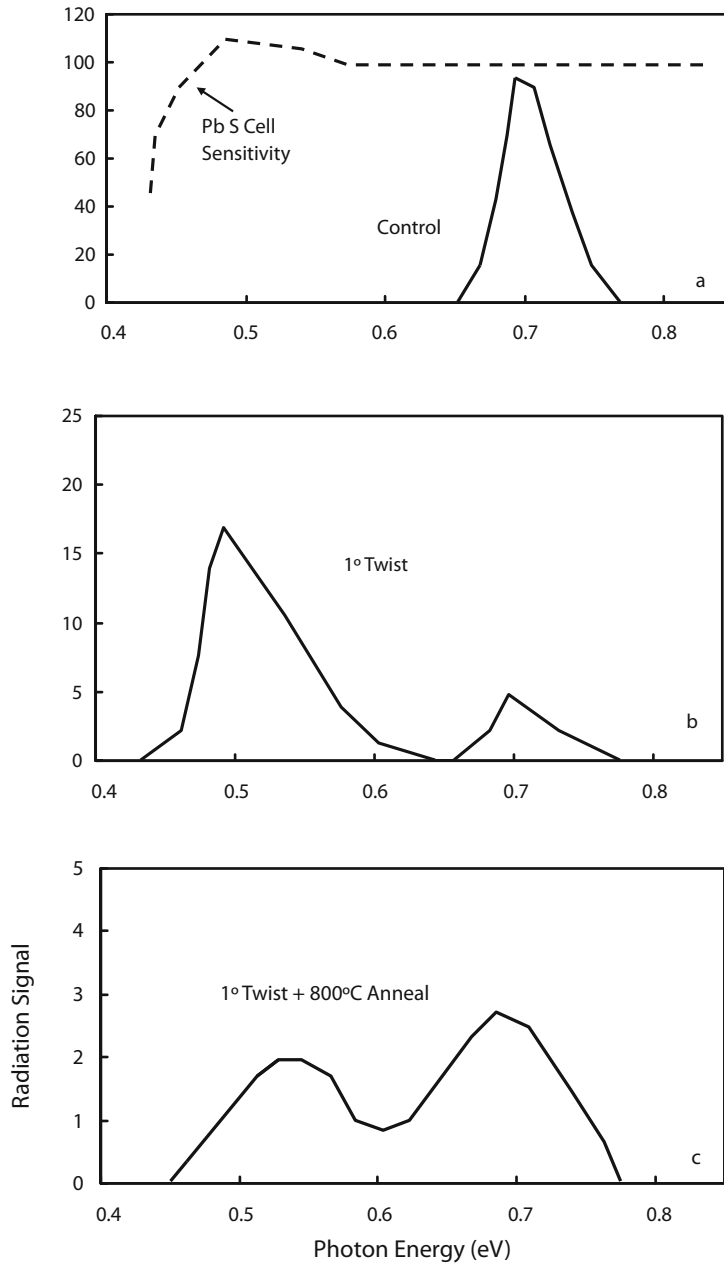


Fig. 2.42. A series of radiation spectra ($T \sim 82$ K) for a Ge junction which had the treatments indicated in the figure. The same current density was used throughout. The 300 K junction characteristics prior to bending were $p \sim 0.01$ ohm cm, $n \sim 1$ ohm cm, $\tau_h \sim 50 \mu\text{s}$ (after [131])

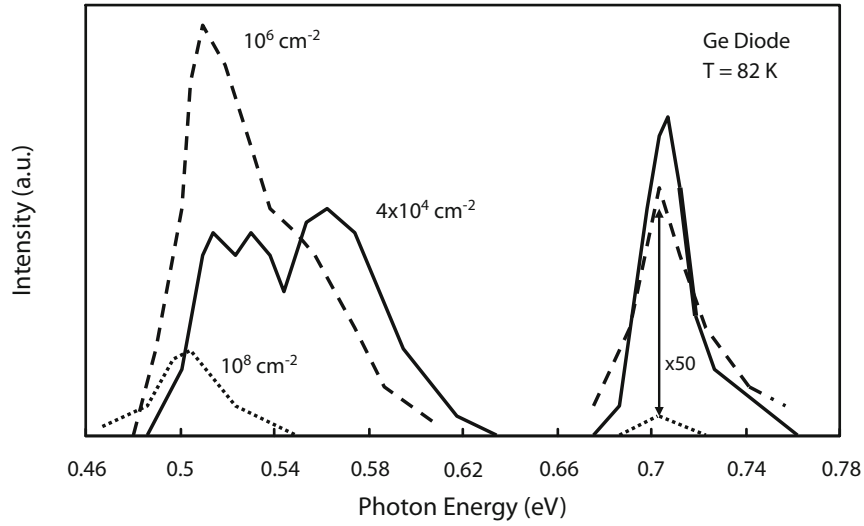


Fig. 2.43. Dependence of the emission spectra on dislocation density N_d (injection current density being constant at 4.1 A cm^{-2}), $N_A = 3 \times 10^{16} \text{ cm}^{-3}$ and $T = 82 \text{ K}$ (after [135])

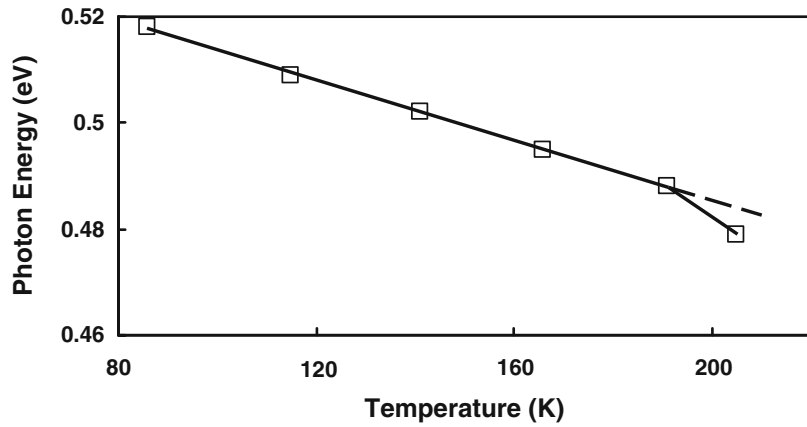


Fig. 2.44. Temperature dependence of the photon energy corresponding to the maximum of the radiation band (after [133])

This could explain the saturation of the emission peak intensity at high current levels (intensity $\sim I^{0.2}$) [133]. A theory for optical absorption and emission was developed by Sokolov [136]. The calculations confirmed that the absorption and radiation by dislocations are small for their usual density in Ge.

2.6.3 Photoconductivity

Dislocations were shown to have a pronounced impact on the steady-state and decay photoconductivity (PC) in germanium [137–145]. The steady-state intrinsic PC ($h\nu > 0.7\text{ eV}$) lifetime exhibits a nonlinear dependence on the injection level Δn or Δp in the intrinsic absorption range [137]: a power law was observed with an exponent in the range 0.6–0.8. This nonlinear PC was related to the occurrence of intense carrier trapping by dislocations [137, 139]. It was found that trapping of both holes (in n-type) and electrons (p-Ge) occurred in deformed Ge, which is unusual compared with the case of metal-doped Ge, where only hole trapping was found in n-type material [137]. The trapping of holes was believed to occur through a dislocation level close to the conduction band, while the trapping in n-type Ge could not be explained on the basis of hole trapping by a single level [137]. The trapping was already strong at room temperature in n-Ge, while it started at 270 K for p-material. The activation energy of the lifetime was found to correspond to 0.46 eV for n- and 0.30 eV for p-type Ge [137].

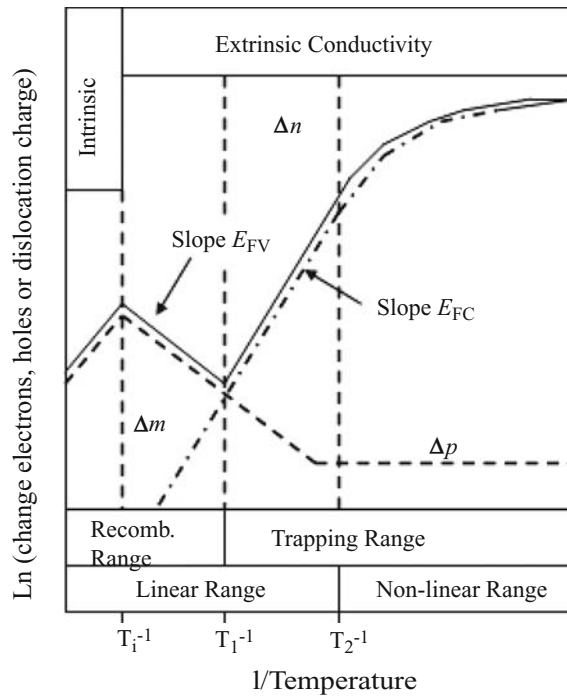


Fig. 2.45. Dependence of excess charge concentrations on reciprocal temperature expected on the barrier model. E_{FC} (E_{FV}) is the difference between the energy of the conduction (valence) band edge and the Fermi energy at the dislocation core (after [145])

The behavior of dislocations as recombination or trapping centers has been explained in a simple manner by Figielski [145], following the scheme of Fig. 2.45 for the intrinsic PC ($h\nu \geq E_G$) and based on the dislocation-charge-dependent potential barrier model. Assuming low-level injection, that is, close to thermal equilibrium conditions, and for n-type Ge, the steady-state excess hole concentration can be expressed as

$$\Delta p = \frac{G}{c_n N_d} \frac{N_V}{n_0} \exp(-[E_F - E_V]/kT) + \frac{G}{c_p N_d}, \quad (2.23)$$

G is the electron-hole generation rate; c_n and c_p is the recombination coefficient for electrons and holes, respectively, and may be expressed in terms of the cross section for that process per unit length of dislocation [145]. In other words, c_n is the product of the thermal velocity times the capture cross section per unit of length; a value of 4×10^{-8} cm was quoted for n-type Ge [145]. Further, N_V is the density of states in the valence band, n_0 is the free electron density in the bulk at zero excitation (equilibrium value), and $E_F - E_V$ is the difference between the Fermi level at the dislocation core and the valence band edge and is a linear function of the Coulomb barrier at the charged dislocation Φ_B . One has further that $n = n_0 + \Delta n$.

For the trapped positive charge at the dislocations, one can equally show that [145]

$$\Delta m = \frac{kT}{q^2} \frac{\eta_0}{\Phi_0} N_d \ln \left[1 + \frac{G}{c_n N_d N_C} \exp([E_C - E_F]/kT) \right], \quad (2.24)$$

with η_0 the linear charge density on the dislocation at equilibrium ($\Delta n = \Delta p = 0$), N_C the density of states in the conduction band. When the relative deviation of the dislocation charge from equilibrium is small, (2.24) reduces to [145]

$$\Delta m = \frac{kT}{q^2} \frac{\eta_0}{\Phi_0} \frac{G}{c_n N_C} \exp([E_C - E_F]/kT). \quad (2.25)$$

We have finally from the condition of crystal neutrality that

$$\Delta n = \Delta m + \Delta p. \quad (2.26)$$

The three excess charges are represented in Fig. 2.45 and based on their behavior, a distinction can be made between dislocations as recombination or as trapping centers. At sufficiently high temperatures, but still in the extrinsic doping range, the first term in (2.23) dominates, following an (exponential) slope $E_F - E_V$. As Δp is proportional with G , a linear recombination occurs so that the relation $\Delta p = G\tau_p$ is valid in steady-state. Consequently, a SRH hole lifetime τ_p can be derived, which is inversely proportional with the dislocation density N_d , as is observed experimentally.

As the temperature is lowered, the first term in (2.24) becomes negligible and the trapped positive (hole) charge starts to increase with a slope $E_C - E_F$.

There is a transition temperature T_1 separating the SRH recombination from the trapping range and given by [142]

$$kT_1 = E_G / \ln \left[\frac{q^2 \Phi_B N_C N_V}{kT_1 \eta_0 N_d n_0} \right]. \quad (2.27)$$

This temperature is nearly proportional with the band gap and increases with dislocation density. In the trapping range, the PC becomes monopolar (electrons only), while it is bipolar in the recombination range. Since T_1 does not depend on the generation rate G , it means that the dislocation charge cannot be changed by illumination at that point [145].

Finally, a second transition temperature can be defined (T_2) below, which the net dislocation charge changes from an exponential increase with $1/T$ to a saturation behavior (Fig. 2.45). A good estimate for T_2 is given by [145]

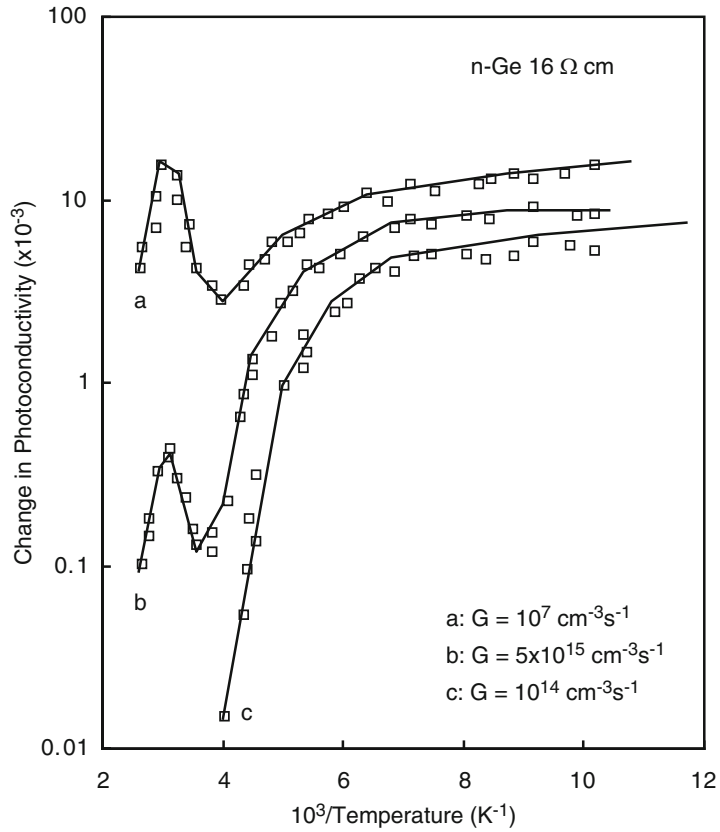


Fig. 2.46. Temperature dependence of the photoconductivity in a plastically bent Ge sample at different rates of generation of electron-hole pairs (after [145])

$$kT_2 = (E_C - E_F) \left/ \ln \frac{c_n N_d N_C}{G} \right., \quad (2.28)$$

T_2 depends on the generation rate per dislocation G/N_d . In the range $T_2 < T < T_1$, Δn is proportional with G , implying that linear recombination occurs and the usual SRH lifetime concept can be applied as well. As can be seen in the experimental curves of Fig. 2.46, this simple theory describes quite well the observations [145].

The most interesting regime in the intrinsic PC, typical for dislocations, is the nonlinear regime at low temperatures ($T < T_2$). Here, a significant deviation from the equilibrium line charge density η_0 exists on the dislocations, that is, $\Delta m \gg 0$ and the barrier height is reduced. In that case, a nonlinear recombination of the carriers is observed, whereby Δn obeys

$$\Delta n = \frac{kT}{q^2} \frac{\eta_0}{\Phi_B} N_d \ln \frac{G}{c_n N_d N_C} + N_d (E_C - E_F) \frac{\eta_0}{q^2 \Phi_B}. \quad (2.29)$$

The steady-state PC grows with N_d although slower than linear in this regime. It is also nonlinear in the generation rate G , as according to (2.29) and Fig. 2.47 it follows an $\ln(G)$ dependence.

The nonlinearity of the recombination process is most easily seen in the decay transient after switching off the illumination. In that case, the excess electrons decay according to [145]

$$\Delta n \approx \Delta m = -\frac{kT}{q^2} \frac{\eta_0}{\Phi_B} N_d \ln \frac{t + t_0}{\tau_n}. \quad (2.30)$$

In (2.30), the “offset” time t_0 equals

$$t_0 = \frac{kT}{q^2} \frac{\eta_0}{\Phi_B} \frac{N_d}{G} \quad (2.31)$$

and the electron “lifetime” τ_n is given by

$$\tau_n = \frac{kT}{q^2} \frac{\eta_0}{\Phi_B} \frac{1}{c_n N_C} \exp([E_C - E_F]/kT). \quad (2.32)$$

The time t_0 is determined by the initial condition of the sample and is smaller than τ_n for $T < T_2$ [145]. The time constant τ_n depends only on material and defect parameters and not on the excitation level or the dislocation density and can be considered as a generalized electron lifetime. It is the characteristic time of the decay process in the nonlinear regime, similar to the SRH lifetime in the linear regime, where the decay is an exponential process with time. The logarithmic nature of the decay is shown in Fig. 2.48, and the x -axis intercept is given by $t = \tau_n - t_0$.

At times comparable with τ_n , the excess carrier concentration is quite small, so that an exponential decay results. On the other hand, the rise of the intrinsic PC in the nonlinear regime is well described by an exponential

$$\Delta n = \Delta n(\infty)(1 - \exp(-t/t_0)). \quad (2.33)$$

As can be seen from (2.32), τ_n is very sensitive to temperature and can become quite large at low T . For T where $\tau_n \geq 10^3$ s, the material becomes extremely photosensitive, as can be derived from Fig. 2.46. It implies that even the lowest background radiation can considerably change the experimental zero level. For long time constants, the excess carrier concentration remains at a practically unchanging level after switching of the light, leading to a so-called photomemory effect [145]. At the same time, both the dislocation density (Fig. 2.49a) and the illumination level (Fig. 2.49b) have a pronounced impact on the intrinsic PC in deformed Ge, particularly at low temperature in the trapping range.

According to (2.29), an activation energy can be derived from the PC in the trapping range. For n-type Ge, values of -0.42 eV were consistently obtained [145], whereby no definite shift with doping level in the range 10^{13} – 10^{15} cm^{-3} was observed. For p-type material $E_C - E_F = 0.24$ – 0.30 eV. These two values add up to the band gap energy in Ge. It should finally be remarked that a similar (complementary) analysis holds for the intrinsic PC in

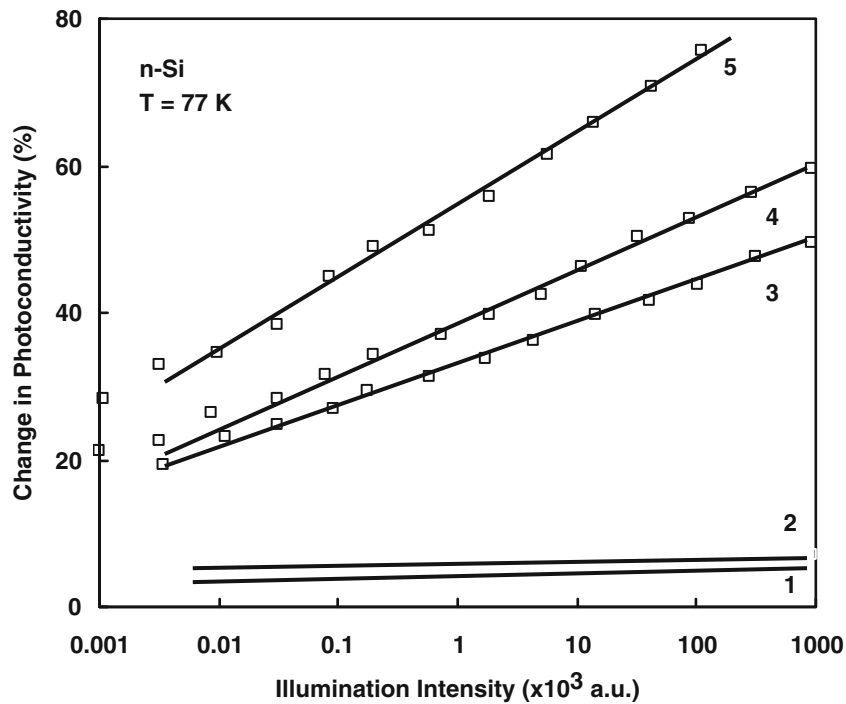


Fig. 2.47. Steady-state photoconductivity in plastically deformed Si vs. illumination intensity: (1) reference sample; (2) heated but unbent sample; (3)–(5) sample bent to the radii of curvature 12, 6, and 3 cm, respectively (after [145])

plastically deformed p-type Ge, whereby in the trapping range, the monopolar conduction is by holes [141]. Finally, under background illumination, a quenching of the intrinsic PC has been observed for n-type Ge samples [144].

The spectral dependence of the extrinsic PC ($h\nu < 0.7$ eV) in deformed Ge has also been the subject of intense studies [144, 146–154]. As the absorption cross section for direct absorption measurements is rather small, it is better to use the more sensitive extrinsic PC measurements at low T . However, the interpretation is not straightforward as both generation and recombination of carriers may contribute to the signal, both in the bulk and at the surface of the sample [148]. A comprehensive summary of the optical excitation of dislocation states in Ge has been provided by Mergel and Labusch [150, 151], where the PC spectra were compared with radiative recombination data. Figures 2.50 and 2.51 summarize the PC spectra in deformed p- and n-type material, respectively. No extrinsic PC was found before deformation below the intrinsic regime [150]. In deformed p-Ge, a peak at 0.18 eV and a second one at 0.48 eV plus a broad band at 0.6 eV was observed [150]. In n-type material, qualitatively similar spectra were obtained (compare Figs. 2.50 and 2.51). This implies that the same kind of transitions was observed in both material types. However, an additional exponential generation band was found in n-Ge, between 0.45 eV and the band gap (Fig. 2.51). The lower G band at 0.2 (+0.27) eV disappears in n-Ge as the response time (time constant) becomes fast.

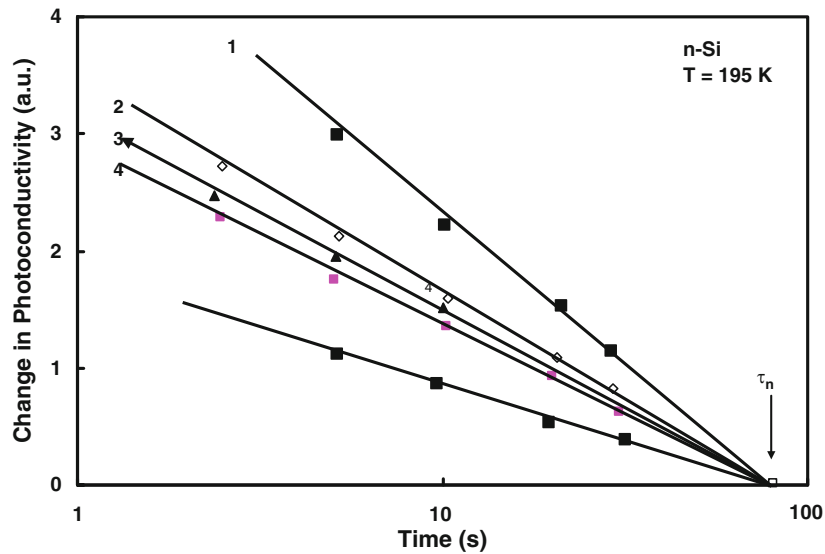


Fig. 2.48. Decay of the photoconductivity after illumination of the sample by a rectangular light pulse. (1) 150 Ω cm sample bent to a curvature radius of 3 cm, (2) and (4) 1,000 Ω cm unbent sample at two different illumination levels, and (3) 35 Ω cm, unbent sample (after [145])

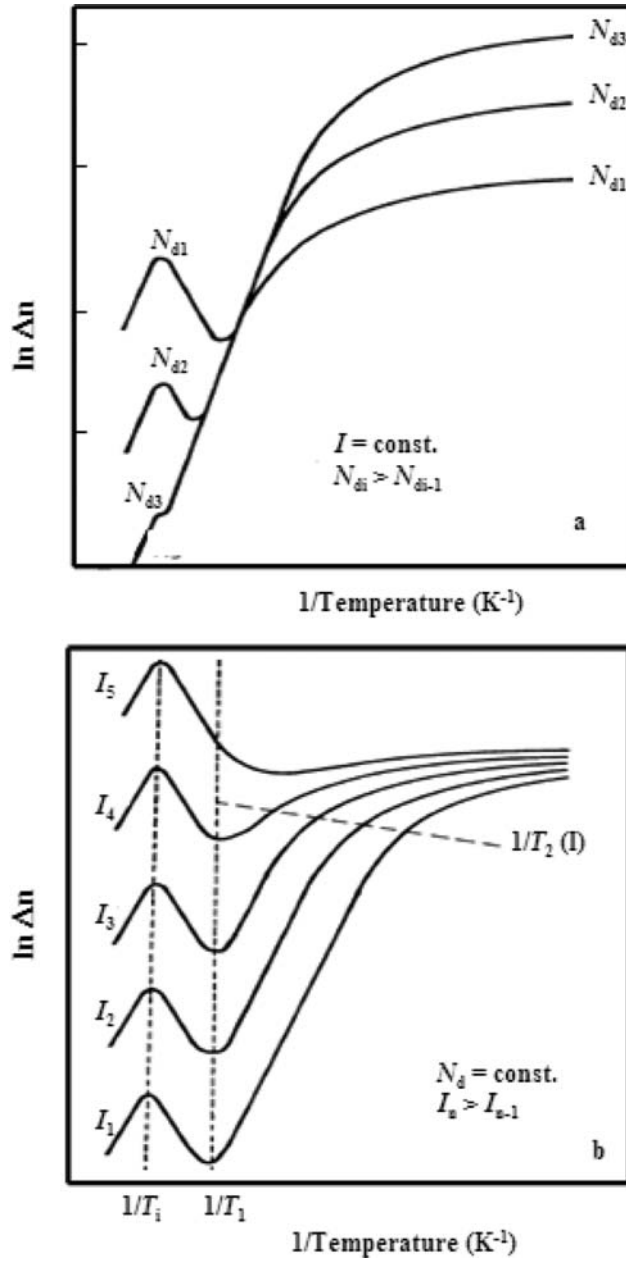


Fig. 2.49. (a) Theoretical dependence of photoconductivity vs. reciprocal temperature for different dislocation densities. (b) Theoretical dependence of photoconductivity vs. reciprocal temperature for different illumination levels (after [145])

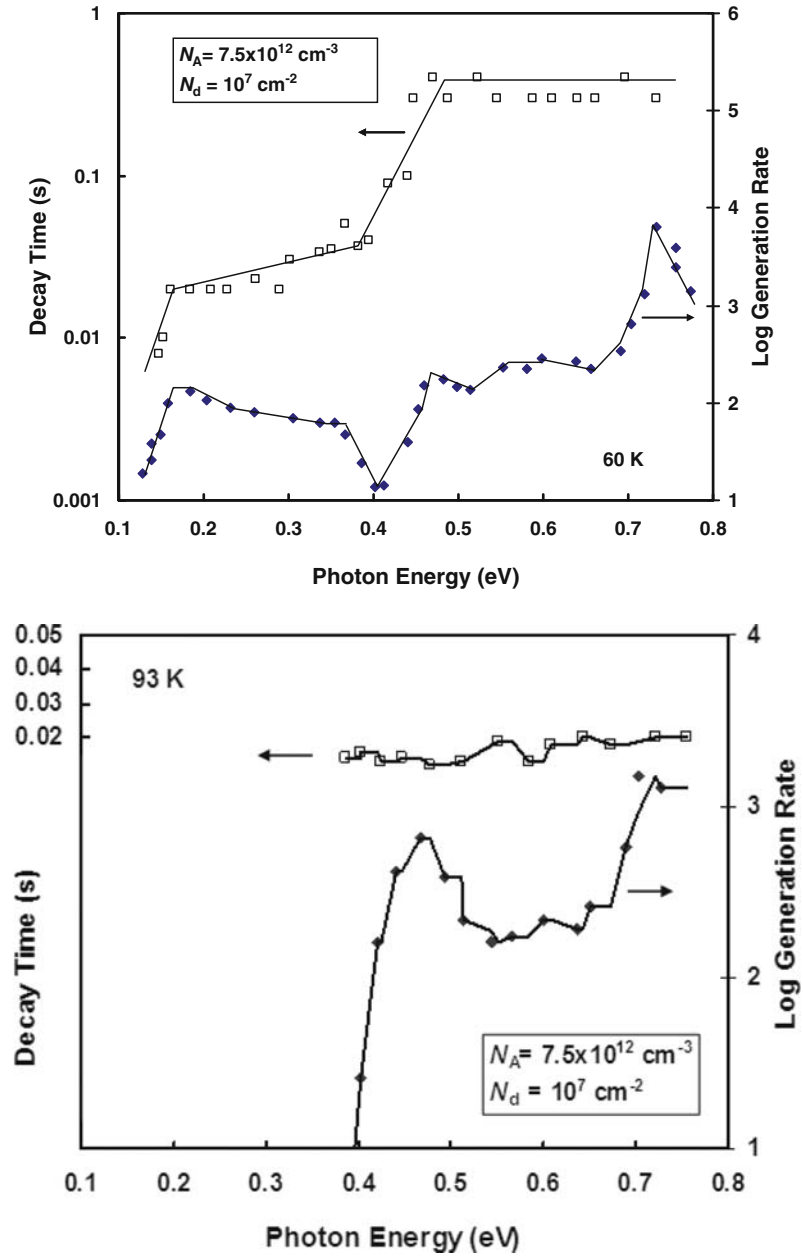


Fig. 2.50. Generation yield G (right) and characteristic decay times (left) vs. the photon energy in deformed p-Ge. The doping concentration was $N_A = 7.5 \times 10^{12} \text{ cm}^{-3}$, the dislocation density $N_d = 10^7 \text{ cm}^{-2}$ (predominantly edge type). $G(h\nu)$ is given in arbitrary units on a logarithmic scale. No signals could be resolved below $h\nu = 0.38 \text{ eV}$ at 93 K (after [150])

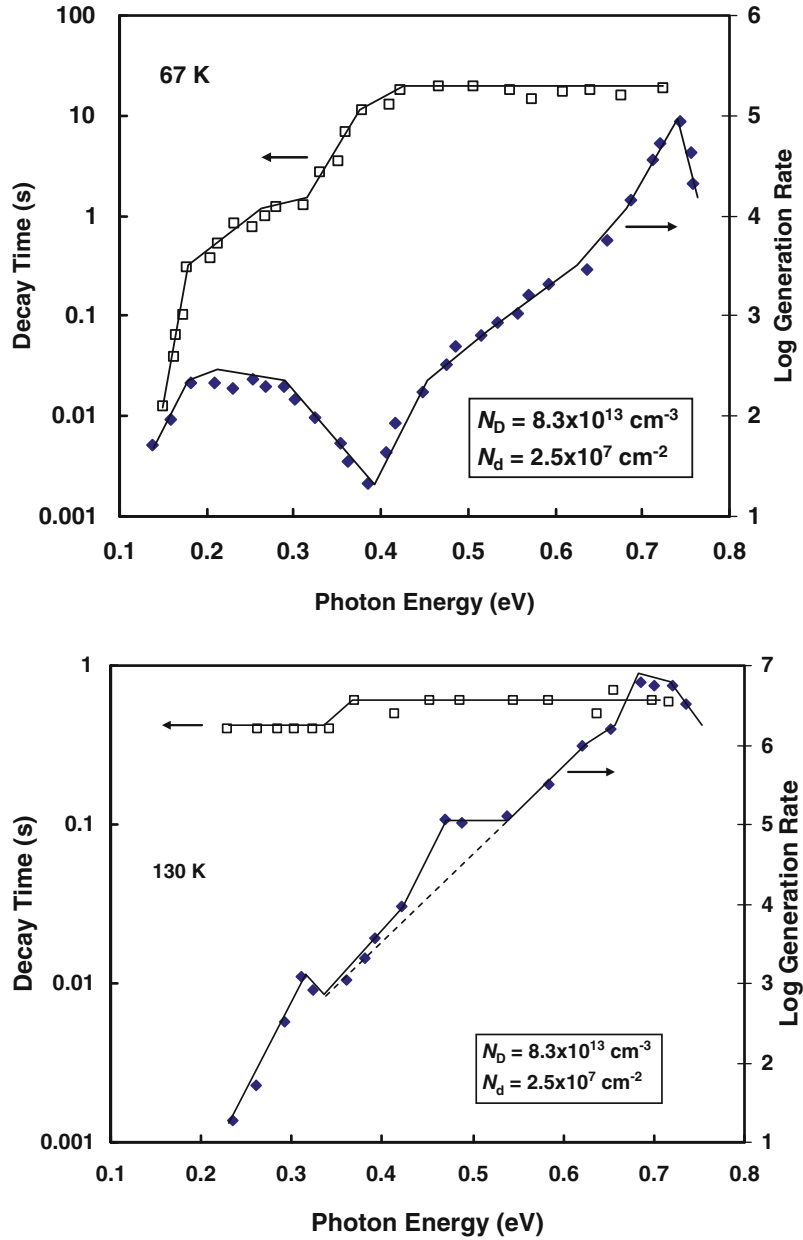


Fig. 2.51. Generation yield G (*right*) and characteristic decay times τ (*left*) vs. the photon energy $h\nu$ in deformed n-Ge. The doping concentration was $N_D = 8.3 \times 10^{13} \text{ cm}^{-3}$, the dislocation density $N_d = 2.5 \times 10^7 \text{ cm}^{-2}$ (predominantly edge type). In the upper half of the energy range $G(h\nu)$ seems to consist of an exponential background and two peaks, similar to those in p-type Ge, as indicated by the *dashed lines* (after [150])

A polarization parallel with the Burgers vector of the predominant dislocation type has been found in the extrinsic PC [146, 148]. Maximum PC was observed parallel and minimum PC perpendicular with the direction of the Burgers vector. As shown in Fig. 2.52, the polarization peaks correspond with the G peaks in n-Ge [150]. Also the recombination peak at ~ 0.51 eV corresponds to one of the PC maxima. The stationary photocurrent is proportional with the decay time τ , so that it is an indirect measurement of this parameter. The photocurrent is temperature activated in a broad observation window, whereby the activation energy E_A only weakly depends on doping and dislocation density. In the lower G band, $E_A \sim 0.1$ to 0.18 eV in n-Ge and 0.1 – 0.15 eV in p-Ge. In the upper G band, one obtains $E_A = 0.4$ – 0.5 eV [150]. From this, it was concluded that the recombination paths are different for the lower and upper G band. For the lower G band, it has been assumed that the half-filled band of acceptor states determines the PC. In the upper band, empty dislocation states close to the conduction band play the key role, whereby transitions occur between the valence band and the upper band [150]. The continuous and exponential generation background in n-type material (Fig. 2.51) is then supposed to originate from transitions from the valence band to tunneling states localized at the dislocations in their potential barrier. The recombination through the exponential and upper G band follows the same path, as can be derived from the lack of structure in τ vs. $h\nu$ (Figs. 2.51 and 2.52) [150].

The nature of the extrinsic PC decay has also been investigated to some extent [147, 149]. It was observed that the relaxation time of PC increases with increasing photon energy, whereby a nonexponential decay was the rule rather than the exception [149]. For $h\nu > 0.5$ eV a slow, logarithmic type of PC dominates, similar as for the intrinsic regime ($h\nu = 0.7$ eV). For $0.25 < h\nu < 0.5$ eV, the PC is characterized by a shorter relaxation time and a different type of PC. For $h\nu < 0.25$ a third type of relaxation occurs, with a fast time constant. At the same time, the intensity of the PC is lower than for the higher energy regimes. The situation is summarized in Fig. 2.53 [149]. The logarithmic type of PC decay was interpreted in terms of the generation of majority carriers whose recombination is governed by the potential barriers at the dislocations (Figielski model [145]). The fast PC at low energies was assumed to originate from the same electronic transitions responsible for an absorption band at 0.1 eV [149].

More recent experiments have used the same arrangement to study the DC conductivity of a small group of dislocations [59] and to measure the related PC along it and towards the Ge bulk [59, 153]. Typical results are shown in Figs. 2.54 and 2.55 [153]. A prominent double peak is observed in Fig. 2.55 at 0.38 eV. The sharp increase at 0.33 eV and the sharp drop at 0.38 eV are characteristic for the singularity in the density of states of a 1D band. According to the model schematically represented in Fig. 2.56 [59], there are three 1D bands associated with a 60° -dislocation. First, we have the primary band with neutral level at $E_V + 0.1$ eV and a small band gap

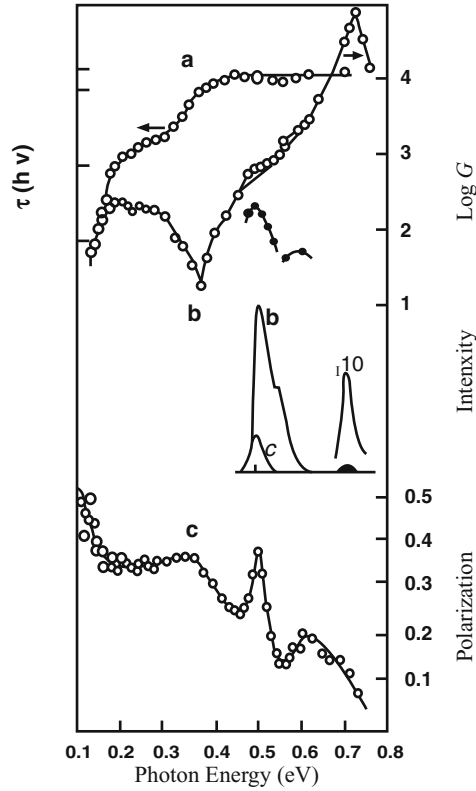


Fig. 2.52. Comparison of (a) $G(h\nu)$ and $\tau(h\nu)$ in n-Ge with (b) measurements of the radiative recombination at dislocations [135] and (c) with the degree of polarization of the PC [148]. The peaks that were only conjectured from the G-spectrum appear very clearly in these experiments (after [150])

(Peierls gap). Next, there is a hole band in the attractive potential of a charged dislocation (more curved than the primary band, with a small gap as well). Finally, a secondary band is considered, residing closer to the conduction band and split-off from it due to the deformation potential of the dislocation.

Labusch and Hess also worked out a theory that takes into account the deformation potential of the dislocation strain field [153]. Here, it is no longer assumed that the core states rigidly shift with electrostatic charging of the dislocations, without accounting for the change in the band gap by the strain field. It is shown that the strain field potential reduces the lowest conduction band states at a distance $r_s \sim 5$ nm (saddle point of the potential) by an amount $\Delta E \approx 0.18$ eV [153]. This implies that the lowest transition from core states to extended conduction band states occurs at $E_G - E_0 - \Delta E \approx 0.43$ eV, explaining the increase of the PC at about 0.42 eV in Fig. 2.54 (E_0 is the

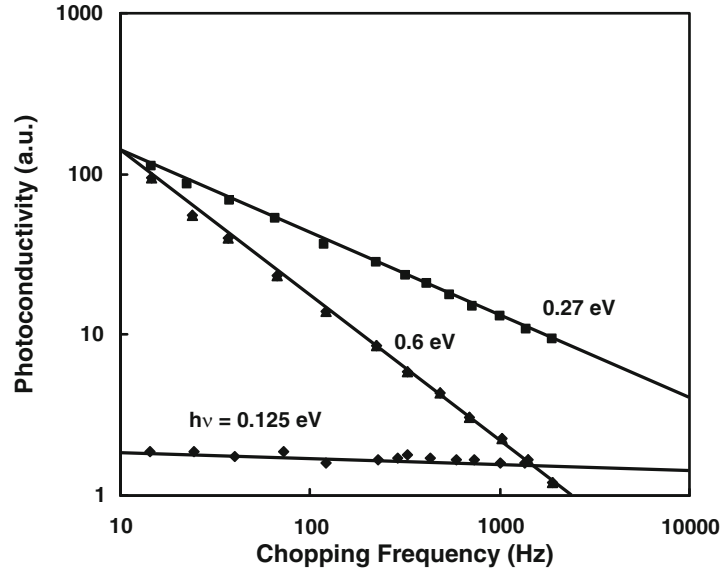


Fig. 2.53. Typical dependences of the photoconductivity on the frequency of light chopping for three photon energies (after [149])

occupation limit of the core states in the absence of an electrostatic potential ~ 0.1 eV).

Based on these considerations, it was concluded that the double peak at 0.37–0.38 eV is related to internal transitions at the core states, while the rise above 0.42 eV is due to transitions from bound dislocation states to free conduction band states in the bulk [153]. The structure around 0.5 eV in Fig. 2.54 (0.49–0.53 eV range) is another contribution by internal core state transitions.

The dependence of the PC in deformed Ge has also been measured as a function of hydrostatic pressure using various gases [155, 156]. It was observed that when helium was used as a pressure-transducing medium, the photoconductivity dropped, for $0.3 \times 10^8 \text{ Pa} < P < 3 \times 10^8 \text{ Pa}$ [157]. This was explained by considering that helium atoms penetrated the material through the dislocation cores. The presence of helium atoms pushes the dangling bonds closer to each other, provoking bond reconstruction to happen. It was assumed that this pushes the associated bands of states outside the band gap and reduces the recombination activity of the dislocations. As such, it can be considered an indirect proof of the existence of dangling bonds in the dislocation core. At $P > 3 \times 10^8 \text{ Pa}$, the PC shows a steep increase, due to the reduction of the band gap with pressure P and the exponential dependence of the PC intensity on E_G . Beyond this range, the photoconductivity is the same for deformed and nondeformed material [157]. It was also found that in the spectral range $0.2 \text{ eV} < h\nu < 0.35 \text{ eV}$ the PC was insensitive to pressure. These transitions

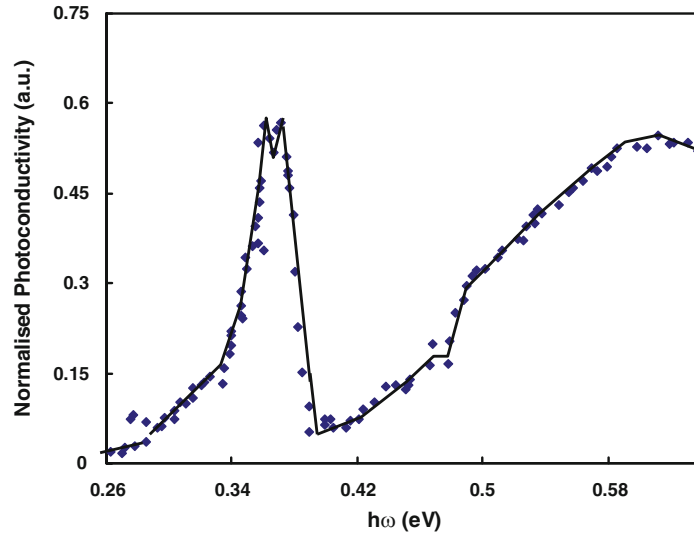


Fig. 2.54. Photoconductivity along a group of twenty dislocations in n-Ge with doping concentration $N_D = 3 \times 10^{13} \text{ cm}^{-3}$ at 90 K. Applied voltage is 0.3 V. The current was normalized by the relative light intensity (after [153])

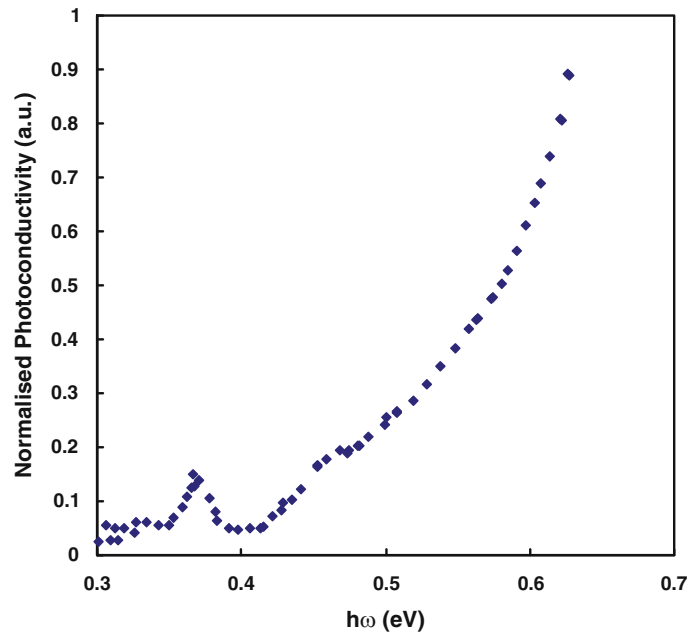


Fig. 2.55. Photoconductivity from the same dislocations as in Fig. 2.53 to the bulk at 60 K. Applied voltage 0.3 V, dislocations negative, bulk contact positive (after [153])

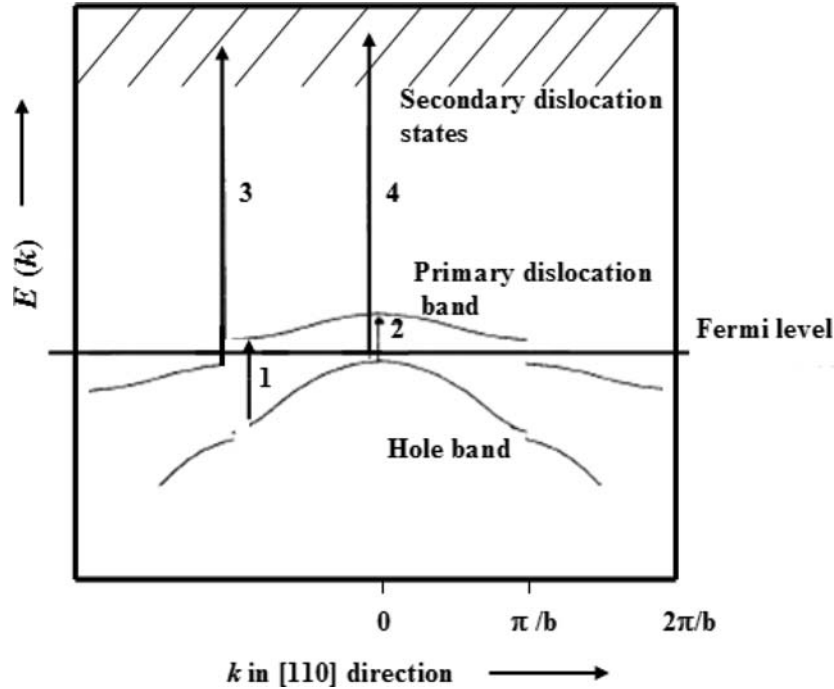


Fig. 2.56. Band structure of 60° -dislocations according to Mergel and Labusch, modified to take into account the Peierls gap (after [59])

were therefore ascribed to electron transitions from the dislocation donor to the acceptor band [157]. A total band width of 0.15 eV was derived, which was split up in 0.09 eV for the acceptor band and 0.06 eV for the donor band. It was assumed that the gap between the two partial dislocation bands widens with pressure, while the core atom spacing reduces at the same time [157].

2.6.4 Photoluminescence

Dislocation photoluminescence has been investigated by a few groups [158–161]. A typical spectrum is represented in Fig. 2.57 [160]. As can be seen, the same spectral features are observed in both PC and PL, indicating that they are due to the same electronic transitions between the conduction band and dislocation states [160].

Moreover, it was found that the PC spectrum is stable against annealing from 420 to 880°C , independent on doping density and dislocation structure [160]. In low-temperature deformed Ge (460°C) some short wavelength features have been ascribed to donor–acceptor (or excited dislocation states) transitions [159]. This was related to the fact that the short wavelength PL increased slowly with pumping intensity and was strongly dependent

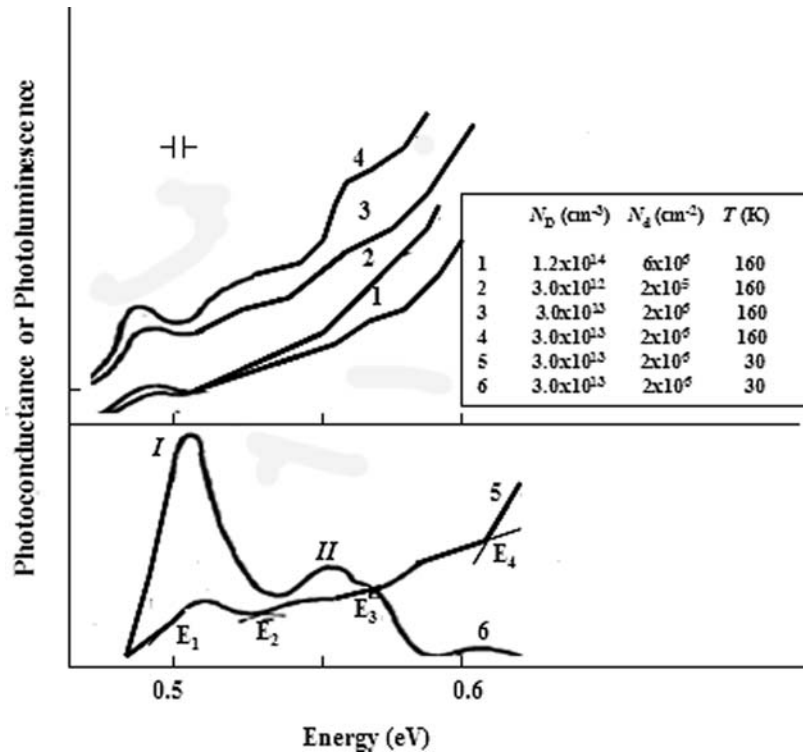


Fig. 2.57. Photoconductivity (PC, curves 1–5) and photoluminescence (PL, curve 6) spectra of deformed n-type germanium samples with different types of doping. Measurement temperature 160 K (1–4) and 30 K (5,6). Annealing after deformation at temperatures 880 °C (4) and 680 °C (1–3,5,6) (after [160])

on doping density. It was also demonstrated that the quantum yield of the dislocation-related PL is low: 10^{-4} at 80 K and 10^{-6} at 130 K [158]. This points out that the majority of the recombination events through dislocations is nonradiative.

PL studies of grown-in dislocations were performed by the Yoffe group, also showing a sharp transition at 513 meV, represented in Fig. 2.58 [161]. The interpretation was that the line results from electron–hole recombination between the two split-off 1D energy bands, at 150 meV below E_C and 80 meV above E_V . The binding energy of the dislocation exciton (DE) was shown to be ~ 2 meV (Fig. 2.59) and is believed to be associated with the 90° partial dislocation [161]. The activation energy of the line intensity at higher T determines the binding energy of the hole to the dislocation (~ 80 meV). The resulting electron binding energy to the 1D energy band is then $E_G - 0.08 - h\nu (= 0.513 \text{ eV})$. According to Fig. 2.60, the line position of the DE line behaves in the same way as the free exciton (FE) with

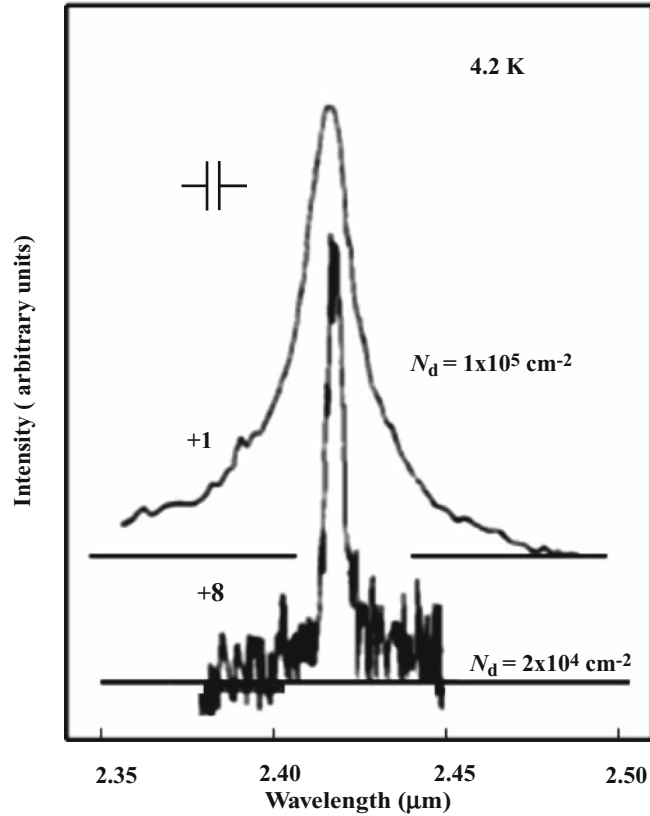


Fig. 2.58. PL-line of DE (after [161])

temperature. The width of the line saturates at higher temperatures and is given by $\sim 2kT$ at lower temperature. This is due to inhomogeneous line broadening [161].

In deformed Ge, a metastable 60° -dislocation luminescence spectrum with several narrow lines (width ~ 3 meV) with limiting energy 0.55 eV may be observed under certain conditions, as represented in Fig. 2.61 [162]. It has been shown that the energy E_n increases with the separation Δ_n between the two partial dislocations. The line d_8 corresponds with an equilibrium separation of $\Delta_0 = 4.9 \pm 0.9$ nm. The lines with $n < 8$ and $8 < n < \infty$ occur on the left and right side of the d_8 line, respectively [162, 163], over the range 0.43–0.55 eV. These narrow lines are found only under specific deformation conditions [163], namely, low temperature and high shear stress deformation, followed by cooling down under load. It is believed that these narrow lines correspond with the optical recombination of carriers at the 90° partial, whereby the potential of the 30° partial acts as a perturbation, whose value depends on the width Δ_n .

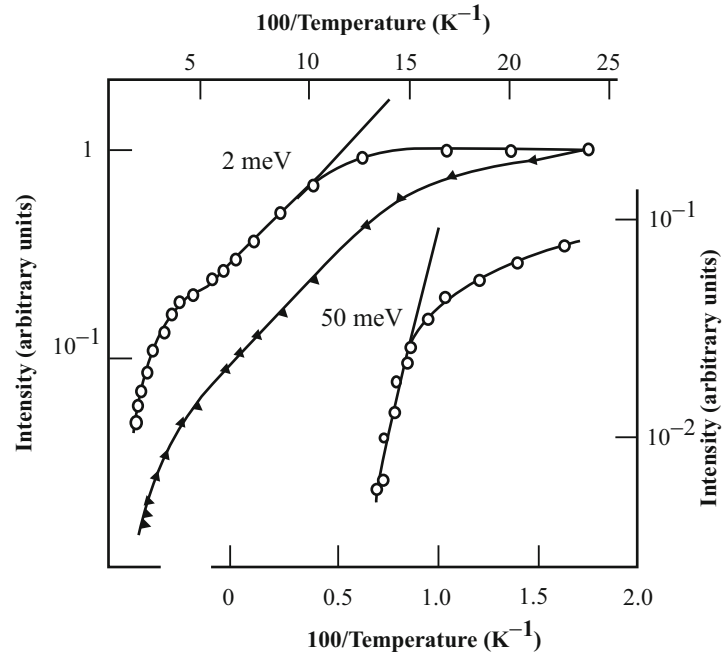


Fig. 2.59. The dependence of DE-line intensity on the inverse temperature: (*open circles*) DE; (*Filled triangles*) (FE) (after [161])

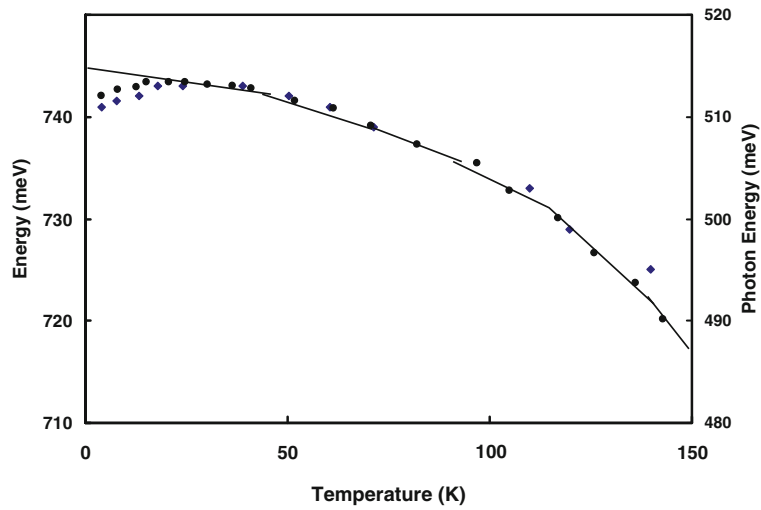


Fig. 2.60. The dependence of the DE-line position on T . (*Filled circle*) DE (*right-hand scale*). (*Filled diamonds*) FE + LA-phonon; *solid line* – energy gap (*left-hand scale*) (after [161])

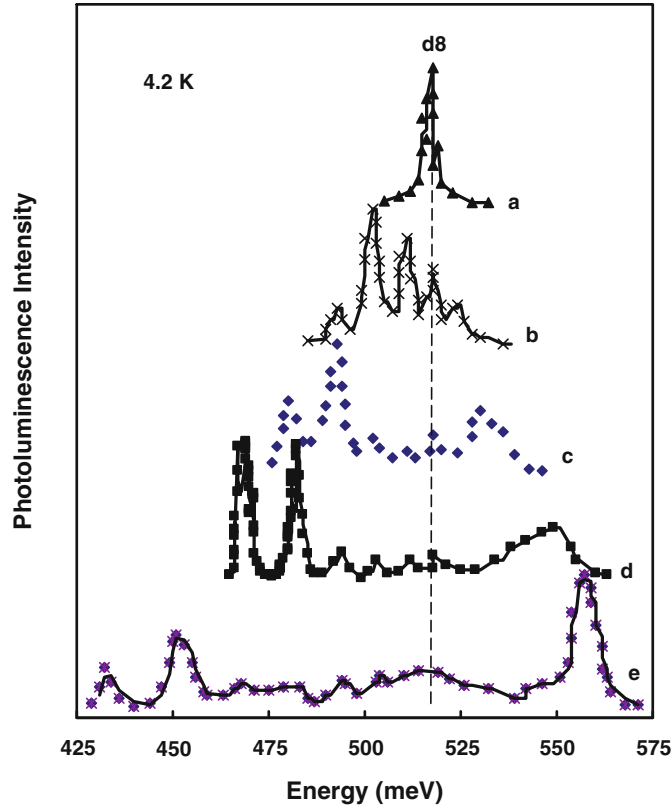


Fig. 2.61. DPL spectra of Ge after standard second stage deformation with stress parallel with $[1\bar{2}3]$: (a) 0, (b) 200, (c) 450, (d) 700, (e) 800 MPa (after [162])

The line number n is given by the relation $n \approx (\Delta_n/a) - 6$, where $a = 0.346$ is the step of changing Δ_n [163]. This nonequilibrium PL structure disappears after annealing above 150°C [163].

A quasi-equilibrium dislocation structure develops under relaxation of the internal stresses in the process of unloaded cooling down to RT after high temperature and low shear stress deformation, as well as after a 150°C (or higher) annealing of high-stress deformed material [163]. In that case, the PL band becomes broad over the range $0.43\text{--}0.60\text{ eV}$ with nonresolved lines. This could be due to the presence of quasi-equilibrium 60° dislocations with various values of Δ_n .

A theory was developed explaining the DE binding energy in terms of the zero-range potential approach to describe the electron-hole interaction, yielding an expression for $E_{\text{DE}} = \mu_{\text{DE}}q^4/(\varepsilon_{\text{Ge}}\varepsilon_0)^2\hbar^2 = 3\text{ meV}$ [161]. μ_{DE} is the reduced mass of the DE, assumed to be small and equal to $0.03m_0$ [161].

The electron–hole pair is thought to be bound by a rectangular potential wall, which is limited by the screening length of the DB charges in the core of the 90° partial dislocation of about 3 nm. The same model was used to explain the observation of DE PL line series in deformed germanium, containing nonequilibrium dislocations (Fig. 2.61). It is thought to be related to the splitting of a 60° dislocation into a 90° and a 30° partial. The presence of the 30° partial can be seen as a perturbation, whereof the impact is inversely proportional with the separation distance (splitting or stacking fault width). Since this can take up only discrete values, a series of spectral lines for the DE may result from this, whereby the E_0 value ($=513$ meV) corresponds with a separation distance of 4.9 nm in Ge and is the only line that survives annealing [161].

It was also observed that there exists a so-called “hot luminescence” background, which has been shown to originate from the nonconstant splitting width along the dislocation core. Finally, a detailed model was proposed to explain e – h recombination and PL through dislocations; for details, the Reader is referred to the work by Lelikov et al. [161].

The photo-Hall effect in deformed germanium has been investigated by Weber [164]. The results show that the dislocations are excited in the whole spectral region of 0.1–0.8 eV.

2.7 Conclusions

Over the years, the model for the deep-level states of dislocations in germanium has evolved from a single energy level associated with DBs to a complex scheme of 1D energy bands, which reasonably well account for the electrical and optical activity. Significant progress in the understanding of the origin of these levels has also been acquired, in spite of some serious experimental difficulties: while deformation conditions are known to activate a single slip system and thus introduce one dominant dislocation type, one is never 100% sure that there are no additional point defects introduced or gettered in the stress field of the dislocations. In addition, dislocations are for the most part split in partials, with a stacking fault in between, so that the observed deep levels should rather be interpreted in terms of 30° or 90° partials and/or the SF in between. Moreover, defects in the dislocations structure (kinks and jogs, etc.) may equally contribute to the electrical activity. A specific problem in the case of germanium is that it is difficult to apply electron spin resonance (ESR) for the identification of dangling bonds in the dislocation core, for example.

Nevertheless, it has become clear that certain features are intrinsic to the dislocation core – the most convincing one perhaps is the 1D microwave conduction pointing to some bands of states in the band gap of Ge. Further proof comes from the anisotropy of the optical dislocation properties (absorption, photoconductivity). In addition, theoretical calculations have pointed out that shallow 1D bands are split off from the valence and conduction band, which

are most likely responsible for the (optical) recombination activity and the PL of dislocations. Referring to the better studied case of silicon, additional deep-level core states are assumed to correspond with impurities and structural defects, thereby strongly enhancing the electrical activity of dislocations. From PL investigations, it has become clear that the optical recombination proceeds through the shallow split-off states and is probably associated with the 90° partial, with little activity for the 30° partial. The latter merely modulates the energy position of the PL line, through a wider splitting (larger SF width).

Similar as for the case of dislocations in silicon, it can be expected that there is potential interest of utilizing dislocations in Ge for certain applications. In principle, a dislocation forms a 1D conductor, similar to a nanowire, so that this could be used as a potential model system for future nanoelectronic applications. The optical recombination, albeit not very efficient, could be exploited for the development of light-emitting diodes in Ge, operating in the (far) infrared region, which is of interest for fiber opto-electronics applications. This requires an optimization of the dislocation structure, produced in a p-n junction. Especially in a Ge-on-Si platform, relying on the epitaxial deposition of Ge directly on silicon or using a SiGe virtual substrate, this could be an interesting option, whereby one can exploit the threading dislocations present in these layers. However, this requires a better understanding of the electrical and optical activity of dislocations in thin Ge layers and on devices produced in them, like MOSFETs and p-n junctions.

References

1. C.J. Gallagher, *Phys. Rev.* **88**, 721 (1952)
2. W.C. Ellis, E.S. Greiner, *Phys. Rev.* **92**, 1061 (1953)
3. G.L. Pearson, W.T. Read Jr, F.J. Morin, *Phys. Rev.* **93**, 666 (1954)
4. A.G. Tweet, *Phys. Rev.* **99**, 1245 (1955)
5. W. Bardsley, *Prog. Semicond.* **4**, 157 (1960)
6. W. Shockley, *Phys. Rev.* **91**, 228 (1953)
7. W.T. Read Jr., *Philos. Mag.* **45**, 775 (1954)
8. W.T. Read Jr., *Philos. Mag.* **45**, 1119 (1954)
9. W. Schröter, *Phys. Stat. Sol.* **21**, 211 (1967)
10. W. Schröter, R. Labusch, *Phys. Stat. Sol.* **36**, 539 (1969)
11. R. Landauer, *Phys. Rev.* **94**, 1386 (1954)
12. V. Celli, V. Gold, R. Thomson, *Phys. Rev. Lett.* **8**, 96 (1962)
13. J.N. Hobstetter, C.A. Renton, *J. Appl. Phys.* **33**, 600 (1962)
14. J.W. Allen, *J. Electron.* **1**, 580 (1956)
15. W. Schröter, H. Cerva, *Solid State Phenom.* **85–86**, 67 (2002)
16. R.M. Broudy, J.W. McClure, *J. Appl. Phys.* **31**, 1511 (1960)
17. R.M. Broudy, *Adv. Phys.* **12**, 135 (1963)
18. J.H.P. van Weeren, G. Koopmans, J. Blok, *Phys. Stat. Sol.* **27**, 219 (1968)
19. J. Krylow, J. Auleytner, *Phys. Stat. Sol.* **32**, 581 (1969)
20. C.V. Collins, M.H. Miles, *J. Appl. Phys.* **42**, 5644 (1971)

21. J.N. Hobstetter, P. Breidt Jr., *J. Appl. Phys.* **28**, 1214 (1957)
22. R.K. Mueller, *J. Appl. Phys.* **30**, 2015 (1959)
23. L. Blik, W. Schröter, *Phys. Stat. Sol.* **14**, K55 (1966)
24. W. Schröter, *Inst. Phys. Conf. Ser.* **46**, 114 (1979)
25. W. Schröter, E. Scheibe, H. Schoen, *J. Microsc.* **118**, 23 (1979)
26. K.D. Usadel, W. Schröter, *Philos. Mag. B* **37**, 217 (1978)
27. R. Labusch, R. Schettler, *Phys. Stat. Sol. (A)* **9**, 455 (1972)
28. H. Veth, M. Lannoo, *Philos. Mag. B* **50**, 93 (1984)
29. S. Mantovani, U. del Pennino, E. Mazzega, *Phys. Stat. Sol. (A)* **35**, 451 (1976)
30. U. del Pennino, S. Mantovani, *Phys. Stat. Sol. (A)* **38**, 109 (1976)
31. R. Wagner, *Phys. Stat. Sol. (A)* **24**, 575 (1974)
32. R. Wagner, P. Haasen, *Inst. Phys. Conf. Ser. No.* **23**, 387 (1975)
33. A.I. Kolyubakin, S.A. Shevchenko, *Phys. Stat. Sol. (A)* **63**, 677 (1981)
34. A.I. Kolyubakin, Y.A. Osip'yan, S.A. Shevchenko, *Sov. Phys. Solid State* **25**, 1234 (1983)
35. W. Güth, *Phys. Stat. Sol. (B)* **51**, 143 (1972)
36. A. Claesson, *Phys. Stat. Sol. (B)* **61**, 599 (1974)
37. S. Winter, *Phys. Stat. Sol. (B)* **79**, 637 (1977)
38. V.L. Bonch-Bruevich, V.B. Glasko, *Sov. Phys. Solid State* **3**, 26 (1961)
39. V. Heine, *Phys. Rev.* **146**, 568 (1966)
40. W. Güth, W. Haist, *Phys. Stat. Sol.* **17**, 691 (1966)
41. R.A. Brown, *Phys. Rev.* **156**, 692 (1967)
42. R.A. Brown, *Phys. Rev.* **156**, 889 (1967)
43. S. Marklund, *Phys. Stat. Sol. (B)* **85**, 673 (1978)
44. A. Osip'yan Yu, I.A. Ryzhkin, *Sov. Phys. JETP* **52**, 489 (1980)
45. I.A. Ryzhkin, *Sov. Phys. Solid State* **24**, 28 (1982)
46. S. Winter, *Phys. Stat. Sol. (B)* **90**, 289 (1978)
47. H. Veth, H. Teichler, *Philos. Mag. B* **49**, 371 (1984)
48. W. Yong-Liang, *Phys. Rev. B* **40**, 5669 (1989)
49. S.N. Karyagin, *Phys. Stat. Sol. (A)* **68**, K113 (1981)
50. E.J. Pakulis, C.D. Jeffries, *Phys. Rev. Lett.* **47**, 1859 (1981)
51. E.J. Pakulis, *J. Magn. Resonance* **51**, 490 (1983)
52. R. Labusch, *Physica* **117B–118B**, 203 (1983)
53. A. Osip'yan Yu, V.I. Tal'yanskiĭ, S.A. Shevchenko, *Sov. Phys. JETP* **45**, 810 (1977)
54. A. Osip'yan Yu, V.I. Tal'yanskiĭ, A.A. Kharlamov, S.A. Shevchenko, *Sov. Phys. JETP* **49**, 840 (1979)
55. A. Osip'yan Yu, V.M. Prokopenko, V.I. Tal'yanskiĭ, A.A. Kharlamov, S.A. Shevchenko, *JETP Lett.* **30**, 111 (1980)
56. A. Osip'yan Yu, S.A. Shevchenko, *JETP Lett.* **20**, 328 (1974)
57. A. Osip'yan Yu, S.A. Shevchenko, *JETP Lett.* **33**, 207 (1981)
58. V.V. Kveder, R. Labusch, A. Ossip'yan Yu, *Phys. Stat. Sol. (A)* **92**, 293 (1985)
59. J. Hess, R. Labusch, *Phys. Stat. Sol. (A)* **138**, 617 (1993)
60. C.A. Hogarth, A.C. Baynham, *Proc. Phys. Soc.* **71**, 647 (1958)
61. J. Kryłow, *Phys. Stat. Sol.* **32**, 589 (1969)
62. S.A. Shevchenko, A.I. Kolyubakin, *Sov. Phys. Semicond.* **13**, 613 (1979)
63. S.A. Shevchenko, L.I. Khodos, I.I. Snighireva, *Phys. Stat. Sol. (A)* **91**, 523 (1985)
64. P. Gondi, S. Mantovani, F. Schintu, *Phys. Stat. Sol. (A)* **7**, 91 (1971)

65. A. Cavallini, P. Gondi, *Lett. Nuovo Cimento* **10**, 115 (1974)
66. A. Cavallini, P. Gondi, A. Castaldini, *Phys. Stat. Sol. (A)*, **43**, K205 (1977)
67. P. Gondi, A. Cavallini, A. Castaldini, *J. de Phys. Colloque C6* **40**, C6-71 (1979)
68. A. Cavallini, P. Gondi, A. Castaldini, *Phys. Stat. Sol. (A)* **63**, 143 (1981)
69. M. Albers, A. Gabriel, W. Schröter, *Inst. Phys. Conf. Ser. No.* **31**, 509 (1977)
70. F.H. Baumann, W. Schröter, *Phys. Stat. Sol. (A)* **79**, K123
71. F.H. Baumann, W. Schröter, *Philos. Mag.* **48**, 55 (1983)
72. G.S. Hubbard, E.E. Haller, *J. Electron Mater.* **9**, 51 (1980)
73. E. Simoen, P. Clauws, J. Vennik, *Solid State Commun.* **54**, 1025 (1985)
74. M. Van Sande, L. Van Goethem, L. De Laet, H. Guislain, *Appl. Phys. A* **40**, 257 (1986)
75. J.B. Arthur, A.F. Gibson, J.W. Granville, E.G.S. Paige, *Philos. Mag.* **3**, 940 (1958)
76. R.A. Logan, G.L. Pearson, D.A. Kleinman, *J. Appl. Phys.* **30**, 885 (1959)
77. B. Pödör, *Phys. Stat. Sol.* **16**, K167 (1966)
78. J.H.P. Van Weeren, R. Struikmans, J. Blok, *Phys. Stat. Sol.* **19**, K107 (1967)
79. J.H.P. Van Weeren, R. Struikmans, G. Koopmans, J. Blok, *Phys. Stat. Sol.* **27**, 225 (1968)
80. F. Calzecchi, P. Gondi, S. Mantovani, *Il Nuovo Cimento* **53B**, 203 (1968)
81. F. Calzecchi, P. Gondi, S. Mantovani, *J. Appl. Phys.* **40**, 82 (1969)
82. D.L. Dexter, F. Seitz, *Phys. Rev.* **86**, 964 (1952)
83. W.T. Read Jr., *Philos. Mag.* **46**, 111 (1955)
84. A.F. Gibson, E.G.S. Paige, *Philos. Mag.* **3**, 950 (1958)
85. E.M. Kuznetsova, *Sov. Phys. Solid State* **3**, 1446 (1962)
86. Y.V. Korniyushin, S.I. Pekar, *Sov. Phys. Solid State* **8**, 895 (1966)
87. R.A. Vardanian, G.G. Kirakosian, *Phys. Stat. Sol. (B)* **126**, K83 (1984)
88. W. Schröter, *Phys. Stat. Sol.* **31**, 177 (1969)
89. A. Osip'yan Yu, S.A. Shevchencko, *Sov. Phys. JETP* **38**, 345 (1974)
90. J. Liu, D.D. Cannon, K. Wada, Y. Shikawa, D.T. Danielson, S. Jongthammurak, J. Michel, L.C. Kimerling, *Phys. Rev. B* **70**, 155309-1/5 (2004)
91. D. Monroe, Y.H. Xie, E.A. Fitzgerald, P.J. Silverman, G.P. Watson, *J. Vac. Sci. Technol. B* **11**, 1731 (1993)
92. E. Simoen, G. Brouwers, G. Eneman, M. Bargallo Gonzalez, B. De Jaeger, J. Mitard, D.P. Brunco, L. Souriau, N. Cody, S. Thomas, M. Meuris, *E-MRS* (2008)
93. G.K. Wertheim, G.L. Pearson, *Phys. Rev.* **107**, 694 (1957)
94. R.A. Logan, M. Schwartz, *Phys. Rev.* **96**, 46 (1954)
95. J. Okada, *J. Phys. Soc. Jpn.* **10**, 1110 (1955)
96. A.D. Kurtz, S.A. Kulin, B.L. Averbach, *Phys. Rev.* **101**, 1285 (1956)
97. A.D. Kurtz, S.A. Kulin, B.L. Averbach, *J. Appl. Phys.* **27**, 1287 (1956)
98. J.P. McKelvey, *Phys. Rev.* **106**, 910 (1957)
99. C.A. Hogarth, P.J. Hoyland, *J. Electron Control* **4**, 60 (1958)
100. F.D. Rosi, *RCA Rev.* **19**, 349 (1958)
101. M.I. Iglitsyn, L.I. Kolesnik, *Sov. Phys. Solid State* **2**, 1400 (1960)
102. A.D. Belyaev, V.N. Vasilevskaya, E.G. Miselyuk, *Sov. Phys. Solid State* **2**, 208 (1960)
103. L.I. Kolesnik, *Sov. Phys. Solid State* **4**, 1066 (1962)
104. P.G. Eliseev, K. Ch'ang-ho, I.A. Nakhodnov, *Sov. Phys. Solid State* **4**, 2109 (1963)

105. R.L. Bell, C.A. Hogarth, *J. Electron Control* **3**, 455 (1957)
106. S.S. Kulin, A.D. Kurtz, *Acta Metall.* **2**, 354 (1954)
107. S.R. Morrison, *Phys. Rev.* **104**, 619 (1956)
108. V. Gulyaev Yu, *Sov. Phys. Solid State* **3**, 796 (1961)
109. E.B. Sokolova, *Sov. Phys. Semicond.* **3**, 1266 (1970)
110. R.A. Vardanyan, *Sov. Phys. JETP* **46**, 1210 (1977)
111. W. Schröter, *Phys. Stat. Sol. (A)* **19**, 159 (1973)
112. V.B. Shikin, N.I. Shikina, *Phys. Stat. Sol. (A)* **108**, 669 (1988)
113. J. Hess, J. Schreiber, S. Hildebrandt, R. Labusch, *Phys. Stat. Sol. (B)* **172**, 225 (1992)
114. S. Roy Morrison, *Phys. Rev.* **99**, 1904 (1955)
115. J.J. Brophy, *J. Appl. Phys.* **27**, 1383 (1956)
116. L. Bess, *Phys. Rev.* **103**, 72 (1956)
117. L. Gousskov, G. Lecoy, C. Llinares, M. Savelli, *Phys. Stat. Sol.* **16**, 721 (1966)
118. S. Schäfer, *Solid-State Electron* **11**, 675 (1968)
119. M. Bernard, B. Leduc, *J. Phys. Chem. Solids* **13**, 168 (1960)
120. O. Ryuzan, *J. Phys. Soc. Jpn.* **16**, 2177 (1961)
121. P.A. Glasow, E.E. Haller, *IEEE Trans. Nucl. Sci.* **NS-23**, 92 (1976)
122. G.S. Hubbard, E.E. Haller, W.L. Hansen, *IEEE Trans. Nucl. Sci.* **NS-26**, 303 (1979)
123. H. Niizuma, T. Imai, *Jpn. J. Appl. Phys.* **4**, 282 (1965)
124. B.S. Muravskii, *Sov. Phys. Solid State* **4**, 1820 (1963)
125. H.G. Lipson, E. Burstein, P.L. Smith, *Phys. Rev.* **99**, 444 (1955)
126. M. Meyer, M.H. Miles, T. Ninomiya, *J. Appl. Phys.* **38**, 4481 (1967)
127. W. Barth, K. Elsässer, *Phys. Stat. Sol. (B)* **48**, K147 (1971)
128. H. Schaumburg, F. Willmann, *Phys. Stat. Sol. (A)* **34**, K173 (1976)
129. W. Barth, L. Elsaesser, W. Güth, *Phys. Stat. Sol. (A)* **34**, 153 (1976)
130. S. Winter, *Phys. Stat. Sol. (B)* **85**, K95 (1978)
131. R. Newman, *Phys. Rev.* **105**, 1715 (1957)
132. C. Benoit À La Guillaume, *J. Phys. Chem. Solids* **8**, 150 (1959)
133. A.A. Gippius, V.S. Vavilov, *Sov. Phys. Solid State* **6**, 1873 (1965)
134. L. Ivanov Yu, *Sov. Phys. Solid State* **7**, 629 (1965)
135. W. Barth, M. Bettini, U. Ostertag, *Phys. Stat. Sol. (A)* **3**, K177 (1970)
136. E.B. Sokolov, *Sov. Phys. Solid State* **7**, 390 (1965)
137. L.I. Kolesnik, A. Kontsevoi Yu, *Sov. Phys. Solid State* **6**, 131 (1964)
138. M. Jastrzebska, T. Figielski, *Phys. Stat. Sol.* **7**, K101 (1964)
139. T.R. Figielski, A.D. Belyaev, *Sov. Phys. Solid State* **6**, 1690 (1965)
140. Z. Gołacki, T. Figielski, M. Jastrzebska, *Phys. Stat. Sol.* **11**, K35 (1965)
141. M. Jastrzebska, T. Figielski, *Phys. Stat. Sol.* **14**, 381 (1966)
142. Z. Gołacki, T. Figielski, *Phys. Stat. Sol.* **20**, K1 (1967)
143. M. Jastrzebska, T. Figielski, *Phys. Stat. Sol.* **32**, 791 (1969)
144. E. Kamieniecki, *Phys. Stat. Sol. (A)* **4**, 257 (1971)
145. T. Figielski, *Solid-State Electron* **21**, 1403 (1978)
146. M.H. Miles, *J. Appl. Phys.* **40**, 2720 (1969)
147. W. Barth, G. Langohr, *Phys. Stat. Sol. (A)* **3**, K289 (1970)
148. E. Kamieniecki, K. Elsässer, *Phys. Stat. Sol. (B)* **56**, K25 (1973)
149. K. Elsässer, E. Kamieniecki, *Phys. Stat. Sol. (A)* **26**, K37 (1974)
150. D. Mergel, R. Labusch, *Phys. Stat. Sol. (A)* **41**, 431 (1977)
151. D. Mergel, R. Labusch, *Phys. Stat. Sol. (A)* **42**, 165 (1977)

152. A.I. Kolyubakin, A. Osipov Yu, S.A. Shevchenko, *Sov. Phys. JETP* **50**, 491 (1979)
153. R. Labusch, J. Hess, *Phys. Stat. Sol. (A)* **146**, 145 (1994)
154. W. Schröter, H. Hedemann, V. Kveder, F. Riedel, *J. Phys. Condens. Matter* **14**, 13047 (2002)
155. B. Pohoryles, R. Piotrkowski, *Phys. Stat. Sol. (A)* **47**, K115 (1978)
156. B. Pohoryles, J. Jung, *J. Phys. Chem. Solids* **45**, 671 (1984)
157. B. Pohoryles, *Phys. Stat. Sol. (A)* **116**, 349 (1989)
158. A.A. Gippius, V.S. Vavilov, V.S. Konoplev, *Sov. Phys. Solid State* **6**, 1741 (1965)
159. E.A. Steinmann, *Crystal Res. Technol.* **16**, 247 (1981)
160. A.I. Kolyubakin, Y.A. Osip'yan, S.A. Shevchenko, *Sov. Phys. JETP* **66**, 142 (1987)
161. S. Lelikov Yu, T. Rebane Yu, G. Shreter Yu, *Inst. Phys. Conf. Ser. No.* **104**, 119 (1989)
162. A.N. Izotov, A.I. Kolyubakin, S.A. Shevchenko, E.A. Steinman, *Phys. Stat. Sol. (A)* **130**, 193 (1992)
163. S. Shevchenko, A. Tereshchenko, *Phys. Stat. Sol. (C)* **4**, 2898 (2007)
164. H.R. Weber, *Phys. Stat. Sol. (A)* **25**, 445 (1974)